NAVAL POSTGRADUATE SCHOOL
Monterey, California

DISSERTATION

SOURCE LOCATION IN THIN PLATES
USING CROSSCORRELATION

by

Steven Michael Ziola

December, 1991

Dissertation Supervisor: Michael R. Gorman

Approved for public release; distribution is unlimited.

REPORT DOCUMENTATION PAGE

Form Approved
OMB No 0704-0188

1a REPORT SECURITY CLASSIFICATION	1b RESTRICTIVE MARKINGS
UNCLASSIFIED	

2a SECURITY CLASSIFICATION AUTHORITY	3 DISTRIBUTION / AVAILABILITY OF REPORT
Multiple Sources	Approved for public release;
2b DECLASSIFICATION / DOWNGRADING SCHEDULE	distribution is unlimited

4 PERFORMING ORGANIZATION REPORT NUMBER(S)	5 MONITORING ORGANIZATION REPORT NUMBER(S)

6a NAME OF PERFORMING ORGANIZATION	6b OFFICE SYMBOL (If applicable)	7a. NAME OF MONITORING ORGANIZATION
Naval Postgraduate School	39	Naval Postgraduate School

6c. ADDRESS (City, State, and ZIP Code)	7b. ADDRESS (City, State, and ZIP Code)
Monterey, CA 93943-5000	Monterey, CA 93943-5000

8a. NAME OF FUNDING / SPONSORING ORGANIZATION	8b. OFFICE SYMBOL (If applicable)	9 PROCUREMENT INSTRUMENT IDENTIFICATION NUMBER

8c. ADDRESS (City, State, and ZIP Code)	10 SOURCE OF FUNDING NUMBERS			
	PROGRAM ELEMENT NO.	PROJECT NO.	TASK NO.	WORK UNIT ACCESSION NO.

11 TITLE (Include Security Classification)
SOURCE LOCATION IN THIN PLATES USING CROSSCORRELATION (UNCLASSIFIED)

12. PERSONAL AUTHOR(S)
Ziola, Steven, M.

13a. TYPE OF REPORT	13b TIME COVERED	14. DATE OF REPORT (Year, Month, Day)	15 PAGE COUNT
Doctoral Dissertation	FROM _____ TO _____	December, 1991	115

16. SUPPLEMENTARY NOTATION

The views expressed in this thesis are those of the author and do not reflect the official policy or position of the Department of defense or the U. S. Government.

17	COSATI CODES		18. SUBJECT TERMS (Continue on reverse if necessary and identify by block number)
FIELD	GROUP	SUB-GROUP	acoustic emission, composites, plate waves, source location, crosscorrelation

19 ABSTRACT (Continue on reverse if necessary and identify by block number)

Alternative methods to first threshold crossing techniques for acoustic emission (AE) source location in dispersive media are presented. The accuracy of source location in dispersive media can be improved by locating frequency components in the transducer outputs to determine the difference in arrival times. Two methods were developed in this study for the arrival time determination. The first involved crosscorrelating the transducer outputs with a cosine wave modulated by a Gaussian pulse to locate a single frequency in the outputs. The second method narrowband filtered the transducer outputs and then crosscorrelated the filtered signals to determine the difference in arrival times. The techniques were experimentally verified by performing lead breaks on the surface of aluminum and graphite/epoxy plates. The results indicate that accurate source location can be attained in dispersive media by taking the wave propagation into account.

20. DISTRIBUTION / AVAILABILITY OF ABSTRACT	21. ABSTRACT SECURITY CLASSIFICATION
☑ UNCLASSIFIED/UNLIMITED ☐ SAME AS RPT ☐ DTIC USERS	Unclassified

22a. NAME OF RESPONSIBLE INDIVIDUAL	22b. TELEPHONE (Include Area Code)	22c. OFFICE SYMBOL
Michael R. Gorman	408-646-2074	AA/Go

DD Form 1473, JUN 86 — Previous editions are obsolete. — SECURITY CLASSIFICATION OF THIS PAGE

S/N 0102-LF-014-6603

Source Location in Thin Plates Using Crosscorrelation

by

Steven M. Ziola
B.S., University of Nebraska at Lincoln, 1982
M.S., University of Nebraska at Lincoln, 1987

Submitted in partial fulfillment of the
requirements for the degree of

DOCTOR OF PHILOSOPHY IN AERONAUTICAL ENGINEERING

from the

ABSTRACT

Alternative methods to first threshold crossing techniques for acoustic emission (AE) source location in dispersive media are presented. The accuracy of source location in dispersive media can be improved by locating frequency components in the transducer outputs to determine the difference in arrival times. Two methods were developed in this study for the arrival time determination. The first involved crosscorrelating the transducer outputs with a cosine wave modulated by a Gaussian pulse to locate a single frequency in the outputs. The second method narrowband filtered the transducer outputs and then crosscorrelated the filtered signals to determine the difference in arrival times. The techniques were experimentally verified by performing lead breaks on the surface of aluminum and graphite/epoxy plates. The results indicate that accurate source location can be attained in dispersive media by taking the wave propagation into account.

TABLE OF CONTENTS

ACKNOWLEDGEMENT

I. INTRODUCTION

A. NEED FOR NONDESTRUCTIVE EVALUATION

In recent years there have been two highly publicized incidents which involved the catastrophic failure of transport systems. The first of these involved the space shuttle Challenger. In this case, the solid rocket booster (SRB) seals failed and allowed hot gases to escape from the SRB joints. This eventually caused the ignition of the oxygen and hydrogen in the external propellant tank, resulting in seven fatalities and the suspension of the space shuttle program [Ref. 1]. The second was the Aloha Airlines incident in which a portion of the fuselage of a Boeing 737-200 tore away from the airframe in flight, resulting in one fatality and injuries to 69 passengers [Ref. 2]. These two incidents are dramatic examples of the need for the monitoring of structures for defect growth. And, while these are two highly visible examples of the failure of engineering structures, there are many more less publicized, but just as critical, examples of the need for defect monitoring. These include cracking in the main wing beam in the E2-C Hawkeye [Ref. 3], the monitoring of defect locations in nuclear reactor pressure vessels [Ref. 4] and the detection of defects in high pressure storage tanks [Ref. 5]. It is the main goal of non-destructive evaluation (NDE) to locate and monitor defect growth in structures so that preventive actions can be taken before the defects reach a critical size and failure occurs.

Toward this end, many non-destructive test (NDT) methods have been employed, and a short list of these includes x-ray, radiography, ultrasonics, magnetic resonance, dye penetrant and eddy current. A common trait of all these techniques is that the energy to be used to detect the defects must by propagated into the structure, and that this energy must then interact with the defect. If the orientation or the size of the defect is such that the energy fails to interact with or be modulated by the defect, the defect will go undetected. Additionally, the methods listed above are, at best, difficult to apply to a structure while it is in service, and thus, flaw growth while the structure is under load is difficult to monitor. A method not yet mentioned which can detect flaw growth while the structure is in service is acoustic emission (AE).

AE is defined as the elastic waves which are generated by rapid local redistributions of stresses which accompany the operation of damage mechanisms. Thus, the defect growth itself supplies the detectable energy. In Figure 1.1 a typical application of the acoustic emission method in a structure is shown. Due to the applied stress σ, a defect begins to grow and releases energy in the form of a stress wave or stress pulse. To detect this stress wave a transducer is attached to the structure and the output from the transducer is captured. This signal is then analyzed to determine the nature of the event.

While current AE techniques are very adept at flaw growth detection, their use for the determination of source location can lead to large errors. The work presented in this study details crosscorrelation methods which were developed to correct these errors by incorporating the wave propagation in a given medium into the source

2

location algorithm. Before the crosscorrelation techniques are discussed however, a review of the current AE methods will be presented to illuminate the shortcomings of the current methods and to illustrate the need for the new techniques.
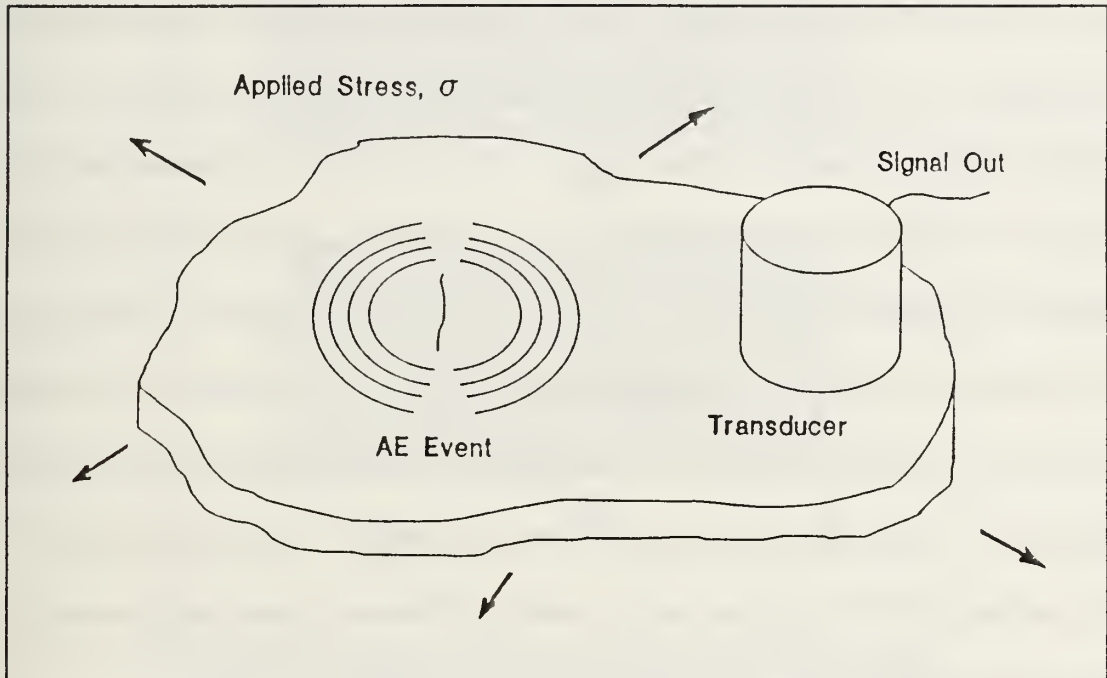
Figure 1.1. Example of acoustic emission technique.

B. BACKGROUND ON ACOUSTIC EMISSION SOURCE LOCATION

If the location of a source is to be determined, then at least two transducers are attached to the structure. By noting the difference in arrival time(s) (Δt('s)) of the stress wave at the transducers and knowing the velocity of propagation of the stress wave, the location of the source can be determined through the use of triangulation.

In commercial AE analyzers, these arrival time differences are determined using first threshold crossing techniques. For example, first threshold crossing could be defined as the time at which the envelope of the AE signal crosses a preset threshold.

3

AE instrumentation of the type described above was used in the testing of flat, plate-like graphite/epoxy coupons, and it was found that errors of up to 5 cm (2 in) occurred in specimens having a 20 cm (8 in) gage length between the AE sensors [Ref. 6]. These errors led to a study of the propagation of acoustic emission waves in plates [Ref. 7], and it was discovered that due to the frequency content of the source (0-1 MHz) and the plate thicknesses (<2.5 mm (0.1 in)) of interest in these tests, only two types of waves propagated in the plate. These two waves were the extensional and flexural plate waves, or modes, and the displacements of these two modes are shown in Figure 1.2. This observation, that only two modes were present, was important since up to this point researchers in AE had assumed that the wave propagation in solid media, such as plates, was too complex to be accounted for in the AE analysis. But with this new understanding, AE measurement could now begin to be based on qualitative rather than quantitative considerations.

The above findings were used by Gorman and Ziola [Ref. 8] to increase the location resolution of conventional AE instrumentation during the testing of tensile graphite/epoxy coupons. From experimental data [Ref. 7] it was found that the extensional mode propagated nearly nondispersively (velocity was independent of frequency) and contained higher frequency components than the flexural mode, which was found to be highly dispersive. By using broadband transducers the two modes could be distinguished and the dispersive, lower frequency flexural mode eliminated by highpass filtering. High amplifier gain was selected and the instrumentation parameters were set so that triggering of the location clocks occurred
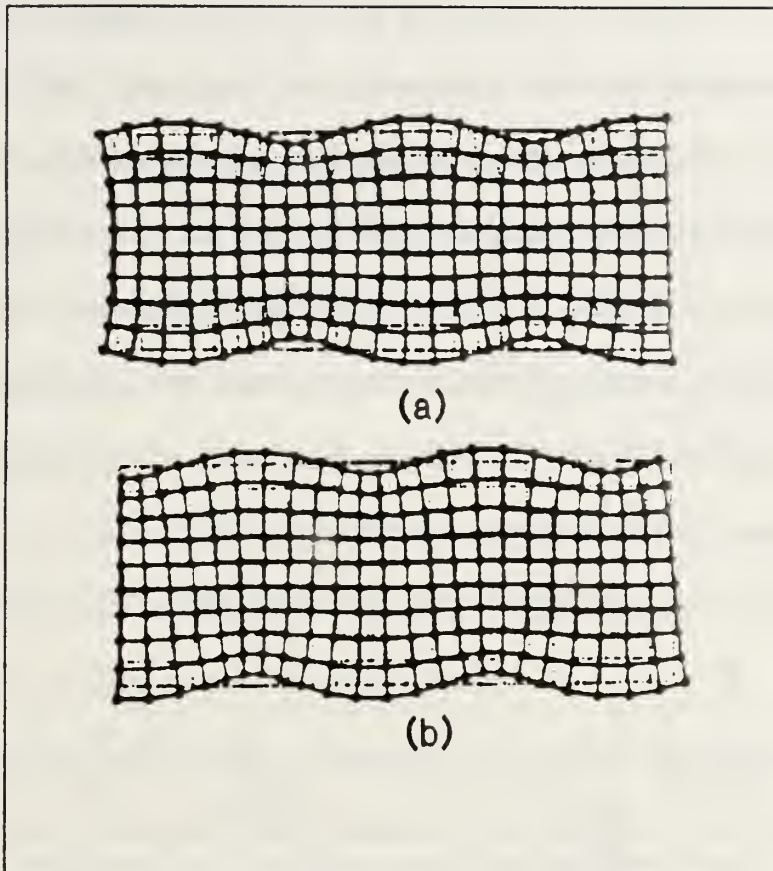
Figure 1.2. Schematic representation of plate wave displacements, (a) extensional plate wave, (b) flexural plate wave (after Beattie [Ref. 9]).

on the first positive going signal due to the nondispersive extensional mode. It was shown that source location accuracy was increased by an order of magnitude using this technique.

While this method worked well on small test coupons, it would not be as effective if the extensional mode was highly attenuated. This would be the case for larger structures, especially those made of composites. Due to the attenuation, the timing clocks would now be triggered by the dispersive flexural wave, leading to timing errors since the AE pulse shape changes as it propagates. An example of the effect

of dispersion on an AE pulse is shown in Figure 1.3. In this figure a flexural wave was excited in an aluminum plate (thickness - 1.42 mm (0.056 in)) by breaking a Pental 2H 0.5 mm lead on the surface of the plate. The resulting wave was then captured at 50.8 mm (2 in) and 304.8 mm (12 in) from the source using broadband sensors and filters. From this it is obvious that the timing clocks would not be triggered on the same frequency point of the waveforms if first threshold crossing techniques were used. This is the main problem with using threshold crossing techniques to locate sources in dispersive media.
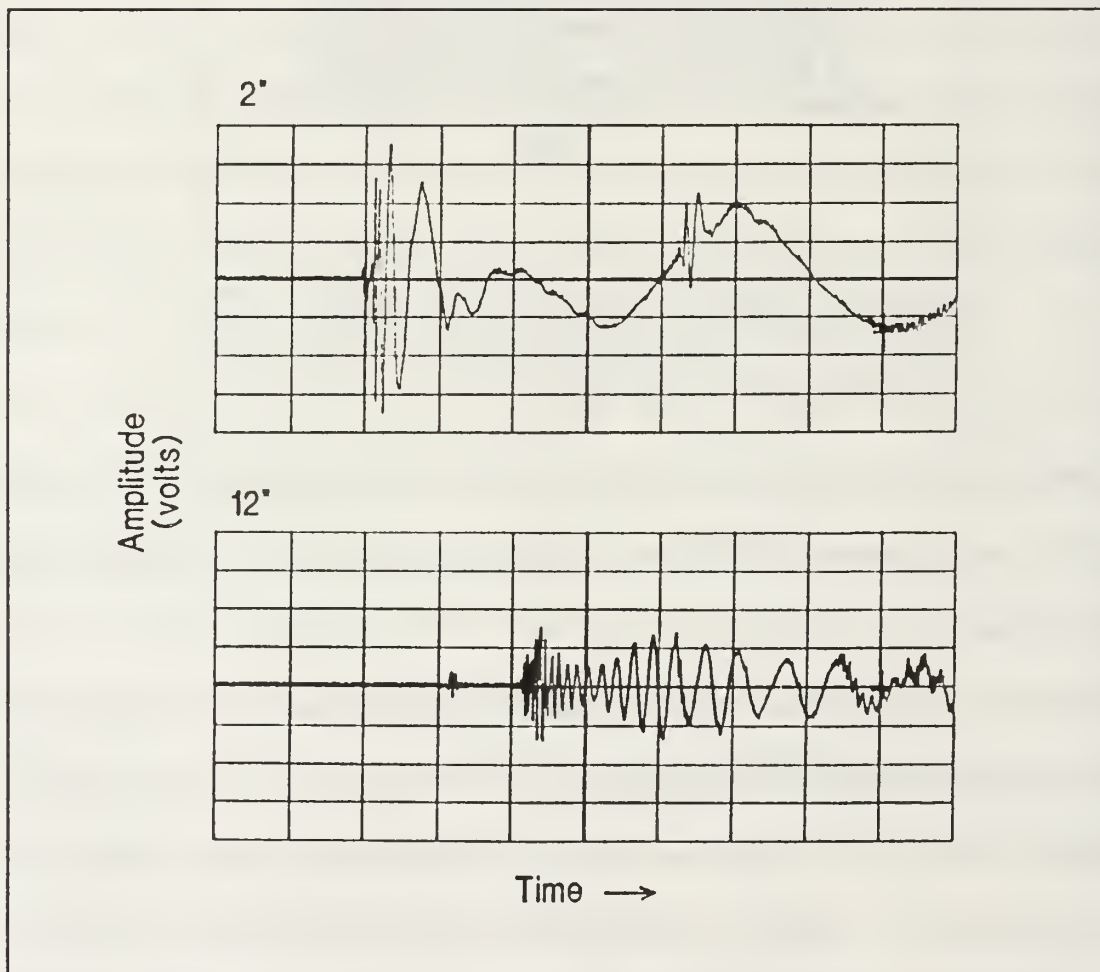

Figure 1.3. Example of dispersion.

C. NEW TECHNIQUES FOR SOURCE LOCATION

The focus of this investigation therefore, was to devise a method which would allow accurate source location by detection of specific frequencies in the waveforms. By using such a method, not only would the problem of first threshold crossing be eliminated, but location measurements could then be performed using the dispersive flexural portion of the waveform. Again, this is of importance in larger structures where, due to attenuation, only the lower frequencies contained in the flexural wave will be able to propagate any great distance, and also in impact studies, such as micrometeriod impacts on space vehicles, where the source motion produces a large flexural wave with little or no extensional component.

A method which does not rely on threshold crossing to determine Δt's is that of crosscorrelation. In this work, crosscorrelation is defined as the time average of the product of two functions, where one function has been delayed relative to the other

$$R_{xy}(\tau) = \lim_{T \to \infty} \frac{1}{2T} \int_{-T}^{T} x(t)y(t+\tau)dt. \tag{1.1}$$

In Section II literature is reviewed in which crosscorrelation was used for time-of-flight determination.

For this study, two crosscorrelation methods were formulated which allowed the use of the dispersive flexural wave (wave propagation theory for thin plates is presented in Section III) for the determination of arrival times at the transducers. The first crosscorrelated the output signals from the transducers with a single frequency cosine wave modulated by a Gaussian pulse. By doing this a single

frequency in the output signals could be isolated, and from this the Δt's needed for the source location could be determined. The second method first narrowband filtered the output signals and then crosscorrelated these filtered signals to determine the arrival times. These methods are detailed in Section IV.

To experimentally verify the above techniques, lead breaks were performed on the surface of both aluminum and graphite/epoxy plates to excite plate waves. Although both the extensional and flexural modes were observed, the lowest order flexural mode was by far the larger wave due to the out-of-plane nature of the lead break. The source location results of the crosscorrelation techniques are compared with conventional AE instrumentation techniques (narrowband filtering and resonant transducers) and also the high gain/broadband technique outlined earlier. The results indicate that the resolution of the crosscorrelation techniques is comparable to that of the high gain methods, thereby allowing accurate source location in structures where, due to attenuation, only the dispersive flexural wave is available. The experimental results are given in Sections V and VI.

II. LITERATURE REVIEW

The ability to locate defects in materials is one of the major attractions of the acoustic emission technique. However, the resolution of the source location is dependent on how accurately the differences in arrival times of the stress wave at the transducers can be measured. As was discussed in the previous section, the method in use in current AE instrumentation, that of threshold crossing, can lead to large errors in location since the wave mechanics of the media are not incorporated into the location analysis. This has lead to the use of crosscorrelation techniques for the determination of arrival times.

Crosscorrelation has been used for many years in acoustics for the determination of propagation paths [Ref. 10]. Typically this is done by sending a known signal, by use of a microphone, into the media, and then having a receiving microphone capture the propagated signal. The known input signal and the captured propagated signal are then crosscorrelated and the peaks in the crosscorrelation will then correspond to the direct propagation path and any paths due to reflections. An example of this is shown in Figure 2.1, where the peaks in the crosscorrelation at 2, 4 and 5 msec correspond to the direct path, the reflection off of the side wall, and the reflection from the back wall, respectively. For the interested reader, Reference 11 contains papers on signal processing and time delay estimation in nondispersive systems.

Smith and Lambert [Ref. 12] used the crosscorrelation technique to measure the
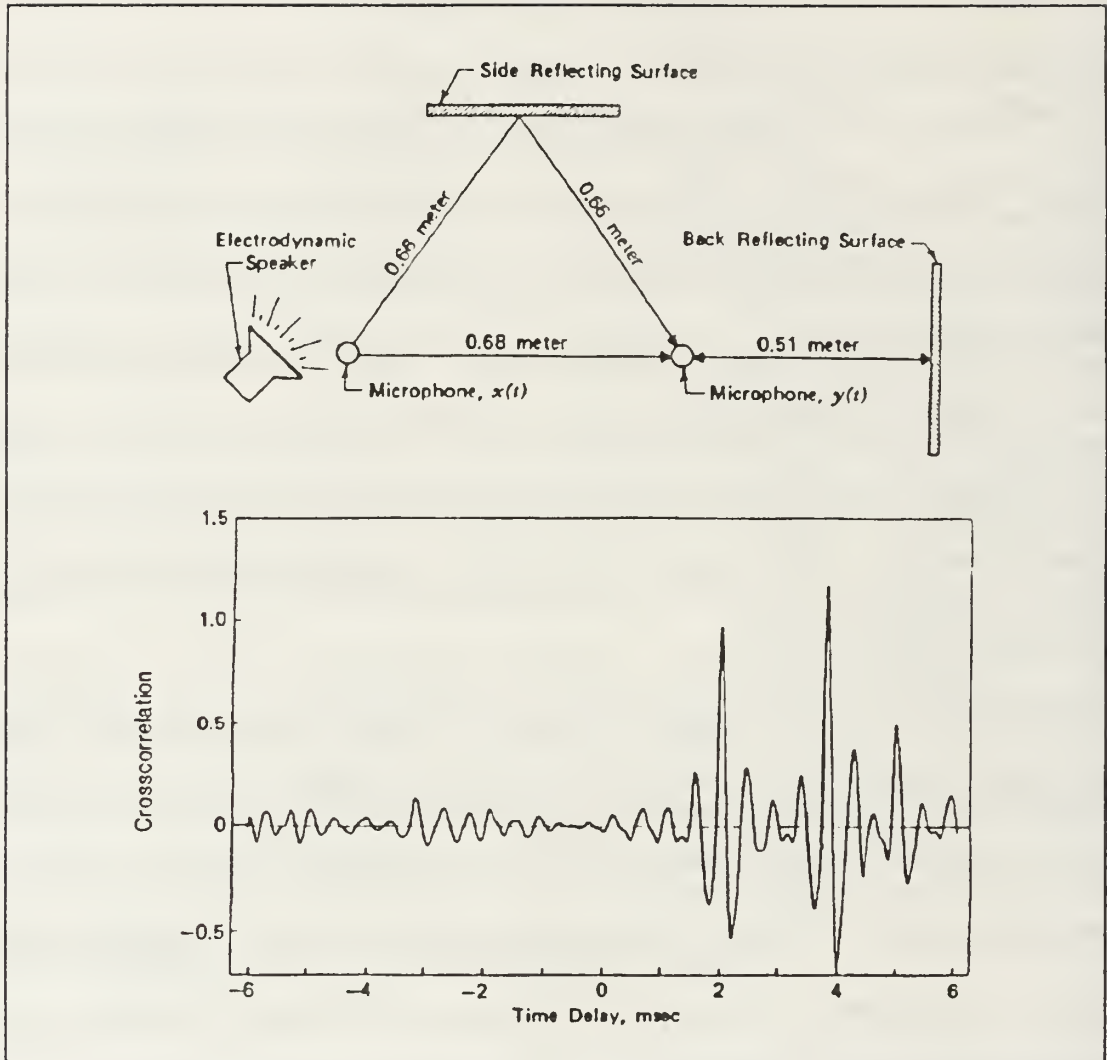
Figure 2.1. Example of propagation path determination using crosscorrelation (after Bendat and Piersol [Ref. 10]).

propagation times of band limited noise in a plane wave tube where the propagation media was air, a nondispersive media. They determined theoretically that the crosscorrelation of band limited noise should result in a cosine wave with a frequency equal to that of the center frequency of the band limited noise modulated by a $\sin x/x$ term which is dependent on the bandwidth of the noise. To experimentally verify the

10

theory, they propagated band limited noise (1 octave) in a plane wave tube and captured the resulting waves using condenser microphones placed a known distance apart. The crosscorrelation of these signals were seen to agree with the theory within experimental error.

Winter and Bies [Ref. 13] used the same approach to measure velocities in a dispersive medium. They attached a shaker to one end of an aluminum bar and placed two transducers a known distance apart near the center of the bar. Damping material was placed at both ends of the bar to eliminate reflections. A flexural wave was then excited in the bar using broadbanded noise (10 octave width) applied to the shaker and the outputs from the two transducers were crosscorrelated. They found that peaks in the crosscorrelations did not seem to correlate to any possible propagation velocities in the bar. It can be seen from Figure 1.3, Section I-B, that crosscorrelation of broadbanded signals in dispersive media will generally lead to inconclusive results.

White [Ref.14] also studied the problem of the measurement of time delays in dispersive media (Novikov [Ref. 15], has performed a similar analysis). The same experimental set-up as Winter and Bies was used, however, instead of using broadbanded noise to excite the bar, White used band limited noise of one octave or less. The theoretical evaluation of the crosscorrelation of band limited noise in a dispersive media given in White's paper resulted in an equation much like that of Smith and Lambert's, where a cosine wave with a frequency equal to that of the center frequency of the bandwidth was modulated by a $\sin x/x$ term dependent on the

11

bandwidth of the noise. For a dispersive media however, White found that the cosine term propagated at the phase velocity, and that this term had a phase shift which was dependent on the distance the pulse had traveled, while the $\sin x/x$ envelope propagated with the group velocity. If the peak of the cosine term was chosen, rather than the peak of the envelope, White determined that an error of up to 1/4 of a cycle at the bandwidth center frequency could be made in the Δt measurement. Thus, White was able to measure group velocities accurately in the bar by choosing the peak of the envelope to determine the arrival time differences.

Time of flight measurements are important not only for source location measurements, but by measuring stress wave velocities in a sample, material constants can be determined. Castagnede, Roux and Hosten [Ref. 16] used ultrasonic transducers, resonant at 1 and 5 MHz, to excite quasi-longitudinal and quasi-transverse waves in a unidirectional fiberglass reinforced sample for the determination of as manufactured material constants. They were then able to determine the time of propagation of the waves through the sample by crosscorrelating the captured waveforms from the sample with a reference waveform from the ultrasonic transducers. In their work however, no correction was made for dispersion, which resulted in a simplification of the problem. The high resolution of the data presented could likely be attributed to frequencies at which the pulses were propagated at, since any errors in the crosscorrelation due to phase shifts would be small.

12

Also for material evaluation purposes, Aussel and Monchalin [Ref. 17] used a pulsed Nd:YAG laser to generate an acoustic displacement in Al_2O_3-Al-SiC. This excited longitudinal and shear waves which were then detected on the opposite face of the sample using a laser-interferometer. The time delay measurements were based on crosscorrelation of the resulting echoes in the sample. The phase velocity dispersion was measured by Fourier transforming the crosscorrelation and using the phase data from the crosscorrelation to calculate the dispersion curve for the material. Using this method they found that the phase velocities varied by approximately 2% in the frequency region studied (10-40 MHz) due to dispersion.

Crosscorrelation techniques have also been used for source location in downhole acoustic emission measurements to monitor subsurface crack extensions in geological studies. Nagano, Niitsuma and Chubachi [Ref. 18] used crosscorrelation of waveforms captured from three orthogonal directions to determine the arrival of the bulk longitudinal or P-wave and the shear horizontal or SH-wave. By knowing the propagation velocity of these two nondispersive modes and the difference in arrival times, the location of the source could be determined.

There has been little work done in the analysis of crosscorrelation techniques in dispersive media due to complexities encountered in the wave propagation. With the exception of White's work, all of the crosscorrelation techniques presented here are based on modes which are nondispersive (bulk longitudinal and bulk shear) or performed at frequencies were the dispersion is insignificant. For acoustic emission however, if crosscorrelation techniques are to be implemented for the use of arrival

13

time determination, then the wave propagation in highly dispersive media must be understood. Hence, a discussion of the wave propagation in thin plates is presented in the next section.

III. WAVE THEORY FOR THIN PLATES

In order to gain insight into acoustic emission (AE) and how improvements can be made in source location, an understanding of the wave mechanics in thin plates must first be arrived at. While this statement may seem obvious, in many AE studies it is largely ignored. This can be attributed to the instrumentation that is used to acquire AE data. In typical AE studies resonant transducers are used to increase the system sensitivity while narrowband filters are used to remove extraneous noise from the AE signals. To illustrate how this can affect the acquired signal an AE source was simulated using a lead break (Pental 2H, 0.5 mm) [Ref. 19] on the surface of an aluminum plate of thickness 1.42 mm. Figure 3.1 (a) shows the wave captured using a resonant transducer (resonant frequency - 150 kHz) and narrowband filtering (100 - 300 kHz) in the preamplifiers. Figure 3.1 (b) shows the same wave, but captured with a broadband transducer and broadband filters in the preamplifiers. The narrowband system has distorted the wave beyond recognition, and much of the information pertaining to the source has been lost. Subsequently, much of the research and theory in AE has been based on these distorted waveforms, [Refs. 20-23], and not on the true wave propagation. Thus, the theory and measurement of waves in thin plates must be thoroughly understood before advances in AE can be made.
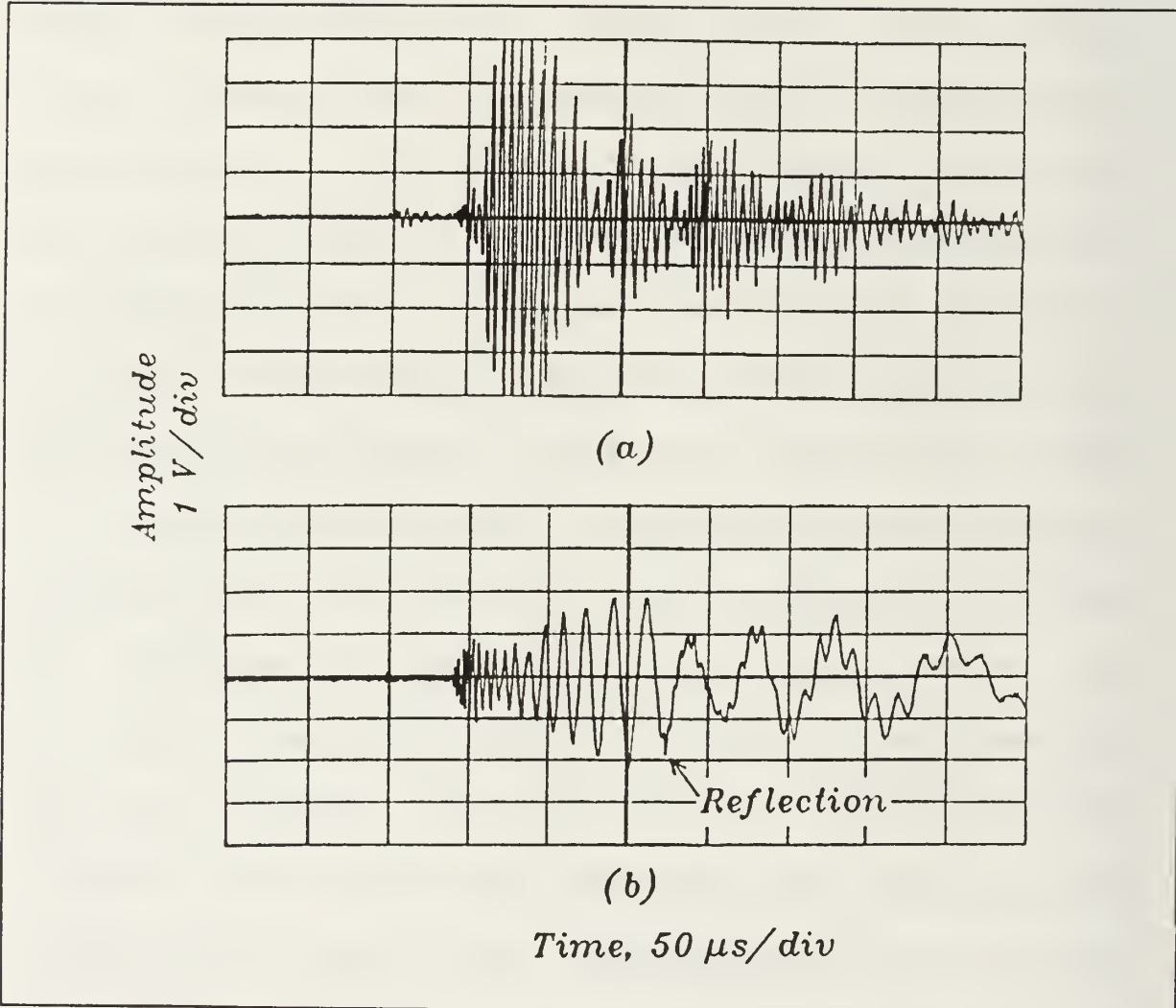
15

Figure 3.1. Captured waveforms.

While many types of waves can propagate in plates, for the purpose of this study only two waves will be considered. These are the extensional plate wave, or an in-plane disturbance, and the flexural plate wave, or an out-of-plane disturbance. The focus of this work will be on the flexural mode since the AE source used for the experiments in this thesis was a lead break on the surface of the plates. This produced an out-of-plane motion, which resulted in exciting primarily the flexural plate wave. Therefore, in this section only the theory of the propagation of flexural waves in thin plates, both isotropic and orthotropic, will be presented. For interested readers analyses for the extensional mode are contained in Graff [Ref. 24], for both the classical plate and exact theory (Rayleigh-Lamb), while Mindlin and Medick [Ref. 25] present an approximate theory in their paper.

A. WAVE THEORY FOR ISOTROPIC PLATES

We will begin the study of the propagation of flexural waves in thin plates using classical plate theory. Consider a plate of thickness h and of infinite extent in the x-y plane as shown in Figure 3.2.

Due to applied stresses, a differential element $h\,dx\,dy$ in the plate will have the various shear forces, bending and twisting moments and external forces acting on it as shown. Summing forces in the z-direction gives

$$\frac{\partial Q_x}{\partial x} + \frac{\partial Q_y}{\partial y} + q = \rho h \frac{\partial^2 w}{\partial t^2} \qquad (3.1)$$

17

where $w(x,y,t)$ measures the displacement of the mid-plane of the plate. Summing moments leaves

$$\frac{\partial M_y}{\partial y} - \frac{\partial M_{xy}}{\partial x} - Q_y = 0, \tag{3.2}$$

$$\frac{\partial M_x}{\partial x} + \frac{\partial M_{xy}}{\partial y} - Q_x = 0. \tag{3.3}$$

If equations (3.2) and (3.3) are solved for Q_y and Q_x and substituted into equation
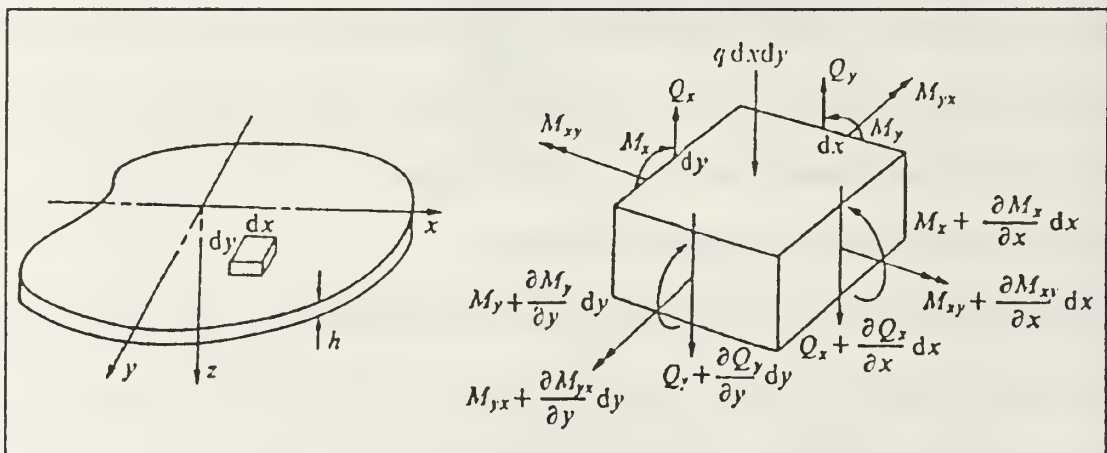
Figure 3.2. Plate element (after Graff [Ref. 24]).

(3.1), a single equation in terms of the various moments is arrived at,

$$\frac{\partial^2 M_x}{\partial x^2} + \frac{\partial^2 M_{yx}}{\partial x \partial y} - \frac{\partial^2 M_{xy}}{\partial y \partial x} + \frac{\partial^2 M_y}{\partial y^2} + q = \rho h \frac{\partial^2 w}{\partial t^2}. \tag{3.4}$$

Now the relationships between the moments and deflections must be established.

As in Bernoulli-Euler theory, it will be assumed that plane sections remain plane and perpendicular to the mid-plane. Shown in Figure 3.3 (a), (b) and (c) is a differential element and the deformations of the element in the x-z and x-y planes.

18

From the figures it follows that the normal strains in the lamina *abcd* are given by

$$\epsilon_x = z/r_x, \qquad \epsilon_y = z/r_y, \qquad (3.5)$$

where r_x and r_y are the radii of curvature in the x-z and y-z planes. If small deflections and slopes are assumed, the curvatures may be approximated by $-\partial^2 w/\partial x^2$ and $-\partial^2 w/\partial y^2$. The strains can then be expressed in terms of the z displacement

$$\epsilon_x = -z\frac{\partial^2 w}{\partial x^2}, \qquad \epsilon_y = -z\frac{\partial^2 w}{\partial y^2}. \qquad (3.6)$$

The shear strain in the lamina is given by

$$\gamma_{xy} = \frac{\partial u}{\partial y} + \frac{\partial v}{\partial x} \qquad (3.7)$$

From Figure 3.3 (b) it can be seen that the displacement component *u* is given by $u = -z\partial w/\partial x$. Similarly, $v = -z\partial w/\partial y$, thus

$$\gamma_{xy} = -2z\frac{\partial^2 w}{\partial x \partial y}. \qquad (3.8)$$

The stresses from Hooke's law are given as

$$\sigma_x = -\frac{Ez}{1-v^2}\left(\frac{\partial^2 w}{\partial x^2} + v\frac{\partial^2 w}{\partial y^2}\right) \qquad (3.9)$$

$$\sigma_y = -\frac{Ez}{1-v^2}\left(\frac{\partial^2 w}{\partial y^2} + v\frac{\partial^2 w}{\partial x^2}\right) \qquad (3.10)$$

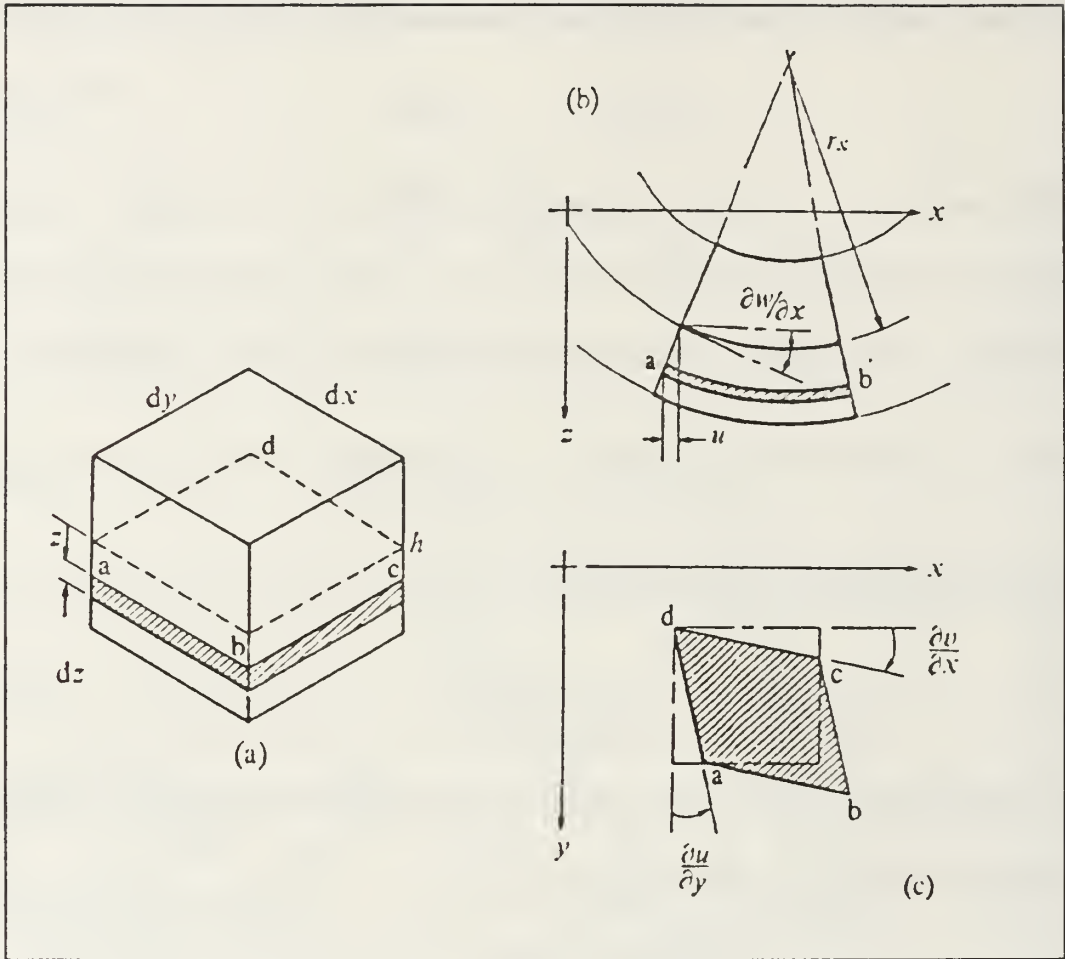$$\tau_{xy} = -2Gz\frac{\partial^2 w}{\partial x \partial y}. \qquad (3.11)$$

19

Figure 3.3. Deformation of differential element (after Graff [Ref. 24]).

The expressions for the bending and twisting moments can now be evaluated. The bending moment due to σ_x on the face of the element in Figure 3.2 (a) defined by $h dy$ is

$$M_x dy = \int_{-h/2}^{h/2} z\sigma_x dy dz \qquad (3.12)$$

or

$$M_x = \int_{-h/2}^{h/2} z\sigma_x \, dz. \tag{3.13}$$

Substituting equation (3.9) into (3.12) and carrying out the integration gives

$$M_x = -D\left(\frac{\partial^2 w}{\partial x^2} + v\frac{\partial w^2}{\partial y^2}\right), \tag{3.14}$$

where $D = Eh^3/12(1-v^2)$. For M_y we obtain

$$M_y = -D\left(\frac{\partial^2 w}{\partial y^2} + v\frac{\partial^2 w}{\partial x^2}\right). \tag{3.15}$$

For M_{xy} the integral is

$$M_{xy} = -\int_{-h/2}^{h/2} z\tau_{xy} \, dz. \tag{3.16}$$

Substituting equation (3.11) into (3.16) and performing the required integration gives

$$M_{xy} = D(1-v)\frac{\partial^2 w}{\partial x \partial y}. \tag{3.17}$$

Also, we have that $M_{yx} = -M_{xy}$. Substituting the expressions for M_x, M_y and M_{xy} into equation (3.4) we obtain the governing equation in terms of the displacement

$$D\left(\frac{\partial^4 w}{\partial x^4} + 2\frac{\partial^4 w}{\partial x^2 \partial y^2} + \frac{\partial^4 w}{\partial y^4}\right) - q = -\rho h\frac{\partial^2 w}{\partial t^2}. \tag{3.18}$$

We can now investigate the conditions under which harmonic plane waves may propagate. Assume a plane wave travelling in the x-direction of the form

21

$$w' = Ae^{i\gamma(x-ct)} \tag{3.19}$$

where A is the amplitude of the wave, γ is the wavenumber (units of 1/length), and c in the velocity of propagation. If we let the external load q be zero, and substitute equation (3.19) into (3.18) we obtain

$$D\gamma^2 - \rho hc^2 = 0, \qquad c = \sqrt{\frac{D}{\rho h}}\,\gamma. \tag{3.20}$$

We can now obtain the relationship between velocity and frequency, knowing that the velocity is defined as $c = \omega/\gamma$, where ω is the circular frequency,

$$c = \sqrt[4]{\frac{D}{\rho h}}\,\omega^{\frac{1}{2}}. \tag{3.21}$$

For long wavelength, low frequency conditions, this theory predicts the correct response, but for short wavelength, high frequency conditions, unbounded wave velocities are predicted. This physically unacceptable situation is the result of imperfections in the model due to rotary inertia and shear effects.

In order to accurately predict the propagation of waves in plates at high frequencies both Lord Rayleigh and H. Lamb in 1899 independently obtained the frequency equation for a plate using the exact equations of elasticity. Their work, now known as the Rayleigh-Lamb theory, pertains to the propagation of continuous, straight crested waves in a plate, which is infinite in extent and has traction-free surfaces. The coordinate system is shown in Figure 3.4, with the x-z plane coinciding with the mid-plane of the plate. To obtain the equation of motion for this case, they

began with the governing equations for a homogeneous isotropic elastic solid

$$\tau_{ij,j} + \rho f_i - \rho \ddot{u}_i \qquad (3.22)$$

$$\epsilon_{ij} - \frac{1}{2}(u_{i,j} + u_{j,i}) \qquad (3.23)$$

$$\tau_{ij} - \lambda \epsilon_{kk} \delta_{ij} + 2\mu \epsilon_{ij} \qquad (3.24)$$
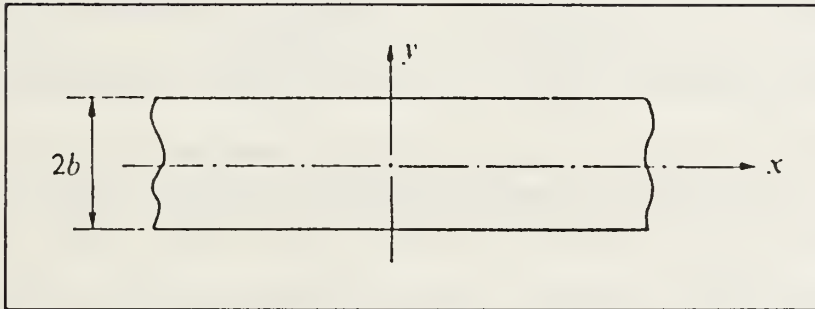
Figure 3.4. Coordinate system, thickness - 2b, (after Graff [Ref. 24]).

where τ_{ij} is the stress tensor at a point and u_i is the displacement vector of a material point. The mass density per unit volume of the material is ρ and f_i is the body force per unit mass of material. The strain tensor is given by ϵ_{ij}. The elastic constants are λ and μ, also known as the Lamé constants.

From this the governing equations in terms of the displacements were obtained by substituting the expressions for strain into the stress-strain relation and that result into the stress equations of motion, which gave

$$(\lambda + \mu)u_{j,ji} + \mu u_{i,jj} + \rho f_i - \rho \ddot{u}_i. \qquad (3.25)$$

23

Solving this equation gave the displacements, and for the flexural mode in a plate these were

$$u_x - i(\gamma A \sin \alpha y - \beta D \sin \beta y)e^{i(\gamma x - \omega t)} \tag{3.26}$$

$$u_y - (\alpha A \cos \alpha y - \gamma D \cos \beta y)e^{i(\gamma x - \omega t)} \tag{3.27}$$

where A and D are amplitudes of the waves and α and β are defined as

$$\alpha^2 - \frac{\omega^2}{c_1^2} - \gamma^2, \qquad \beta^2 - \frac{\omega^2}{c_2^2} - \gamma^2, \tag{3.28}$$

where c_1 and c_2 are the bulk longitudinal and shear velocities. Figure 3.5 shows the
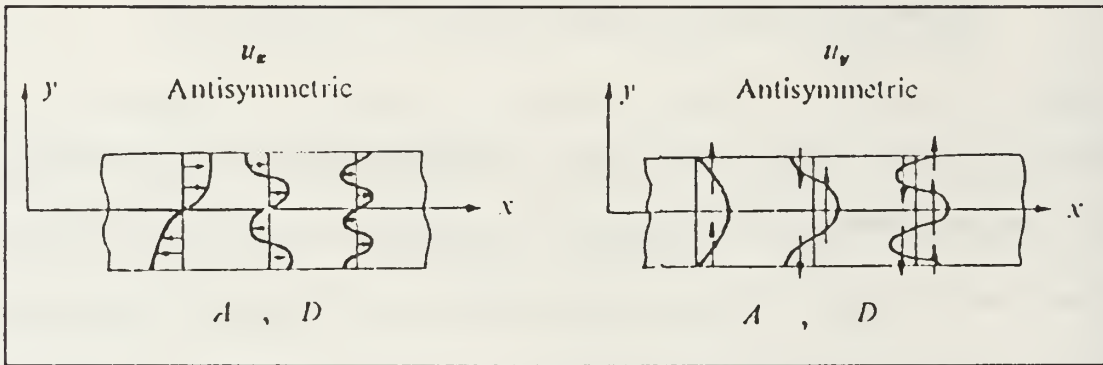

Figure 3.5. Flexural mode displacements (after Graff [Ref. 24]).

general form of these displacements. The boundary conditions for a plate with stress free surfaces are

$$\tau_{yy} - \tau_{xy} - \tau_{zy} - 0, \qquad y - \pm b, \tag{3.29}$$

24

where τ_{zy} is identically zero. Substituting the equations (3.26) and (3.27) into the expressions for τ_{yy} and τ_{xy} and setting these equations equal to zero gave the Rayleigh-Lamb frequency equation for flexural waves in a plate

$$\frac{\tan\beta b}{\tan\alpha b} = -\frac{(\gamma^2 - \beta^2)^2}{4\alpha\beta\gamma^2}.$$
(3.30)

Thus, given the frequency, ω, the wavenumbers, γ, are determined which satisfy equation (3.30) and from the relationship $c = \omega/\gamma$, the velocity of propagation of the wave can be calculated. Shown in Figure 3.6 is a plot of nondimensionalized phase velocity (c/c_2) versus nondimensionalized wavenumber $(2b\gamma/\pi)$. In the bottom half of the graph is plotted the lowest order flexural mode which corresponds to the velocities predicted by the classical plate theory. However, it can be seen that in the Rayleigh-Lamb theory the velocity no longer goes to infinity at high frequencies. In fact, the velocity approaches the Rayleigh, or surface wave velocity at high frequencies (short wave lengths), as would be expected. The curves in the upper half of the plot are higher modes predicted by equation (3.30), and illustrate that a single frequency (or wavenumber) can propagate at more than one velocity. For the experiments in this study however, $\bar{\gamma}$ is in the range of 0-1, and therefore these higher modes are not excited.

    R. Mindlin [Ref. 26] in 1951 developed an approximate theory for flexural wave propagation in plates which included corrections for both rotary inertia and shear effects. The mathematical formulation will not be presented here, since a similar theory will be presented in the next section for orthotropic plates. The shear
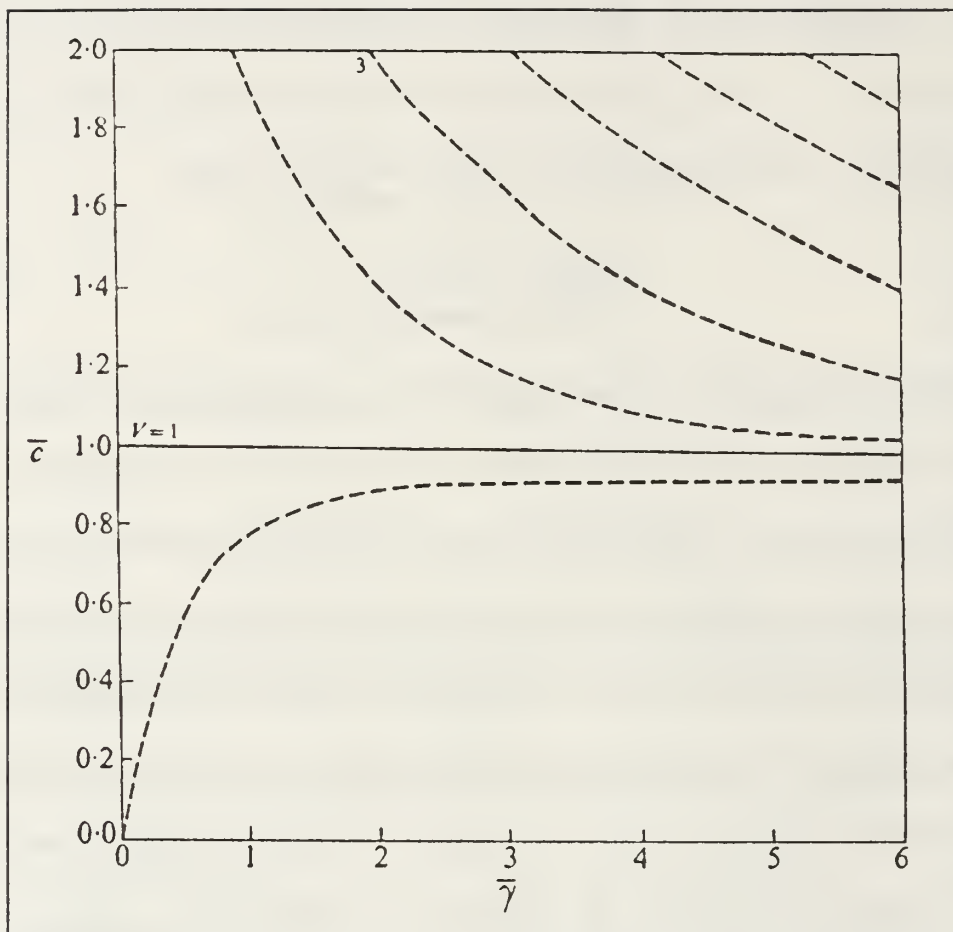
Figure 3.6. Rayleigh-Lamb dispersion theory for the flexural mode
(after Graff [Ref. 24]).

correction in Mindlin's theory was obtained by using a correction factor similar to

that in Timoshenko beam theory, in which the variations in shear stress across the

section are accounted for by inclusion of an adjustment coefficient. The results using

these corrections are nearly identical to that of the lowest order mode in the

Rayleigh-Lamb theory, but the resulting equation has a closed form solution, making

the numerical evaluation of the dispersion curve easier. The dispersion equation

from Mindlin's theory is

26

$$\left(\frac{c^2}{c_2^2}\right)^2 - \left(\kappa^2 + \frac{c_p^2}{c_2^2} + \frac{12\kappa^2}{h^2\gamma^2}\right)\left(\frac{c^2}{c_2^2}\right) + \kappa^2\frac{c_p^2}{c_2^2} = 0, \qquad (3.31)$$

where

$$c_p = \left(\frac{E}{\rho(1-v^2)}\right)^{\frac{1}{2}}, \qquad (3.32)$$

which is the plate velocity and h is the plate thickness. As in the Rayleigh-Lamb theory, values for the wavenumber are assumed and the equation is solved for the velocity, c. To find the shear adjustment coefficient, κ, the behavior of equation (3.31) as $\gamma \to \infty$ (high frequency) is examined. In this case two roots for c^2 are found, $c^2 = \kappa^2 c_2^2$, and $c^2 = c_p^2$. Since c should approach the surface, or Rayleigh velocity, c_R, as $\gamma \to \infty$, then $\kappa = c_R/c_2$.

Figure 3.7 shows a comparison several dispersion theories for the lowest flexural mode. The theories presented here were II, classical plate theory, I, exact solution of three dimensional equations and IV, classical plate theory + rotary inertia and shear corrections. Marked on the graph is the point at which classical plate theory begins to deviate from the exact theory. It should also be noted that I and IV are practically identical in the lowest mode.

B. WAVE THEORY FOR ORTHOTROPIC PLATES

The dispersion theory presented for the orthotropic plates [Ref. 27] is an extension of the work that Mindlin performed on isotropic plates, which included both rotary inertia and shear corrections. For a graphite/epoxy laminate, because of the
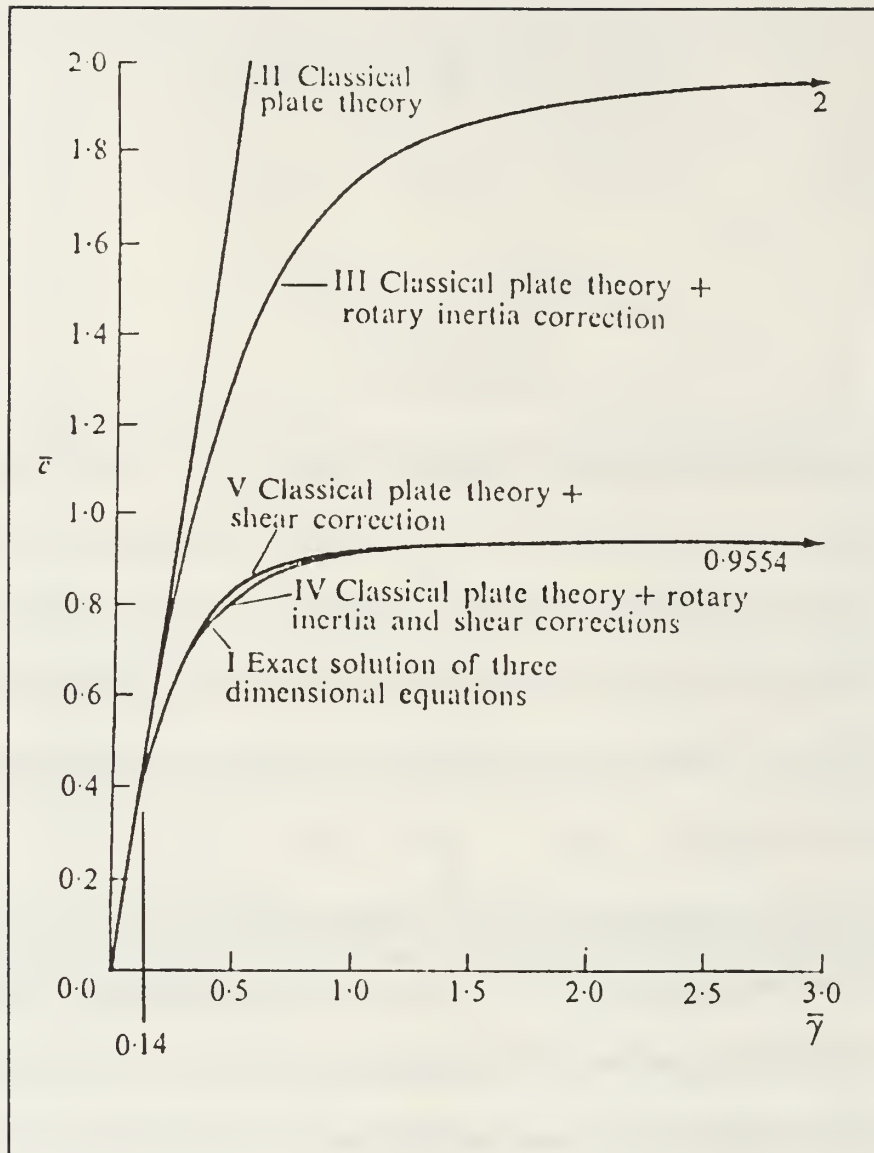
Figure 3.7. Dispersion theories (after Graff [Ref. 24]).

relatively low transverse shear modulus, the effects of transverse shear deformation

are large even at low frequencies, and thus classical plate theory is inaccurate even

in this region. Therefore, classical plate theory will not be discussed in this section.

Also, no exact solutions, such as the Rayleigh-Lamb theory for isotropic plates, will

be presented since only the lowest order flexural mode is of interest. If higher order

theory should be needed though, the work of Noiret and Roget [Ref. 28] and Datta

et. al. [Ref 29] both contain solutions for multilayered plates which predict the higher modes.

To begin the analysis, consider a laminated composite plate of thickness h, with the same coordinate system as shown in Figure 3.2. The following displacement fields are assumed.

$$u = u_0(x,y,t) + z\psi_x(x,y,t) \tag{3.33}$$

$$v = v_0(x,y,t) + z\psi_y(x,y,t) \tag{3.34}$$

$$w = w(x,y,t), \tag{3.35}$$

where u, v and w are the displacement components in the x, y and z directions, u_0 and v_0 are midplane displacement components, and ψ_x and ψ_y are the rotation components along the x and y axes, respectively. From the strain-displacement relations

$$\epsilon_x = \frac{\partial u_0}{\partial x} + z\frac{\partial \psi_x}{\partial x} \tag{3.36}$$

$$\epsilon_y = \frac{\partial v_0}{\partial y} + z\frac{\partial \psi_y}{\partial y} \tag{3.37}$$

$$\epsilon_z = 0 \tag{3.38}$$

$$\gamma_{xy} = \frac{\partial u_0}{\partial y} + \frac{\partial v_0}{\partial x} + z\left(\frac{\partial \psi_x}{\partial y} + \frac{\partial \psi_y}{\partial x}\right) \tag{3.39}$$

29

$$\gamma_{xz} = \psi_x + \frac{\partial w}{\partial x} \tag{3.40}$$

$$\gamma_{yz} = \psi_y + \frac{\partial w}{\partial y}. \tag{3.41}$$

The stress-strain relations for a given lamina are

$$
\begin{bmatrix} \sigma_x \\ \sigma_y \\ \tau_{yz} \\ \tau_{xz} \\ \tau_{xy} \end{bmatrix} =
\begin{bmatrix}
Q_{11} & Q_{12} & 0 & 0 & Q_{16} \\
Q_{12} & Q_{22} & 0 & 0 & Q_{26} \\
0 & 0 & Q_{44} & Q_{45} & 0 \\
0 & 0 & Q_{45} & Q_{55} & 0 \\
Q_{16} & Q_{26} & 0 & 0 & Q_{66}
\end{bmatrix}
\begin{bmatrix} \epsilon_x \\ \epsilon_y \\ \gamma_{yz} \\ \gamma_{xz} \\ \gamma_{xy} \end{bmatrix} \tag{3.42}
$$

where Q_{ij} for i, j = 1, 2 and 6 are plane-stress reduced stiffnesses, and Q_{ij} for i, j = 4 and 5 are transverse shear stiffnesses. The force and moment resultants per unit length acting on the laminate are obtained by integration of the stresses in each layer,

$$(N_x, N_y, N_{xy}) = \int_{-h/2}^{h/2} (\sigma_x, \sigma_y, \tau_{xy}) dz \tag{3.43}$$

$$(Q_x, Q_y) = \int_{-h/2}^{h/2} (\tau_{xz}, \tau_{yz}) dz \tag{3.44}$$

$$(M_x, M_y, M_{xy}) = \int_{-h/2}^{h/2} (\sigma_x, \sigma_y, \tau_{xy}) z \, dz. \tag{3.45}$$

30

We now substitute equations (3.36-41) and (3.43-45) into equation (3.42) to obtain

$$
\begin{bmatrix} N_x \\ N_y \\ Q_y \\ Q_x \\ N_{xy} \\ M_x \\ M_y \\ M_{xy} \end{bmatrix} = \begin{bmatrix} A_{11} & A_{12} & 0 & 0 & A_{16} & B_{11} & B_{12} & B_{16} \\ A_{12} & A_{22} & 0 & 0 & A_{26} & B_{12} & B_{22} & B_{26} \\ 0 & 0 & A_{44} & A_{45} & 0 & 0 & 0 & 0 \\ 0 & 0 & A_{45} & A_{55} & 0 & 0 & 0 & 0 \\ A_{16} & A_{26} & 0 & 0 & A_{66} & B_{16} & B_{26} & B_{66} \\ B_{11} & B_{12} & 0 & 0 & B_{16} & D_{11} & D_{12} & D_{16} \\ B_{12} & B_{22} & 0 & 0 & B_{26} & D_{12} & D_{22} & D_{26} \\ B_{16} & B_{26} & 0 & 0 & B_{66} & D_{16} & D_{26} & D_{66} \end{bmatrix} \begin{bmatrix} \partial u_0/\partial x \\ \partial v_0/\partial y \\ \partial w/\partial y + \psi_y \\ \partial w/\partial x + \psi_x \\ \partial u_0/\partial y + \partial v_0/\partial x \\ \partial \psi_x/\partial x \\ \partial \psi_y/\partial y \\ \partial \psi_x/\partial y + \partial \psi_y/\partial x \end{bmatrix} \qquad (3.46)
$$

where the extensional stiffnesses, A_{ij}, coupling stiffnesses, B_{ij}, and bending stiffnesses, D_{ij}, are given by

$$
(A_{ij}, B_{ij}, D_{ij}) = \int_{-h/2}^{h/2} (Q_{ij})_k (1, z, z^2) dz, \qquad i, j = 1, 2, 6 \qquad (3.47)
$$

and

$$
A_{ij} = \kappa_i \kappa_j \int_{-h/2}^{h/2} (Q_{ij})_k dz, \qquad i, j = 4, 5. \qquad (3.48)
$$

The shear correction factors $\kappa_i \kappa_j$ are included to account for the fact that the transverse shear strain distributions are not uniform across the thickness of the plates.

Summing forces and moments on a differential element and neglecting body forces, the equations of motion are obtained

31

$$\frac{\partial N_x}{\partial x}+\frac{\partial N_{xy}}{\partial y}-\rho^*\cdot\frac{\partial^2 u_0}{\partial t^2}+R\frac{\partial^2 \psi_x}{\partial t^2} \qquad (3.49)$$

$$\frac{\partial N_{xy}}{\partial x}+\frac{\partial N_y}{\partial y}-\rho^*\cdot\frac{\partial^2 v_0}{\partial t^2}+R\frac{\partial^2 \psi_y}{\partial t^2} \qquad (3.50)$$

$$\frac{\partial Q_x}{\partial x}+\frac{\partial Q_y}{\partial y}-\rho^*\cdot\frac{\partial^2 w}{\partial t^2} \qquad (3.51)$$

$$\frac{\partial M_x}{\partial x}+\frac{\partial M_{xy}}{\partial y}-Q_x-R\frac{\partial^2 u_0}{\partial t^2}+I\frac{\partial^2 \psi_x}{\partial t^2} \qquad (3.52)$$

$$\frac{\partial M_{xy}}{\partial x}+\frac{\partial M_y}{\partial y}-Q_y-R\frac{\partial^2 v_0}{\partial t^2}+I\frac{\partial^2 \psi_y}{\partial t^2} \qquad (3.53)$$

where ρ is the mass density and

$$(\rho^*,R,I)=\int_{-h/2}^{h/2}\rho(1,z,z^2)dz. \qquad (3.54)$$

Substituting equation (3.46) into equations (3.49-53) the equations of motion in terms of the displacements are obtained. For this work, only symmetric laminates will be considered, and for symmetric laminates the coupling stiffnesses, B_{ij}, and the coupling normal-rotary inertia coefficient, R, are identically zero. For the flexural mode, the governing equations of motion are

$$A_{55}(\frac{\partial \psi_x}{\partial x}+\frac{\partial^2 w}{\partial x^2})+A_{45}(\frac{\partial \psi_x}{\partial y}+\frac{\partial \psi_y}{\partial x}+2\frac{\partial^2 w}{\partial x\partial y})+A_{44}(\frac{\partial \psi_y}{\partial y}+\frac{\partial^2 w}{\partial y^2})-\rho^*\cdot\frac{\partial^2 w}{\partial t^2} \qquad (3.55)$$

$$D_{16}\frac{\partial^2\psi_x}{\partial x^2}+(D_{12}+D_{66})\frac{\partial^2\psi_x}{\partial x\partial y}+D_{26}\frac{\partial^2\psi_x}{\partial y^2}+D_{66}\frac{\partial^2\psi_y}{\partial x^2}+2D_{26}\frac{\partial^2\psi_y}{\partial x\partial y}$$
$$+D_{22}\frac{\partial^2\psi_y}{\partial y^2}-A_{45}(\psi_x+\frac{\partial w}{\partial x})-A_{44}(\psi_y+\frac{\partial w}{\partial y})-I\frac{\partial^2\psi_y}{\partial t^2} \tag{3.56}$$

$$D_{11}\frac{\partial^2\psi_x}{\partial x^2}+2D_{16}\frac{\partial^2\psi_x}{\partial x\partial y}+D_{16}\frac{\partial^2\psi_y}{\partial x^2}+(D_{12}+D_{66})\frac{\partial^2\psi_y}{\partial x\partial y}$$
$$+D_{26}\frac{\partial^2\psi_y}{\partial y^2}-A_{55}(\psi_x+\frac{\partial w}{\partial x})-A_{45}(\psi_y+\frac{\partial w}{\partial y})-I\frac{\partial^2\psi_x}{\partial t^2} \tag{3.57}$$

For wave propagation, we consider plane waves of the type

$$w=We^{i[k(l_1x+l_2y)-\omega t]} \tag{3.58}$$

$$\psi_x=\Psi_xe^{i[k(l_1x+l_2y)-\omega t]} \tag{3.59}$$

$$\psi_y=\Psi_ye^{i[k(l_1x+l_2y)-\omega t]} \tag{3.60}$$

where k is the wavenumber, l_1 and l_2 are the direction cosines of the wave vector in the x and y directions, ω is the circular frequency, and W, Ψ_x and Ψ_y are the amplitudes of the plane harmonic waves. Substituting equations (3.58-60) into equations (3.55-57), the determinant of the resulting set of equations gives the dispersion relation for flexural wave propagation. If we further exclude ourselves to symmetric quasi-isotropic laminates, then $A_{16}=A_{26}=A_{45}=0$ and $D_{16}=D_{26}$. This results in the following set of equations

$$
\begin{vmatrix}
D_{11}k^2l_1^2 + 2D_{16}k^2l_1l_2 & D_{16}k^2 + (D_{12}+D_{66})k^2l_1l_2 & iA_{55}kl_1 \\
+D_{66}k^2l_2^2 + A_{55} - I\omega^2 & & \\
& & \\
D_{16}k^2 + (D_{12}+D_{66})k^2l_1l_2 & D_{66}k^2l_1^2 + 2D_{16}l_1l_2 & iA_{44}kl_2 \\
& +D_{22}k^2l_2^2 + A_{44} - I\omega^2 & \\
& & \\
-iA_{55}kl_1 & -iA_{44}kl_2 & A_{55}k^2l_1^2 + A_{44}k^2l_2^2 - \rho^*\omega^2
\end{vmatrix} = 0 \qquad (3.61)
$$

Again, a value of k is chosen, and equation (3.61) is then solved for ω, however, only one root approaches zero circular frequency as the wavenumber approaches zero, and this is the root corresponding to the lowest flexural branch of the frequency spectrum for plate waves.

C. PHASE AND GROUP VELOCITY

In the previous sections it was stated that the velocity of propagation was defined as

$$
c = \frac{\omega}{k} \qquad (3.62)
$$

for continuous harmonic plane waves of the form in equation (3.19). An acoustic emission pulse however, consists of many frequencies, and in a dispersive medium, such as a plate, they propagate at differing velocities. Therefore, how pulses propagate must also be understood if improvements are to be made in source location using AE.

An illustration [Ref. 30] of the behavior of the propagation of pulses in dispersive media can be shown by considering two propagating harmonic waves of equal

amplitude but slightly different frequency ω_1 and ω_2, given by

$$y = A\cos(k_1 x - \omega_1 t) + A\cos(k_2 x - \omega_2 t), \tag{3.63}$$

where $\omega_1 = k_1 c_1$ and $\omega_2 = k_2 c_2$. This can be rewritten as

$$y = 2A\cos[\frac{1}{2}(k_2 - k_1)x - \frac{1}{2}(\omega_2 - \omega_1)t] \times \cos[\frac{1}{2}(k_1 + k_2)x - \frac{1}{2}(\omega_1 + \omega_2)t]. \tag{3.64}$$

Since the frequencies are only slightly different, the wavenumbers will also differ only slightly, and these can be written as

$$\omega_2 - \omega_1 = \Delta\omega, \qquad k_2 - k_1 = \Delta k. \tag{3.65}$$

The average frequency and wavenumber are defined as

$$\omega = \frac{1}{2}(\omega_1 + \omega_2), \qquad k = \frac{1}{2}(k_1 + k_2), \tag{3.66}$$

and the resulting average velocity by $c = \omega/k$. Thus (3.63) can be rewritten as

$$y = 2A\cos(\frac{1}{2}\Delta kx - \frac{1}{2}\Delta\omega t)\cos(kx - \omega t). \tag{3.67}$$

The cosine term containing the difference terms Δk and $\Delta\omega$ is a low frequency term since $\Delta\omega$ is a small number. It will have a propagation velocity c_g where

$$c_g = \frac{\Delta\omega}{\Delta k}. \tag{3.68}$$

The cosine term containing the average wavenumber and frequency k and ω will be a high frequency term, propagating at the average velocity c. The effect of the low frequency term will be to act as a modulation on the high frequency carrier. The

appearance of the motion is shown if Figure 3.8. It is the overall wave group that propagates at the velocity c_g in the figure. The velocity of the high frequency carrier may be greater than, equal to, or less than the velocity c_g.
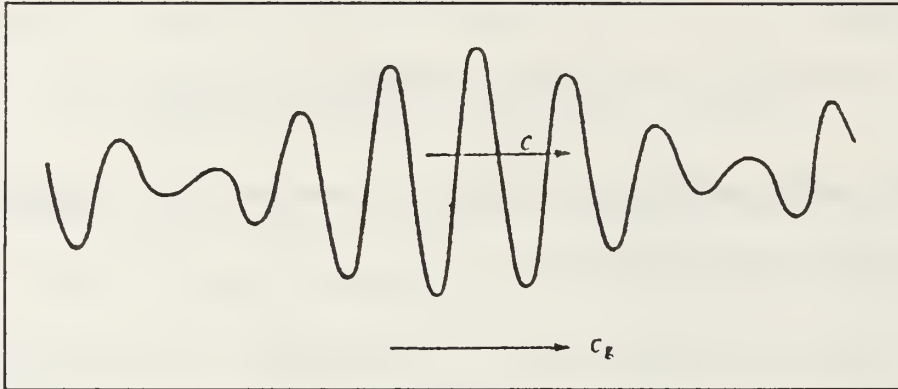

Figure 3.8. Simple wave group (after Graff [Ref. 24]).

If we wish to generalize to a pulse consisting of many frequencies, we consider a superposition of a number of waves

$$y = \sum_{i=1}^{n} A_i \cos(k_i x - \omega_i t + \phi_i), \qquad (3.69)$$

where k_i and ω_i differ only slightly. The phase angle of a given frequency is ϕ_i.

Assume that at some time $t = t_0$ and location $x = x_0$, the phases of the various wave trains are approximately the same so that a wave group has been formed. At a time $t = t_0 + dt$ and location $x = x_0 + dx$, the change in phase dP_i of any individual components is

$$dP_i = [k_i(x_0 + dx) - \omega_i(t_0 + dt) + \phi_i] - [k_i x_0 - \omega_i t_0 + \phi_i] \qquad (3.70)$$
$$= k_i dx - \omega_i dt.$$

36

In order for the wave group to be maintained, the change in phase for all of the terms must be approximately the same. This restriction is enforced by requiring that $dP_j - dP_i = 0$, which gives

$$(k_j - k_i)dx - (\omega_j - \omega_i)dt = 0. \tag{3.71}$$

Since k_i, k_j and ω_i, ω_j differ only slightly, we let $dk = k_j - k_i$ and $d\omega = \omega_j - \omega_i$. Therefore equation (3.71) becomes

$$dk\, dx - d\omega\, dt = 0. \tag{3.72}$$

The velocity of the group is then given by

$$c_g = \frac{dx}{dt} = \frac{d\omega}{dk} \tag{3.73}$$

This expression is taken as the definition of group velocity.

37

IV. SOURCE LOCATION THEORY FOR THIN PLATES

A. SOURCE LOCATION

Once the wave propagation in the media has been established, there are two other issues that must be given consideration for source location. The first if these deals with the determination of the arrival times of the wave at the transducers, and the second is, given the arrival times, how is the source located? We will begin by analyzing the second of these two problems.

A simple example of source location is given by the testing of narrow tensile coupons, where one of the specimen dimensions is on the order of the diameter of the transducers used to detect the wave, as shown in Figure 4.1. If this is the case, then the defect growth, or AE source, can be assumed to be constrained to lie between the two transducers. This assumption results in the simple location algorithm of $x = c(t_2 - t_1)/2$, where c is the velocity of propagation of the wave and t_1 and t_2 are the arrival times of the wave at sensors S_1 and S_2 respectively. However, in this work we would like to extend source location from one-dimensional, or linear location, to planar, or two-dimensional location. The next two sections will discuss this extension for isotropic and orthotropic plates.

1. Planar Source Location in Isotropic Plates

For isotropic materials, the location of the emission source calculated form the time difference from a pair of transducers can be shown to lie on a hyperbola with the two sensors as foci. For planar location, to uniquely locate the source at least
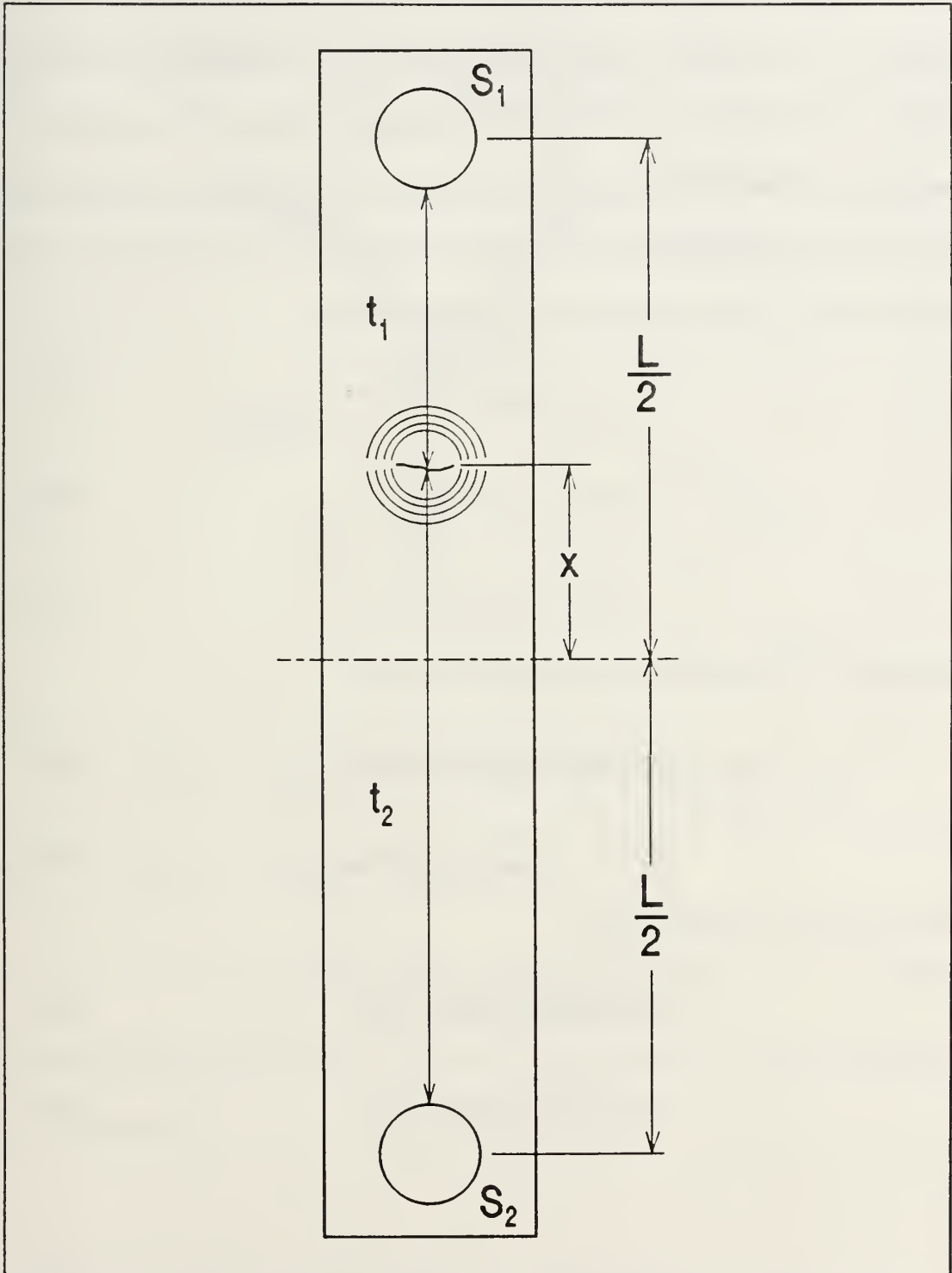
Figure 4.1. Linear location.

39

three transducers must be used. Tobias [Ref. 31], considered an arbitrary three-transducer array with transducers located at point $S_0(0,0)$, $S_1(x_1,y_1)$, $S_2(x_2,y_2)$ as shown in Figure 4.2. The acoustic emission source at $P(x,y)$ is located at the point of intersection of the circles about S_0, S_1 and S_2 as centers with radii r, $r+\delta_1$ and $r+\delta_2$. δ_1 and δ_2 are defined by $\delta_1=ct_1$ and $\delta_2=ct_2$ where c is the velocity of propagation and t_1 and t_2 are the difference in arrival times measured for transducers S_1-S_0 and S_2-S_0 respectively. The equations of the three circles are

$$x^2+y^2-r^2 \tag{4.1}$$

$$(x-x_1)^2+(y-y_1)^2-(r+\delta_1)^2 \tag{4.2}$$

$$(x-x_2)^2+(y-y_2)^2-(r+\delta_2)^2. \tag{4.3}$$

Subtracting the first equation from the other two gives

$$2xx_1+2yy_1-(x_1^2+y_1^2-\delta_1^2)-2r\delta_1 \tag{4.4}$$

$$2xx_2+2yy_2-(x_2^2+y_2^2-\delta_2^2)-2r\delta_2. \tag{4.5}$$

Changing to polar coordinates gives

$$2r(x_1\cos\theta+y_1\sin\theta+\delta_1)-A_1 \tag{4.6}$$

$$2r(x_2\cos\theta+y_2\sin\theta+\delta_2)-A_2 \tag{4.7}$$

where

$$A_1-x_1^2+y_1^2-\delta_1^2, \qquad A_2-x_2^2+y_2^2-\delta_2^2. \tag{4.8}$$

40

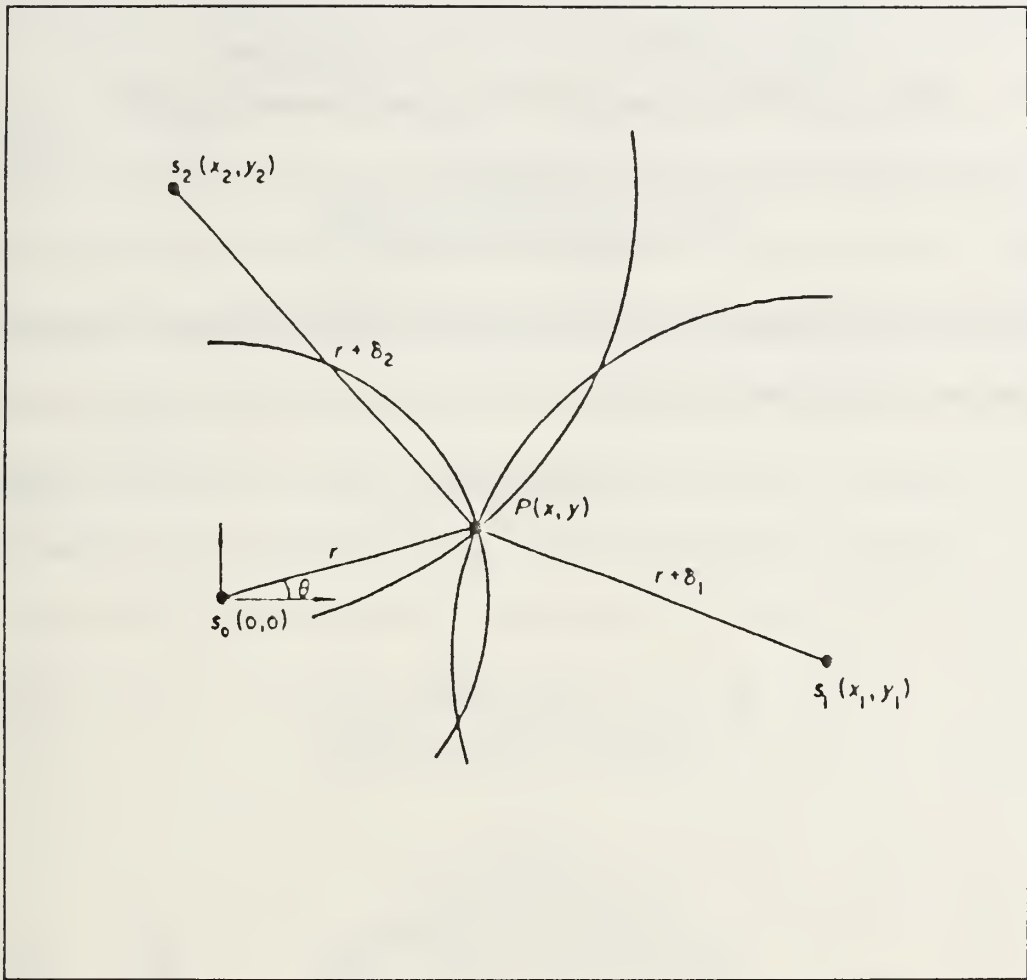**Figure 4.2.** Source and transducer locations (after Tobias [Ref. 31]).

Solving for r results in the following equations

$$r = \frac{A_1}{2(x_1\cos\theta + y_1\sin\theta + \delta_1)} - \frac{A_2}{2(x_2\cos\theta + y_2\sin\theta + \delta_2)} \tag{4.9}$$

from which it follows that $(A_1x_2 - A_2x_1)\cos\theta + (A_1y_2 - A_2y_1)\sin\theta = A_2\delta_1 - A_1\delta_2$. Normalizing

this equation yields

41

$$\frac{(A_1x_2-A_2x_1)\cos\theta}{[(A_1x_2-A_2x_1)^2+(A_1y_2-A_2y_1)^2]^{1/2}}+\frac{(A_1y_2-A_2y_1)\sin\theta}{[(A_1x_2-A_2x_1)^2+(A_1y_2-A_2y_1)^2]^{1/2}}$$

$$-\frac{A_2\delta_1-A_1\delta_2}{[(A_1x_2-A_2x_1)^2+(A_1y_2-A_2y_1)^2]^{1/2}}. \tag{4.10}$$

Since, in this form, the coefficients of the $\cos\theta$ and $\sin\theta$ terms are less than unity, the equation can be rewritten in the form

$$\cos(\theta-\phi)=K \tag{4.11}$$

where

$$K=\frac{(A_2\delta_1-A_1\delta_2)}{[(A_1x_2-A_2x_1)^2+(A_1y_2-A_2y_1)^2]^{1/2}} \tag{4.12}$$

and

$$\tan\phi=\frac{(A_1y_2-A_2y_1)}{(A_1x_2-A_2x_1)}. \tag{4.13}$$

Since both the numerator and denominator in the term for $\tan\phi$ can be determined exactly from the known positions of the transducers and the measured arrival time differences t_1 and t_2 and the propagation velocity c, the angle ϕ can also be determined. This result is substituted into equation (4.11) to determine θ, which in turn is used to determine r, from equation (4.9).

2. Planar Location in Anisotropic Plates

In the previous section an exact analytical solution for the location of sources based on the difference in arrival times of the wave at the transducers was discussed.

42

The solution in this case was made possible due to the fact that in isotropic materials, the velocity curve is circular. This allowed equations (4.1-3) to be written and solved in terms of the source location. In anisotropic media however, the velocity is dependent on the direction of propagation in the material, $c(\theta)$. Figure 4.3 shows the velocity curves for a $[0_2/90_2]_s$ graphite/epoxy plate based on calculations for the flexural mode at several frequencies. Since these curves are calculated using equation (3.61) evaluating an exact analytical expression for the source location is no longer just a matter of solving geometric equations.
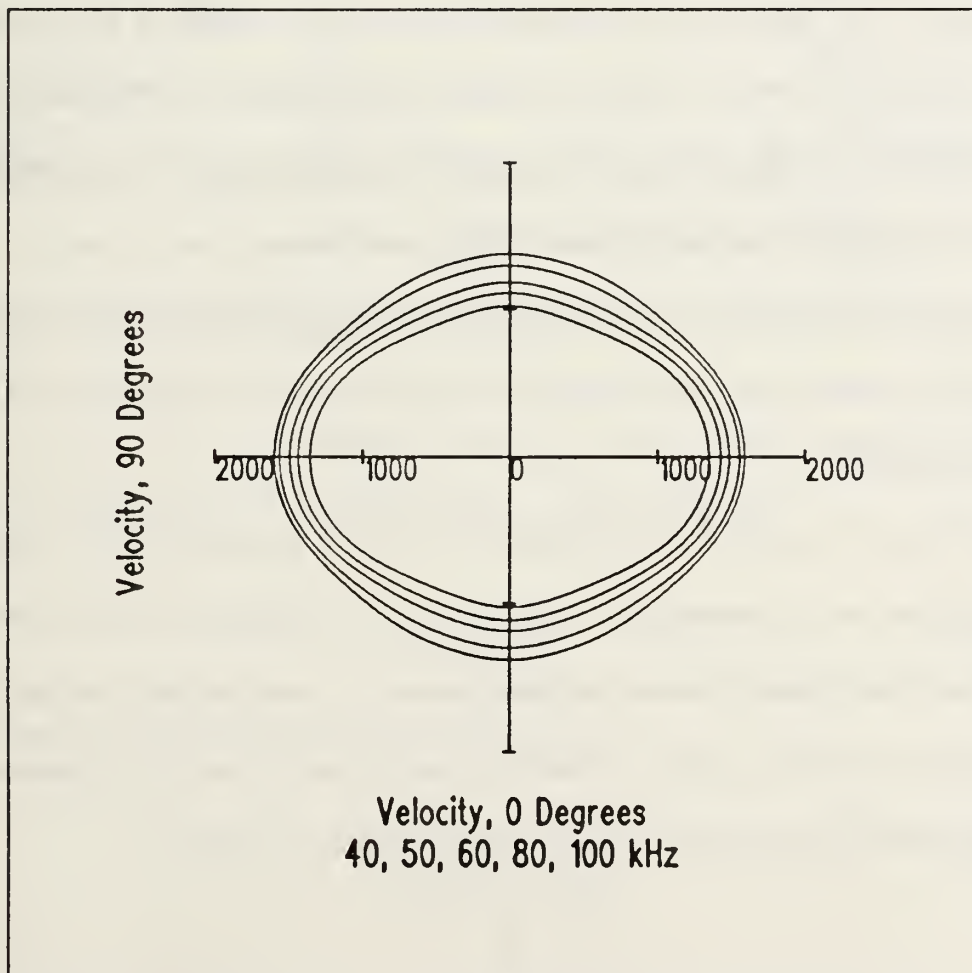

Figure 4.3. Velocity curves for $[0_2/90_2]_s$ graphite/epoxy plate, m/s.

Castagnede, Sachse and Kim [Ref. 32] used an overdetermined system to locate sources in anisotropic media. By using more than three transducers an overdetermined system of equations could be written in terms of the source coordinates. To solve the overdetermined system a Euclidian functional was defined and then minimized using a modified Newton-Raphson algorithm. However, the wavespeeds used for this analysis were based on the quasi-longitudinal mode which has a deterministic solution, unlike the flexural plate mode, thus allowing the above analysis to be performed. A similar approach was used by Buttle and Scruby [Ref. 33], however they experimentally measured the velocity curves in the composite plates used in their work. They then used a cubic spline or polynomial fit to mathematically describe these curves, and then used these fits in the minimization of the set of equations containing the location coordinates.

A new anisotropic source location algorithm developed in this work, based on an iterative scheme using the velocity curves calculated from equation (3.61), will now be discussed.

In Figure 4.4 is shown the transducers, S_0, S_1 and S_2 and the source location, $P(x,y)$, relative to the transducers. For now, only transducers S_0 and S_1 will be considered. The distance between the two sensors is l_{01}, and the distances and times of propagation from the source to sensors S_0 and S_1 are l_0, l_1 and t_0, t_1, respectively. The difference of the arrival times of a wave at sensors S_0 and S_1 is

$$t_0 - t_1 = \frac{l_0}{c_0} - \frac{l_1}{c_1},$$

(4.14)

44
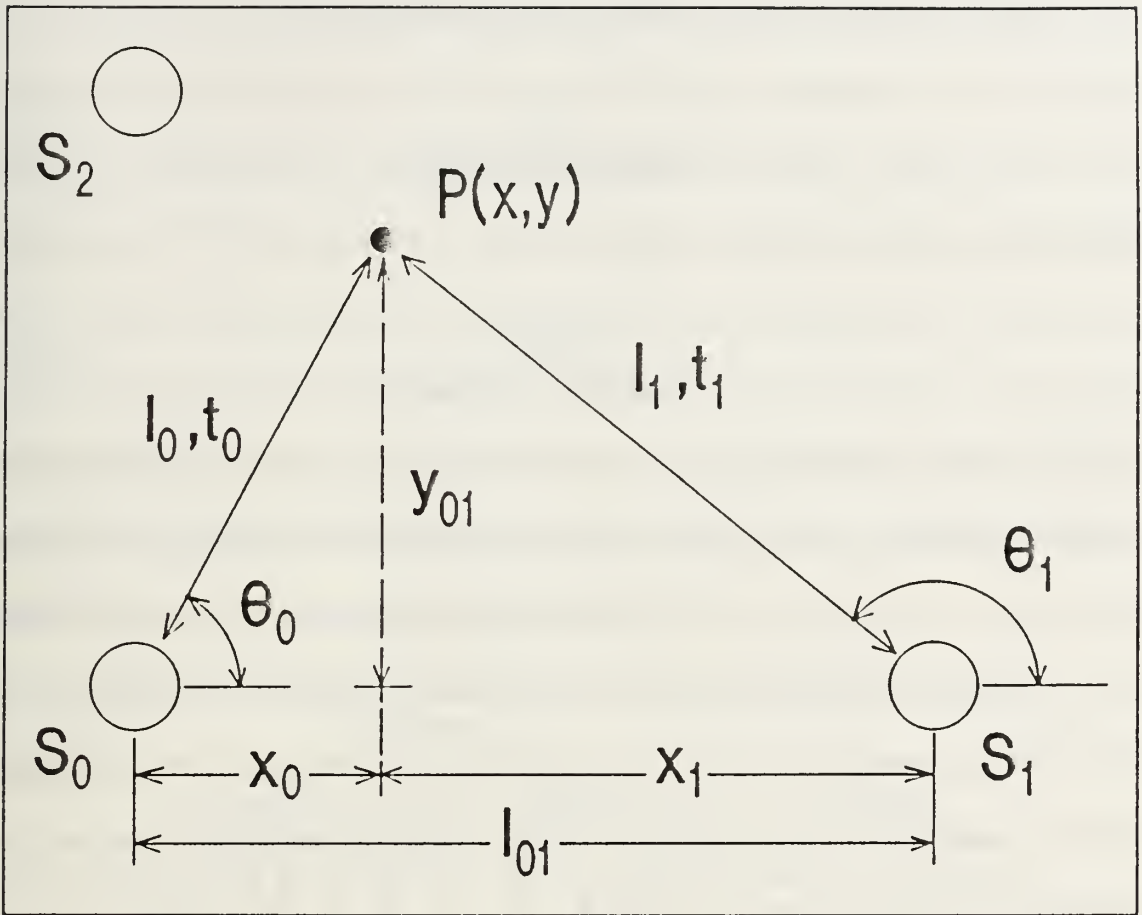
Figure 4.4. Source and transducer locations.

where c_0 and c_1 are the propagation velocities in the θ_0 and θ_1 directions. From geometric considerations, $y_{01} = l_0\sin\theta_0 = l_1\sin\theta_1$, so we can write

$$l_1 = l_0\left(\frac{\sin\theta_0}{\sin\theta_1}\right). \tag{4.15}$$

Furthermore, $l_0\cos\theta_0 - l_1\cos\theta_1 = l_{01}$, and solving for l_1

$$l_1 = l_0\left(\frac{\cos\theta_0}{\cos\theta_1}\right) - \frac{l_{01}}{\cos\theta_1}. \tag{4.16}$$

45

We now set equation (4.15) equal to (4.16) and solve for l_0.

$$l_0 = \frac{l_{01}}{\cos\theta_0 - \sin\theta_0 \cot\!an\theta_1}. \tag{4.17}$$

Substituting equation (4.17) into (4.15) gives

$$l_1 = \frac{l_{01}\sin\theta_0}{\cos\theta_0\sin\theta_1 - \cos\theta_1\sin\theta_0}. \tag{4.18}$$

Equations (4.17) and (4.18) can then be substituted into equation (4.14) to calculate the time difference. Values of θ_0 and θ_1 are then iterated through and calculated values of $t_0 - t_1$ are found which equal the measured value of $t_0 - t_1$. As before, using only two sensors will give ambiguous location results, so the procedure must also be repeated for the sensor pair S_0-S_2. Each of these two sets of transducers will produce a loci of possible location points, and it will be the intersection of these loci that determines where the source is located.

B. ARRIVAL TIME DETERMINATION

In conventional AE instrumentation, the signals from the transducers are enveloped and when this envelope crosses a preset voltage threshold, as shown in Figure 4.5, the timing clocks are triggered, which then allows the determination of the arrival time differences between the transducers. As was seen in Figure 1.3, in dispersive media this is no longer an acceptable method due to the change in shape of the wave as it propagates. Also, even in nondispersive media, if attenuation is present triggering of the location clocks can still occur on different points of the waveforms, leading to incorrect location results. Therefore we would like to be able

46

to measure arrival times independent of triggering voltage threshold or signal gain settings. Toward this end, two methods of arrival time determination were developed based on crosscorrelation techniques. The crosscorrelation methods have the advantage over first threshold crossing techniques of gain and voltage threshold independence. Also, the use of a point transducer to eliminate phase cancellation is no longer needed because if the crosscorrelation is done at frequencies where the wavelength is greater than the diameter of the transducer, phase cancellation of the wave due to the finite area of the transducer is no longer a consideration. The two crosscorrelation methods will now be discussed.
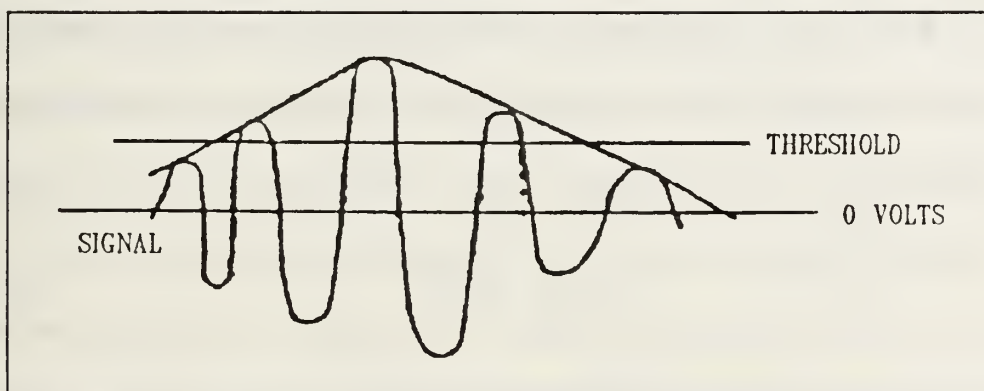
Figure 4.5. Schematic of threshold crossing.

1. Gaussian Crosscorrelation

The Gaussian crosscorrelation method can be thought of as a narrowband filter in time space. The idea behind this was that if a single frequency in the output waveform from each transducer could be isolated, than the time differences due to the propagation of that frequency component could be used for the location analysis. The velocity of this frequency component could be either calculated from theory or experimentally determined. To locate a single frequency in the transducer output,

47

the output was crosscorrelated with an input pulse consisting of a cosine wave modulated by a Gaussian pulse. The Gaussian pulse was chosen since it allowed a gradual tapering of the cosine, thereby narrowing the frequency content of the input signal.

To determine if the crosscorrelation technique could accurately determine time differences, the response of a thin plate to an impulse loading was calculated. From Medick [Ref. 34] the displacement is,

$$w(r,t) - 2\left(\frac{\pi}{2} - Si\left[\frac{r^2}{4bt}\right]\right)$$

(4.19)

where $b^2 = Eh^2/12\rho(1-\nu^2)$, r is the distance from source to transducer, and t is the time. If the argument of the sine integral is large, then $Si(z)$ can be approximated by [Ref. 35],

$$Si(z) - \frac{\pi}{2} - \frac{\cos(z)}{z}.$$

(4.20)

Substituting equation (4.20) into (4.19) gives

$$w(r,t) - 2\frac{\cos(r^2/4bt)}{r^2/4bt}$$

(4.21)

for the displacement of the flexural mode. Figure 4.6 (a) shows the calculated response of the flexural mode using equation (4.21) for sources at 305 and 610 mm from the receiver. For the calculation the plate thickness used was 1.42 mm and the material properties were, E = 70 GPa, ρ = 2750 kg/m^3 and ν = 0.33. The modulated cosine

$$x(t) - e^{-(t-t_1)^2/\sigma^2} \cos(\omega_1 t) \qquad (4.22)$$

used for the crosscorrelation is shown in Figure 4.6 (b). For this particular simulation, ω_1 = 6.283×10^5 rad/s (f_1 = 100 kHz), t_1 = 100 μs and σ = 40 μs. The two functions were then digitally crosscorrelated using

$$R_{xy}(r\Delta t) - \frac{1}{N-r} \sum_{n-1}^{N-r} x_n y_{n+r} \qquad (4.23)$$

where x is defined in equation (4.22) and y in equation (4.21), N is the number of digital samples and r is the lag number, r = 0, 1, 2,..., m, where m is the maximum lag number and m < N [Ref. 36]. For the crosscorrelation, the total number of points was 2500, and the time step, Δt, was 0.2 μs. These values were chosen to correspond with the experimental data, presented later in Section VI. The crosscorrelations are shown in Figure 4.6 (c). The cursors mark the peaks in the crosscorrelations and the measured time difference between the cursors was 131.0 μs. Using equation (4.21), the time at which the 100 kHz component occurs in each of the waveforms in Figure 4.6 (a) can be determined, and from this the actual time difference can be calculated. This was found to be 130.6 μs, the crosscorrelation being in error by 0.3%. From this simulation it would seem that the resolution of this technique is well within any experimental errors which may be encountered.
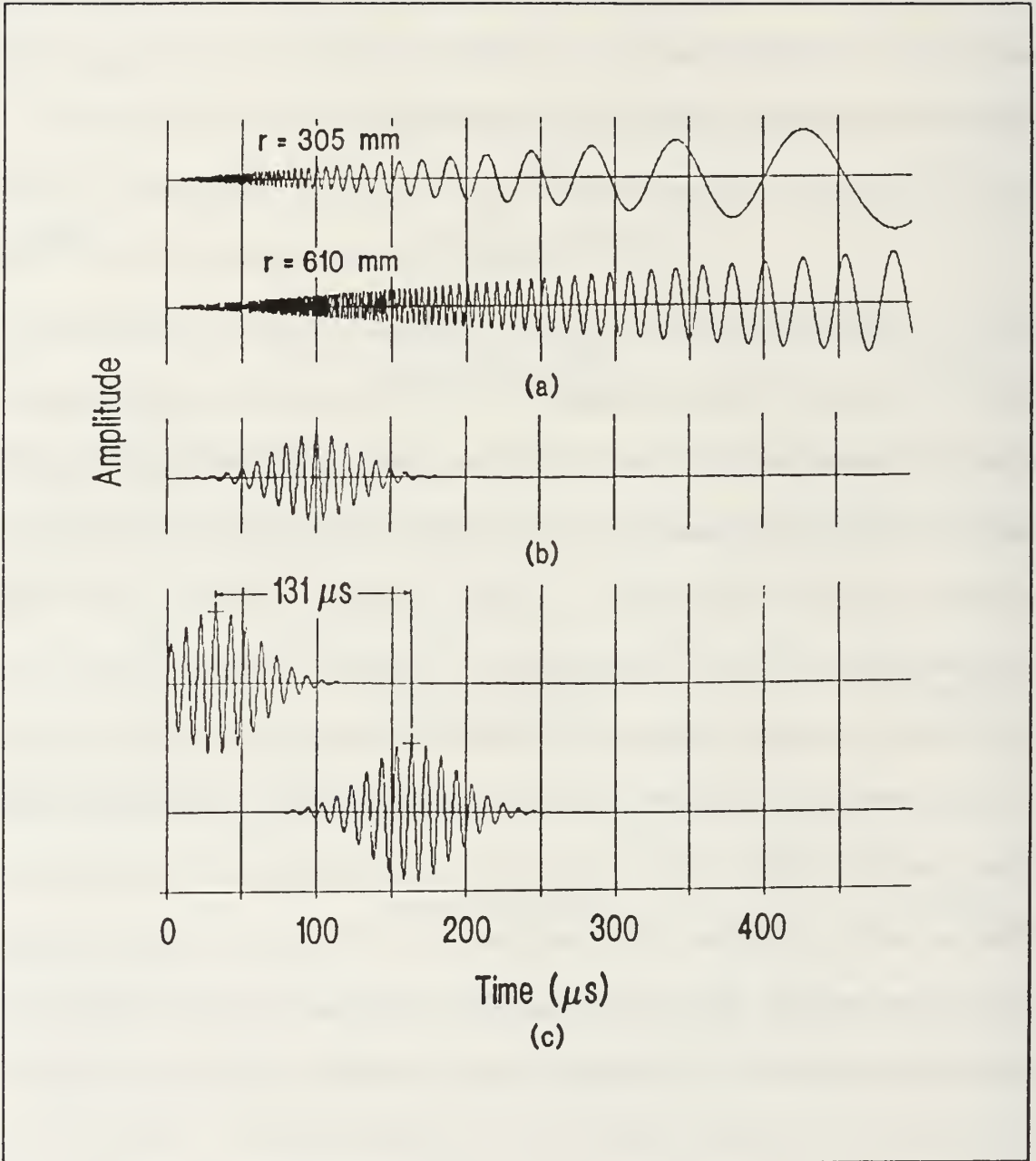
Figure 4.6. Crosscorrelation analysis.

50

2. Crosscorrelation Using Narrowband Filtering

The second method used for arrival time determination is again a crosscorrelation method, based on theory developed by White [Ref. 14]. The experimental work has been discussed in Section II.

We begin the analysis by using the result for the phase velocity obtained from classical plate theory, equation (3.21),

$$c_p - \sqrt[4]{\frac{D}{\rho h}} \, \omega^{1/2}. \tag{4.24}$$

From this the phase shift of a sinusoidal wave propagating through a path l is,

$$\phi(\omega) - \frac{l\omega}{c_p(\omega)} \tag{4.25}$$

where ω is the circular frequency. The cross spectrum of the input and output of this path is

$$G_{xy}(\omega) - G_x(\omega)G_y(\omega)A(\omega)e^{-i\phi(\omega)} \tag{4.26}$$

where $G_x(\omega)$ and $G_y(\omega)$ are Fourier transformed transducer signals, and $A(\omega)$ is the attenuation factor for the path. The crosscorrelation is given by

$$R_{xy}(t) - \int_0^\infty G_x(\omega)G_y(\omega)A(\omega)\cos[\omega t - \phi(\omega)]d\omega. \tag{4.27}$$

Equation (4.27) gives the exact crosscorrelation function for the process, but generally this cannot be evaluated, except for special cases of $G_x(\omega)$ and $G_y(\omega)$.

Consider a random excitation of suitable spectrum shape such that $G_x(\omega)$ and

51

$G_y(\omega)$ are ideally band limited, i.e.,

$$G_x, G_y - B, \qquad \omega_0(1-\Delta/2)<\omega<\omega_0(1+\Delta/2) \qquad (4.28)$$
$$-0, \qquad \text{otherwise,}$$

where B is the amplitude of the frequency spectrum, and will assumed to be 1, and ω_0 is the center frequency of the bandwidth. Substituting equation (4.28) into (4.27) gives

$$R_{xy}(t) - \int_{\omega_0(1-\Delta/2)}^{\omega_0(1+\Delta/2)} \cos(\omega t - a\omega^{1/2})d\omega \qquad (4.29)$$

where $a = l/(D/\rho h)^{1/4}$. This can be evaluated exactly, but the result is cumbersome and leads to no intuitive results. If the bandwidth is restricted to an octave or less $(\Delta < 1)$, then ω can be written as

$$\omega - \omega_0(1+\epsilon). \qquad (4.30)$$

Using this relation in equation (4.29) gives

$$R_{xy}(t) - \omega_0 \int_{-\Delta/2}^{\Delta/2} \cos[\omega_0 t(1+\epsilon) - a\omega_0^{1/2}(1+\epsilon)^{1/2}]d\epsilon. \qquad (4.31)$$

By expanding $(1+\epsilon)^{1/2}$ in a Taylor series

$$(1+\epsilon)^{1/2} - 1 + \frac{\epsilon}{2} - \frac{\epsilon^2}{8} + \dots \qquad (4.32)$$

and taking only the first two terms, equation (4.31) can be rewritten as

52

$$R_{xy}(t) = \omega_0 \int_{-\Delta/2}^{\Delta/2} \cos\left[\omega_0 t - a\omega_0^{1/2} + \left(\omega_0 t - \frac{a\omega_0^{1/2}}{2}\right)\epsilon\right] d\epsilon. \qquad (4.33)$$

Expanding the cosine of the sum of two arguments and integrating results in

$$R_{xy}(t) = \cos\left[\omega_0\left(t - \frac{a}{\omega_0^{1/2}}\right)\right] \times \frac{\sin\left[\frac{\Delta\omega_0}{2}\left(t - \frac{a}{2\omega_0^{1/2}}\right)\right]}{\frac{1}{2}\left(t - \frac{a}{2\omega_0^{1/2}}\right)}. \qquad (4.34)$$

To understand the results of equation (4.34), we must now return to equations (3.20-21). If we solve equations (3.20) and (3.21) for ω in terms of γ we get

$$\omega = \sqrt{\frac{D}{\rho h}}\gamma^2. \qquad (4.35)$$

Using equation (3.12) we can obtain the group velocity from equation (4.35)

$$c_g = 2\sqrt{\frac{D}{\rho h}}\gamma. \qquad (4.36)$$

Rewriting equation (4.36) in terms of ω gives

$$c_g = 2\sqrt[4]{\frac{D}{\rho h}}\omega^{1/2}. \qquad (4.37)$$

Thus, the group velocity is twice the phase velocity, and equation (4.34) can be rewritten as

53

$$R_{xy}(t) - B\cos\left[\omega_0\left(t - \frac{l}{c_p}\right)\right] \times \frac{\sin\left[\frac{\Delta\omega_0}{2}\left(t - \frac{l}{c_g}\right)\right]}{\frac{1}{2}\left(t - \frac{l}{c_g}\right)}. \tag{4.38}$$
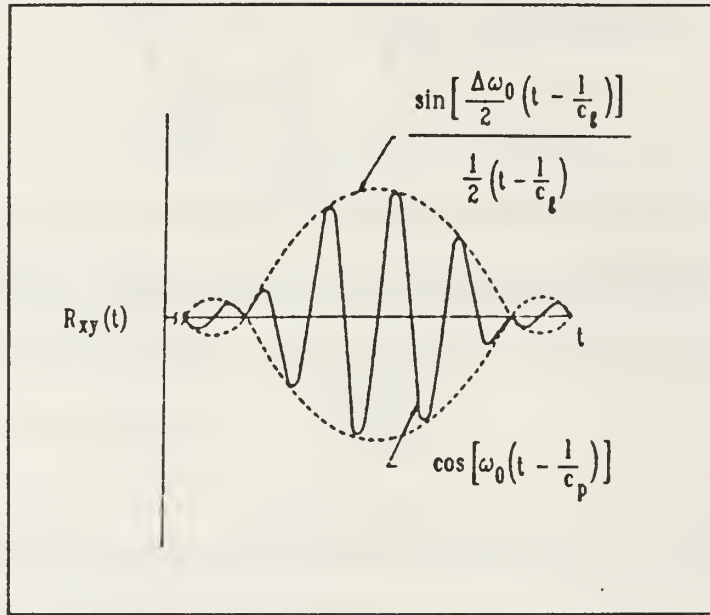
This function is shown in Figure 4.7.

Figure 4.7. Crosscorrelation of dispersive waves (after White [Ref. 14]).

There are several features to be noted about this function. The first is that the modulated cosine travels at the phase velocity of the center frequency, ω_0. The second is that the envelope, or the $\sin x/x$ term, travels at the group velocity of the center frequency, ω_0. Thus, the cosine term has a phase lag which is dependent on the phase velocity, but the maximum amplitude of the modulating function $\sin x/x$ occurs at a time delay appropriate to the group velocity.

To apply this theory to AE source location however, the signal from the transducers must first be modified. AE from defect growth can typically be modeled

54

as a delta function [Ref. 37], which by definition is broadbanded. If the signals from the transducers due to the defect growth are narrowband filtered first, then the narrowband pulse needed for the analysis can be obtained. Shown in Figure 4.8 are the flexural waves predicted by equation (4.21), using a time step of 0.5 μs, at distances of 305 and 610 mm. The time step was imposed due to memory limitations of the computer. To simulate the analysis, these waveforms were then narrowband filtered, with a center frequency ω_0 of 100 kHz and a bandwidth of 1/2 octave (80-120 kHz). Figure 4.9 shows the filtered signals. The two signals were crosscorrelated and the crosscorrelation then enveloped, using a Hilbert transform (Appendix A) as shown in Figure 4.10. The peak of the crosscorrelation was located at 132.5 μs, slightly off from the calculated value of 130.6 μs. Figure 4.11 shows the crosscorrelation as predicted by White's theory, and the peak was found to be at 131.0 μs.

It should be noted that the amplitudes predicted by equation (4.21) increase linearly with time, t. Thus, in the above example, the filtered pulse is no longer square, as in equation (4.28). To see if the shape of the crosscorrelation changes due to the linear increase in amplitude, $A(\omega)$ in equation (4.27) was set equal to $1/\omega$ to account for this, and the resulting integral was obtained

$$R_{xy}(t) = \int_{\omega_0(1-\Delta/2)}^{\omega_0(1+\Delta/2)} \frac{1}{\omega}\cos(\omega t - a\omega^{1/2})d\omega. \qquad (4.39)$$
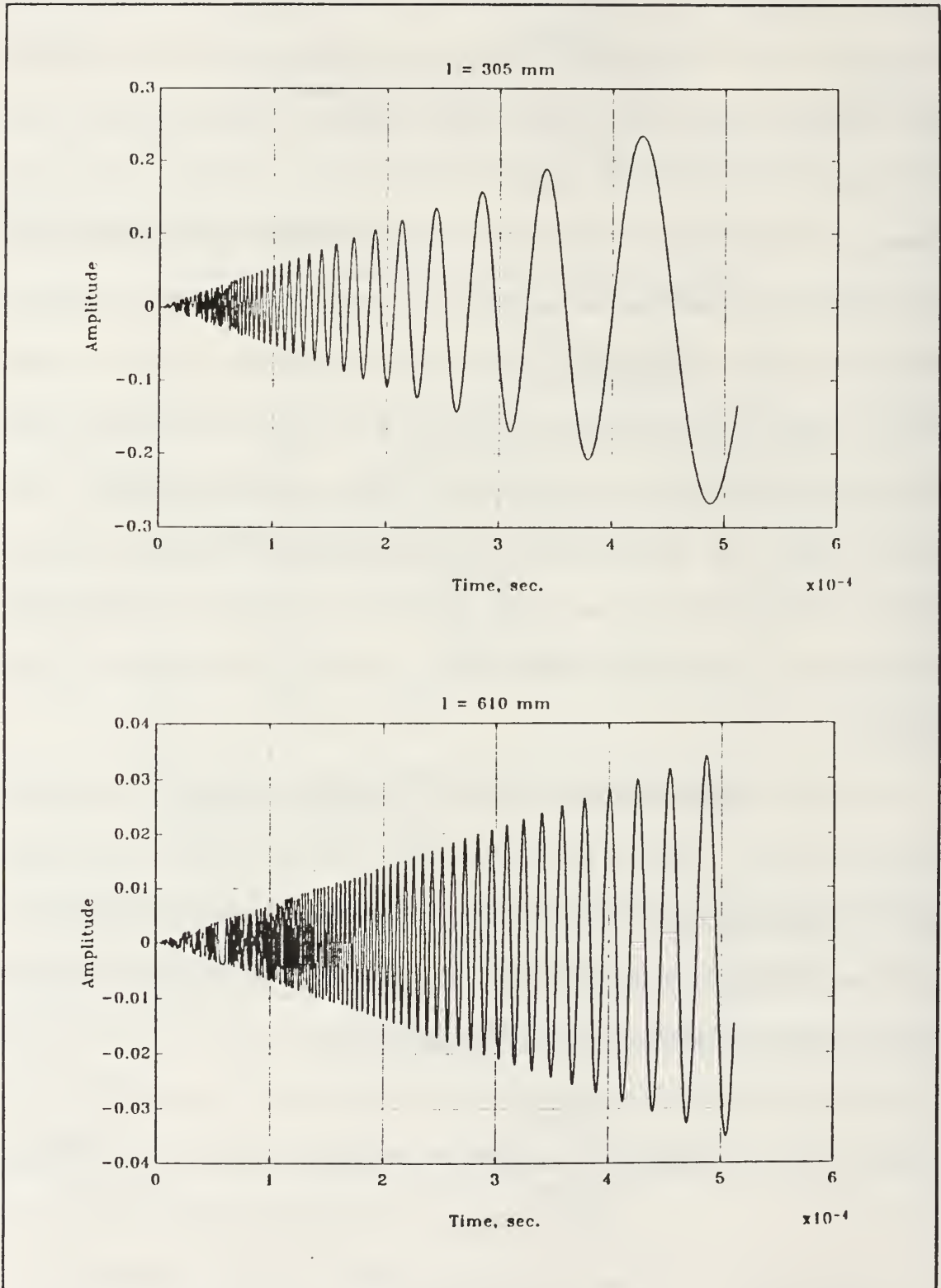
Figure 4.8. Theoretical waveforms.

Figure 4.9. Filtered waveforms.
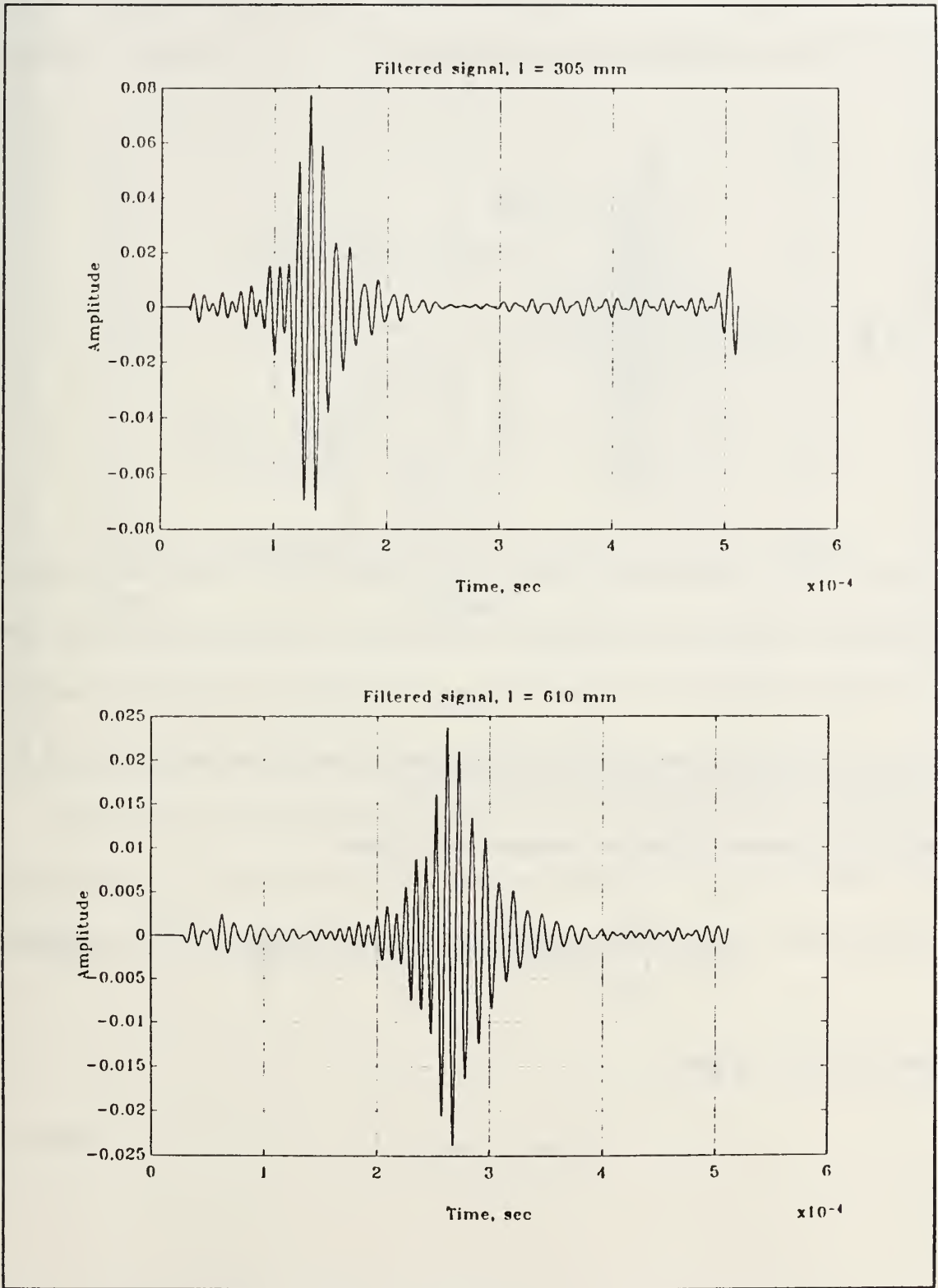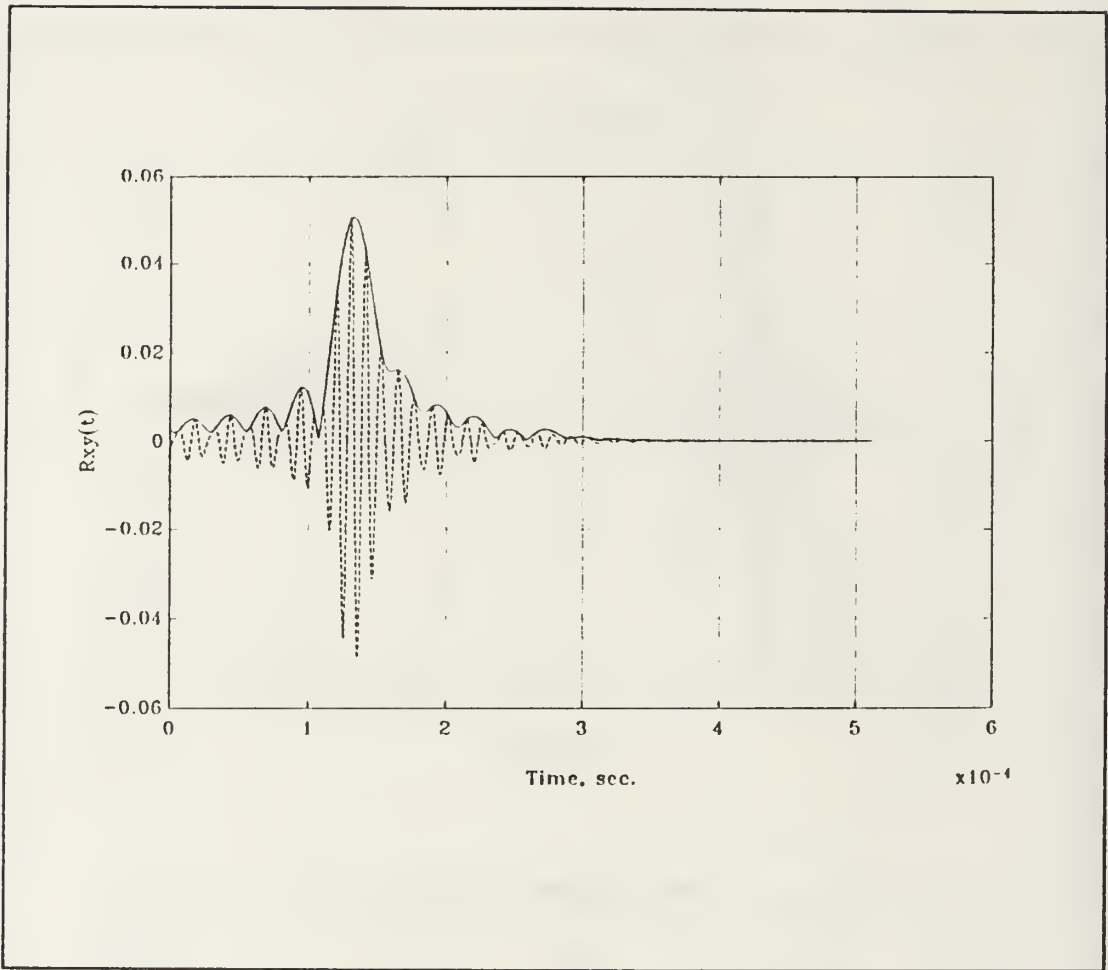
57

Figure 4.10. Crosscorrelation of filtered signals.

Substituting equation (4.30) into equation (4.39) gives

$$R_{xy}(t) - \int_{-\Delta/2}^{\Delta/2} \frac{1}{1+\epsilon} \cos\left[\omega_0 t(1+\epsilon) - a\omega_0^{1/2}(1+\epsilon)^{1/2}\right] d\epsilon. \tag{4.40}$$

Expanding $1/(1+\epsilon)$ gives

$$(1+\epsilon)^{-1} - 1 - \epsilon + \epsilon^2 - \dots \tag{4.41}$$

The first two terms are then substituted into equation (4.40) and the resulting equation is evaluated as before. The crosscorrelation including the attenuation term is

$$
\begin{aligned}
R_{xy}(t) &= \cos\left[\omega_0\left(t-\frac{l}{c_p}\right)\right] \times \frac{\sin\left[\frac{\Delta\omega_0}{2}\left(t-\frac{l}{c_g}\right)\right]}{\frac{\omega_0}{2}\left(t-\frac{l}{c_g}\right)} \\
&+ \sin\left[\omega_0\left(t-\frac{l}{c_p}\right)\right] \times \left\{ \frac{\sin\left[\frac{\Delta\omega_0}{2}\left(t-\frac{l}{c_g}\right)\right]}{\frac{\omega_0^2}{2}\left(t-\frac{l}{c_g}\right)^2} - \frac{\cos\left[\frac{\Delta\omega_0}{2}\left(t-\frac{l}{c_g}\right)\right]}{\frac{\omega_0}{\Delta}\left(t-\frac{l}{c_g}\right)} \right\}
\end{aligned}
\tag{4.42}
$$

where the first term is White's solution for the narrowband pulse, and the second term is due to the attenuation. Numerically evaluating this expression, it was found that the two terms in the brackets in the attenuation term canceled one another, and thus the attenuation had no affect on the shape of the crosscorrelation.

From this it can be concluded that the error in the determination of the Δt was most likely due to the step size of 0.5 μs that was used in the numerical analysis, and any errors that could occur in the calculation of the envelope of the crosscorrelation.
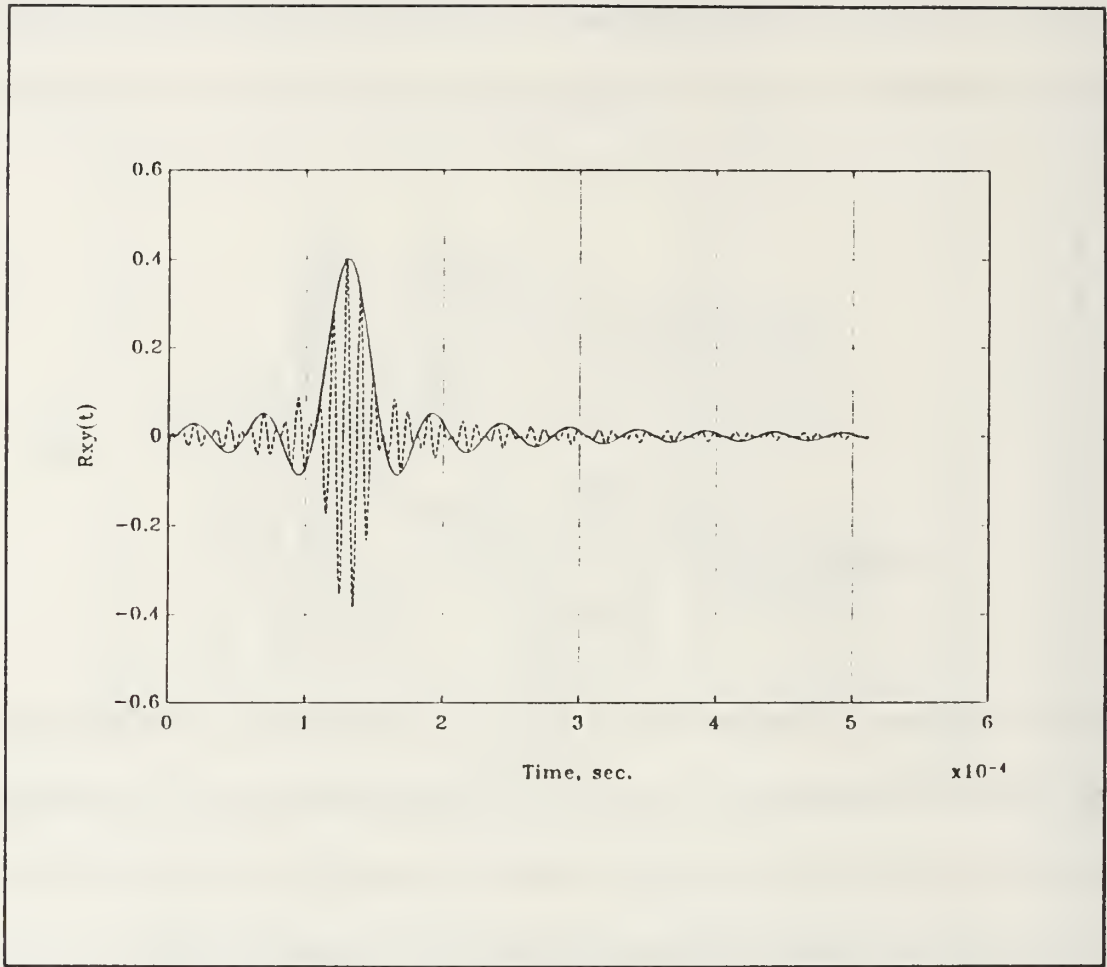
Figure 4.11. Theoretical analysis.

60

V. DISPERSION MEASUREMENTS

While there have been many papers presented on the measurement of the higher modes in plates for applications in ultrasonic NDT [Refs. 38-40], there are few experimental results for the lowest mode which was discussed in Section III. Stiffler and Henneke [Ref. 41] and Tang, Henneke and Stiffler [Ref. 27] have presented experimental results for the lowest plate modes in aluminum and graphite/epoxy plates, for use in the determination of material constants. In these papers however, only the phase velocities were measured, and there was little discussion of the measurement technique used to determine these velocities. To illuminate some of the subtleties associated with the measurement of phase and group velocities in plates, and to verify the theory discussed in Section III, measurements were performed on both isotropic and orthotropic plates. We will begin this section with the experimental set-up used for wave propagation velocity measurements, and then present the results for the isotropic and orthotropic cases.

A. INSTRUMENTATION AND EXPERIMENTAL PROCEDURE

Shown in Figure 5.1 is a schematic of the instrumentation used for the phase velocity measurements. A LeCroy 9100 arbitrary function generator (AFG) was used to generate a 20 volt peak-to-peak gated seven cycle sine wave tone burst, shown in Figure 5.2. The repetition rate of the tone burst was controlled by a Wavetek model 145, 20 MHz pulse generator. The tone burst from the AFG was then amplified (if
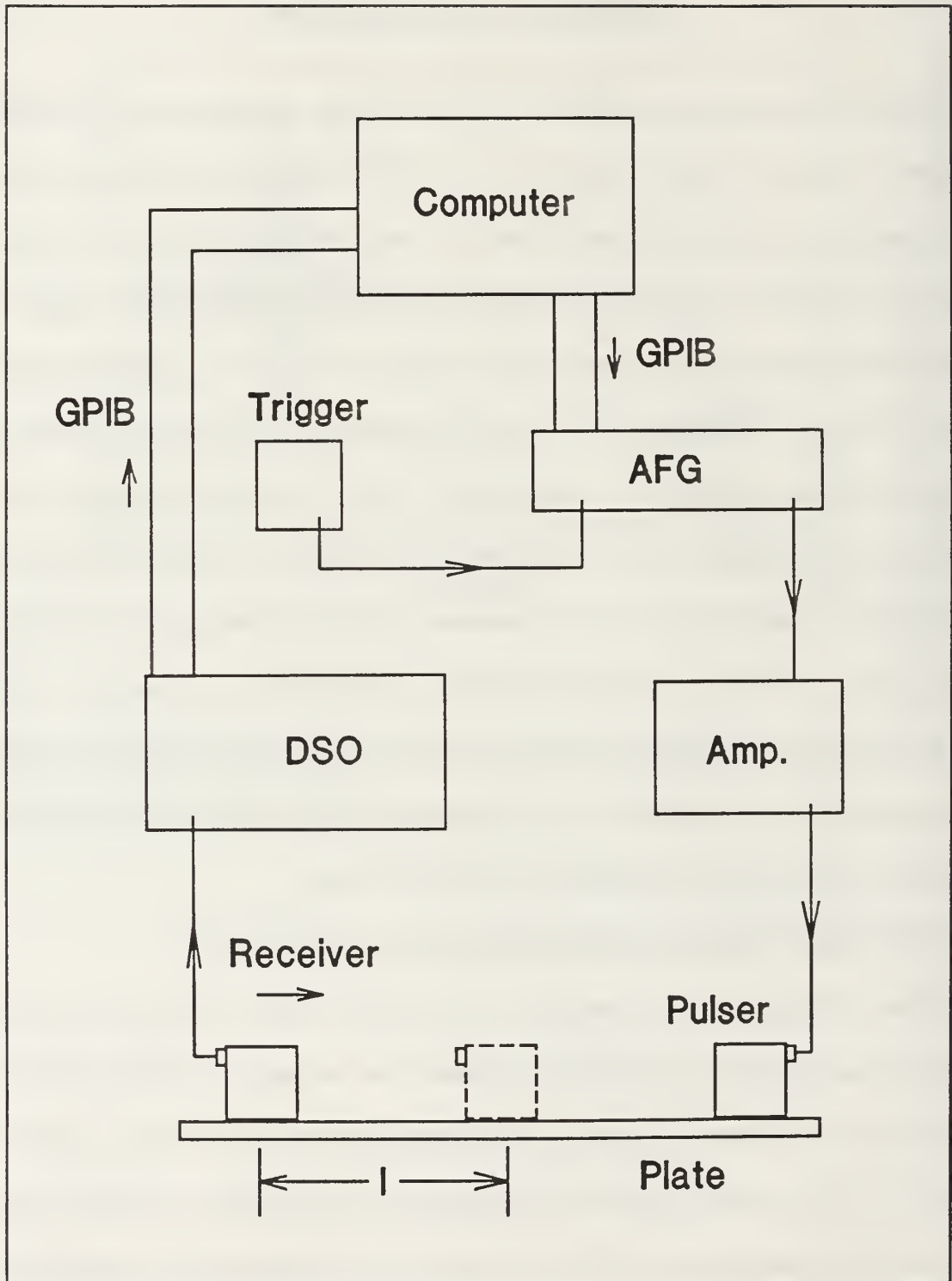
Figure 5.1. Instrumentation set-up.
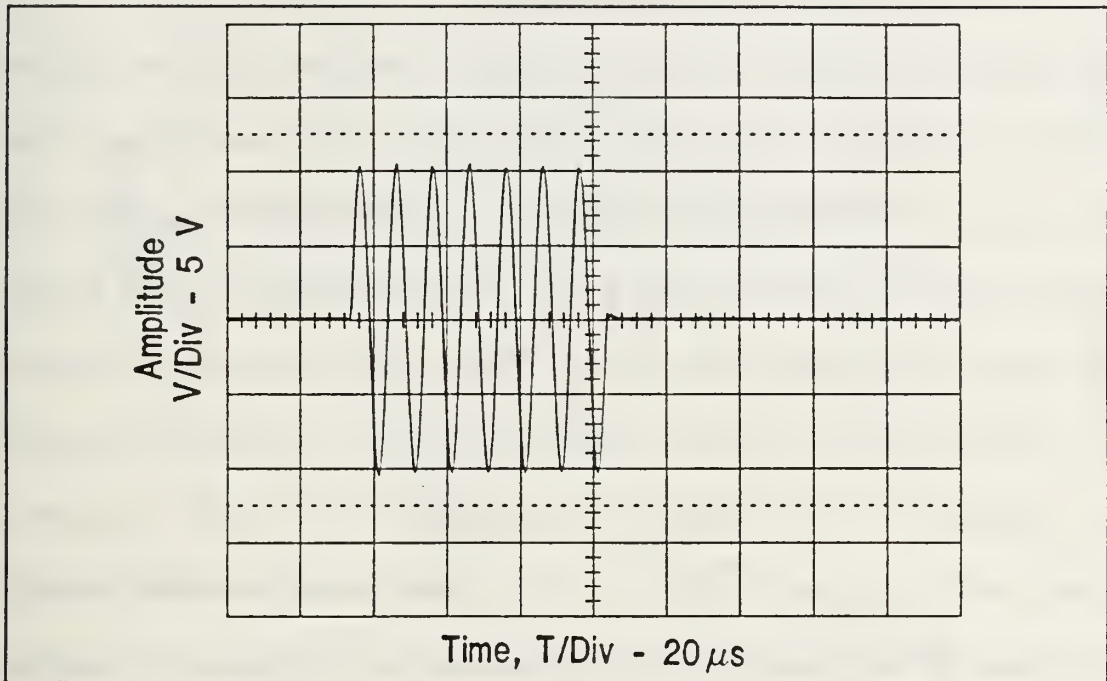
Figure 5.2. Input pulse.

needed) using a Krohn-Hite model DCA-50 direct coupled amplifier (frequency range of 0-500 kHz), which in turn was input into a Krohn-Hite model MT-55 matching transformer. The amplified signal was then input into a Harisonic model HC-483 piezoelectric transducer, which was resonant at 2.25 MHz and had a diameter of 12.7 mm (0.5 in). The receiving transducer was a Harisonic G0504 piezoelectric transducer resonant at 5 MHz and with a diameter of 6.35 mm (0.25 in). Both transducers were coupled to the plate using vacuum grease. The signal from the receiving transducer was then amplified 60 dB using a Physical Acoustics Corporation (PAC) preamplifier, model 1220A, in which the filter had been modified for broadband operation. The toneburst from the AFG was used to trigger a LeCroy

63

9400A digital storage oscilloscope (DSO) which was then used to capture the waveform detected by the receiving transducer.

To determine the phase velocity, the receiving transducer was moved a known distance, l, and the time difference of a phase point on the waveform was noted. Figures 5.3-5 show the flexural wave (100 kHz) at a reference point, and after being moved 40 and 80 mm, and the cursor marks the same phase point at each location. It can be seen that the phase point seems to shifting as the sensor is moved. Because of the abrupt cutoff of the sine wave, additional frequencies are introduced, and the wave propagates as a narrowband pulse. As was noted in Section III-C, because of this there will be a group velocity, as well as a phase velocity and, from equation (4.25), there will be a phase shift which is dependent on the distance the transducer has been moved. Thus, if the time difference is measured by using what looks to be the same phase point, say by always choosing the center cycle of the waveform, in actuality the group velocity will be measured. Therefore, from the above figures it can be seen that one must be careful when measuring the phase velocity so as to pick the correct phase point on the wave.

To measure the group velocity, a different technique was used. Instead of using a tone burst and trying to measure the group velocity from a point on the envelope, the crosscorrelation technique discussed in Section IV-B.2 was used to determine the group velocity. A flexural wave was excited by breaking a lead on the surface of the plate and detecting it using a broadband conical point transducer. This transducer was chosen since it had a better lower frequency response than the Harisonic

64
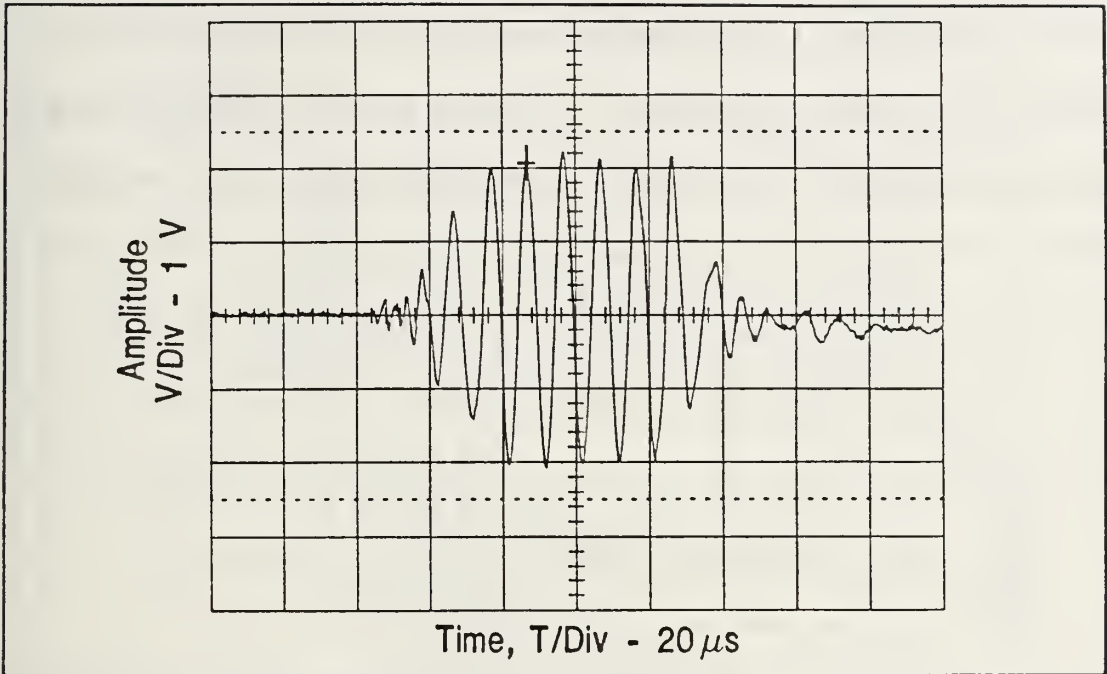
Figure 5.3. Reference waveform.
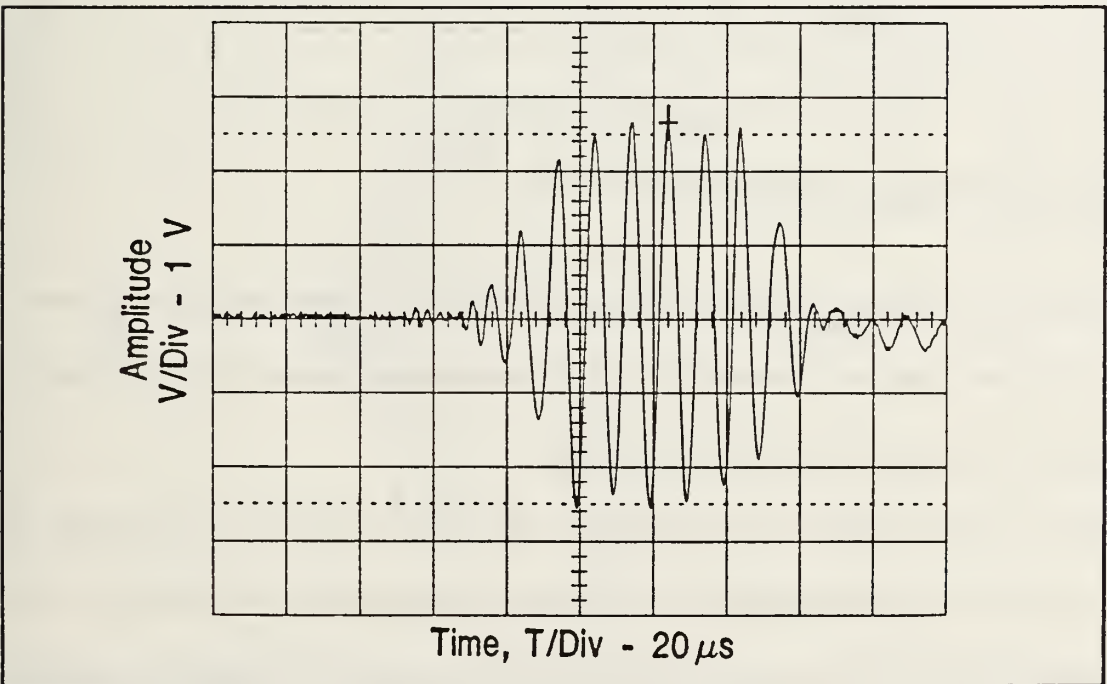
Figure 5.4. Distance moved, 40 mm.

65

piezoelectric transducers. This was important in the graphite/epoxy plate due to the attenuation of the higher frequencies. The signal was then amplified using a broadband PAC amplifier with 40 dB gain, and digitized using the LeCroy DSO.
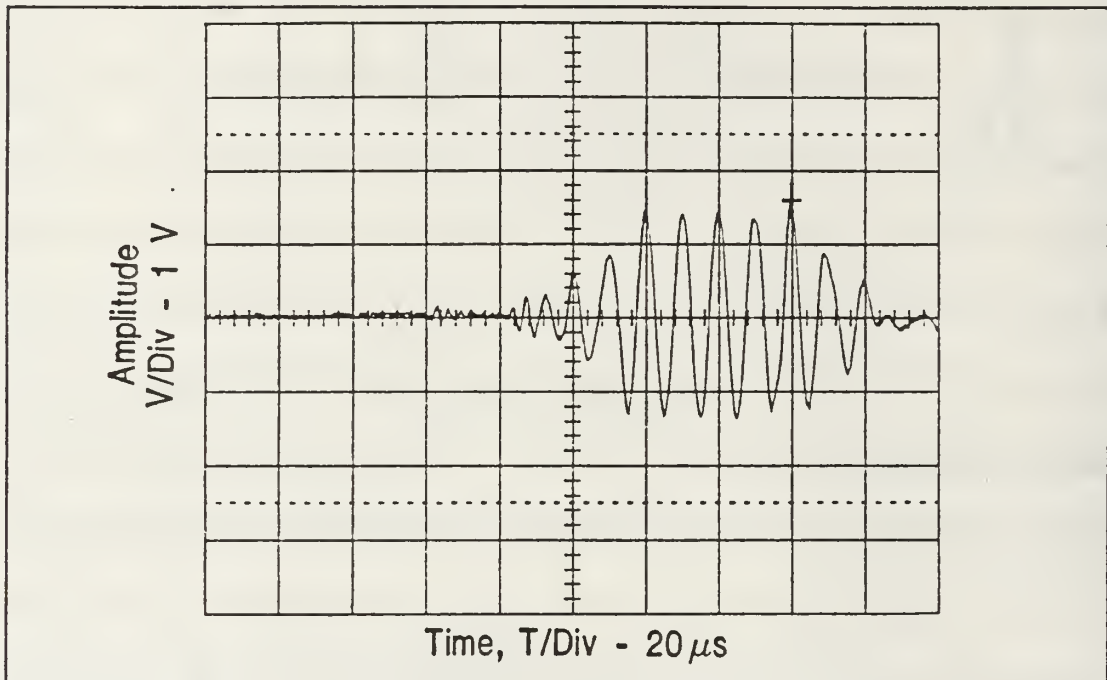
Figure 5.5. Distance moved, 80 mm.

The transducer was then moved a known distance and the above procedure repeated. The waveforms were then narrowband filtered and crosscorrelated to determine the propagation times at the various frequencies.

Figures 5.6 and 5.7 show the waveforms at 120 and 220 mm from a lead break on the surface of an aluminum plate (7178-T6) with a thickness of 1.42 mm (0.056 in). The basic shape of the waveform can be seen to agree with Medick's solution, equation (4.21). The distortion in the latter portions of the waves are due to reflections and the response of the transducer. Also, it should be noted that because of the frequency content of the pulse created by the lead break (0-1 MHz), and the

66
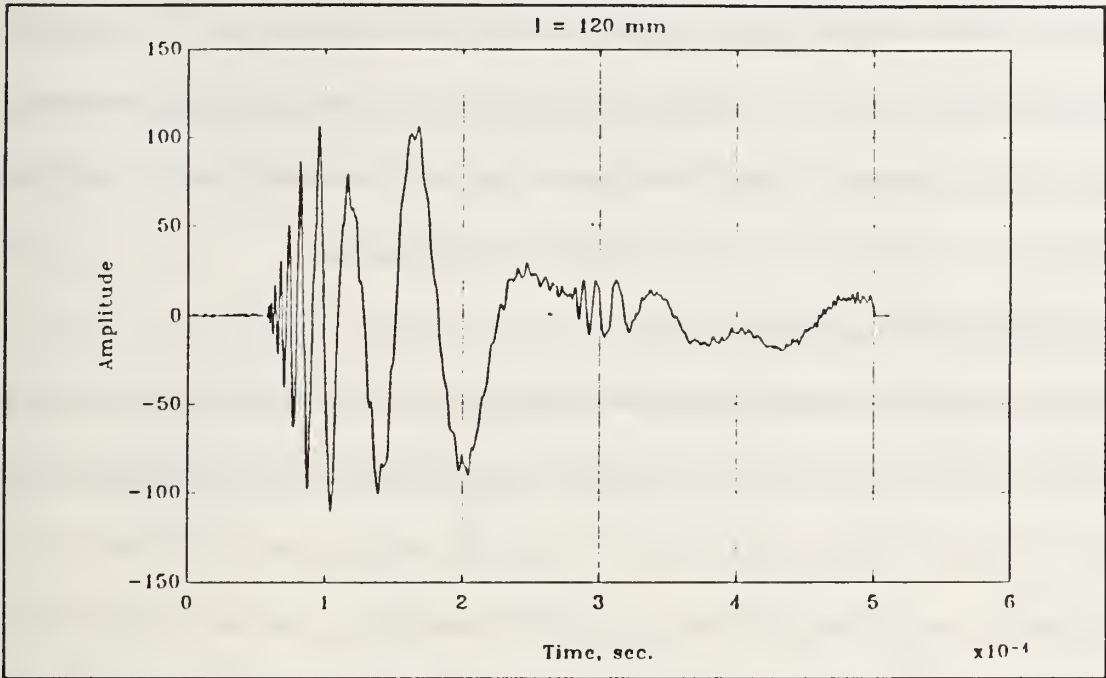
Figure 5.6. Waveform from lead break, l=120 mm.
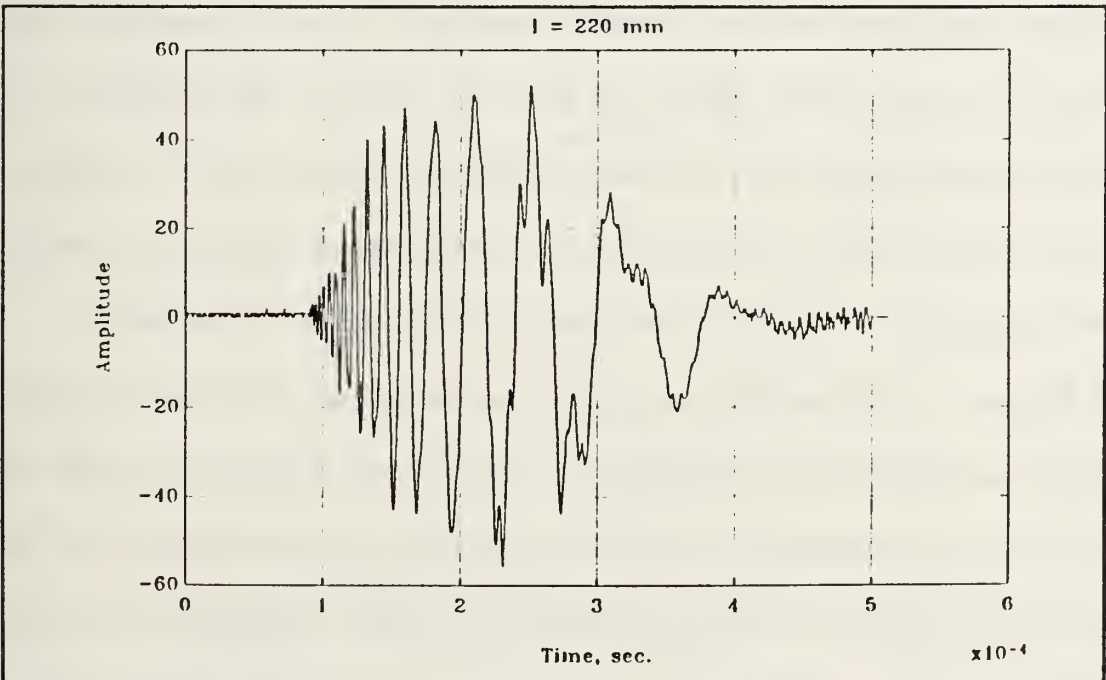
Figure 5.7. Waveform from lead break, l=220 mm.

thickness of the plate, only the lowest order flexural mode is excited. This simplifies the analysis since none of the higher modes predicted by the Rayleigh-Lamb theory, Figure 3.6, are present. For thicker plates, the analysis would need to include a method for determination of which modes are propagating.

B. EXPERIMENTAL RESULTS

Shown in Figure 5.8 is the theoretical dispersion curve for the phase velocity in an aluminum plate calculated using Mindlin's theory. The material constants used are given in Section IV-B.1, and $\kappa = 0.926$. The group velocity curve in Figure 5.8 was calculated by numerically differentiating the theoretical phase velocity data from Mindlin's theory. Also shown are the dispersion measurements made on the aluminum plate described in the preceding paragraph. A small discrepancy is seen between the phase velocity theory and data, and likely can be attributed to the material constants used in the calculation of the theoretical curves. The scatter in the group velocity data is most likely due to errors in the calculation of the envelope of the crosscorrelation caused by the time step of 0.5 μs used in the analysis.

In Figures 5.9, 5.10 and 5.11 are shown the theoretical curves based on Tang, Henneke and Stiffler's higher order plate theory, Section III-B, and the phase and group velocity measurements for a $[0_2/90_2]_s$ AS4/3501-6 graphite/epoxy plate. The figures are for the 0^0, 45^0 and 90^0 directions in the plate respectively, where 0^0 is taken as along the outer fibers. The material constants for the plate are as follows; $E_{11} = 142.3$ GPa, $E_{22} = 9.31$ GPa, $G_{12} = 4.90$ GPa, $G_{23} = 3.45$ GPa, $\nu_{12} = 0.29$, $\nu_{23} = 0.34$ and $\rho = 1583$ kg/m^3. The value used for κ_i and κ_j, the shear correction factors, was

5/6, based on Tang, Henneke and Stiffler's results. Again, a slight difference is seen between the phase velocity measurements and theory, and there is some scatter in the group velocity data, with the same conclusions regarding these errors as in the isotropic case.

From the above data it was felt that the velocity measurements were sufficiently understood to be applied to source location. The results of the source location will be discussed in the following section.
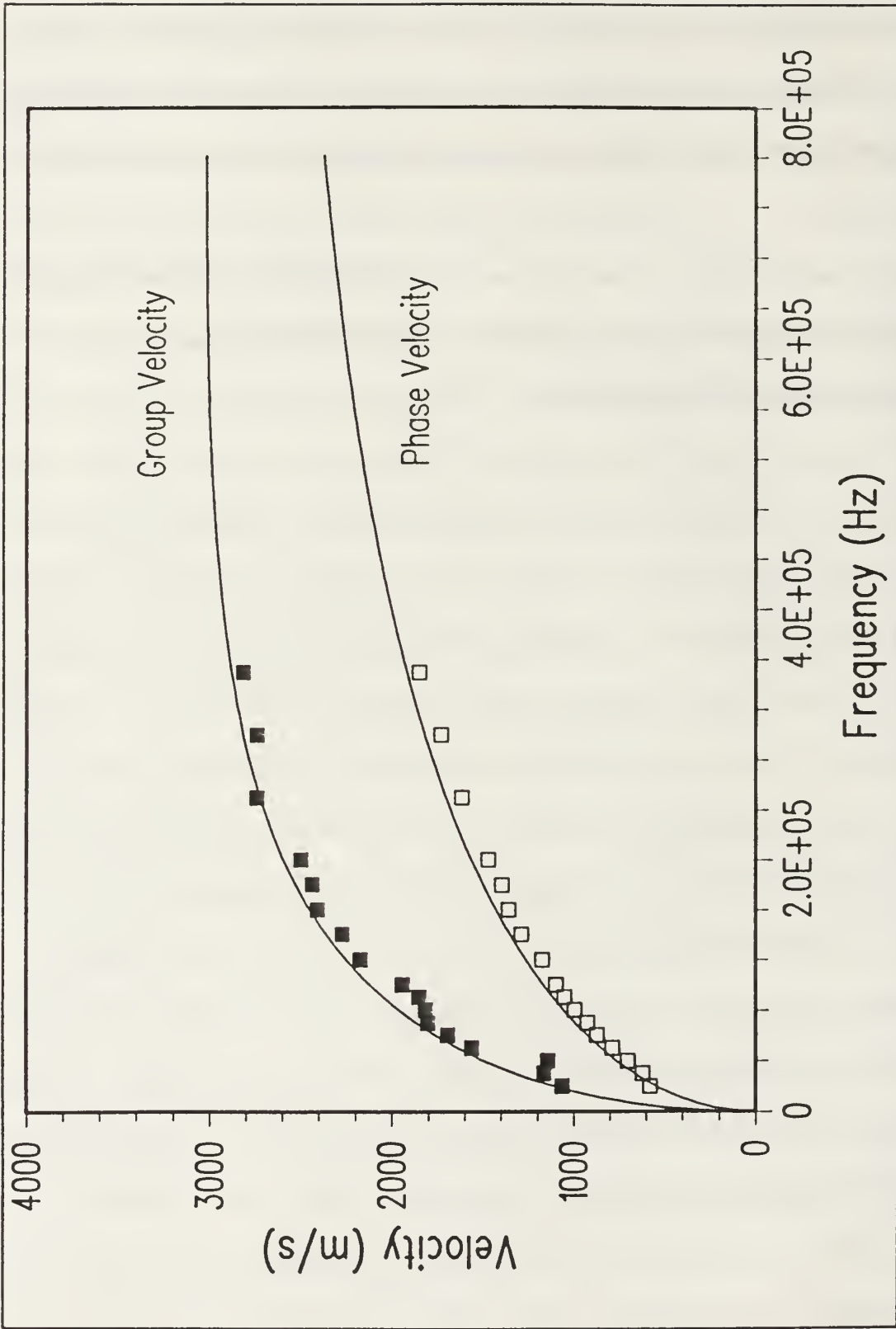
Figure 5.8. Theoretical dispersion curves and data for the aluminum plate.

70
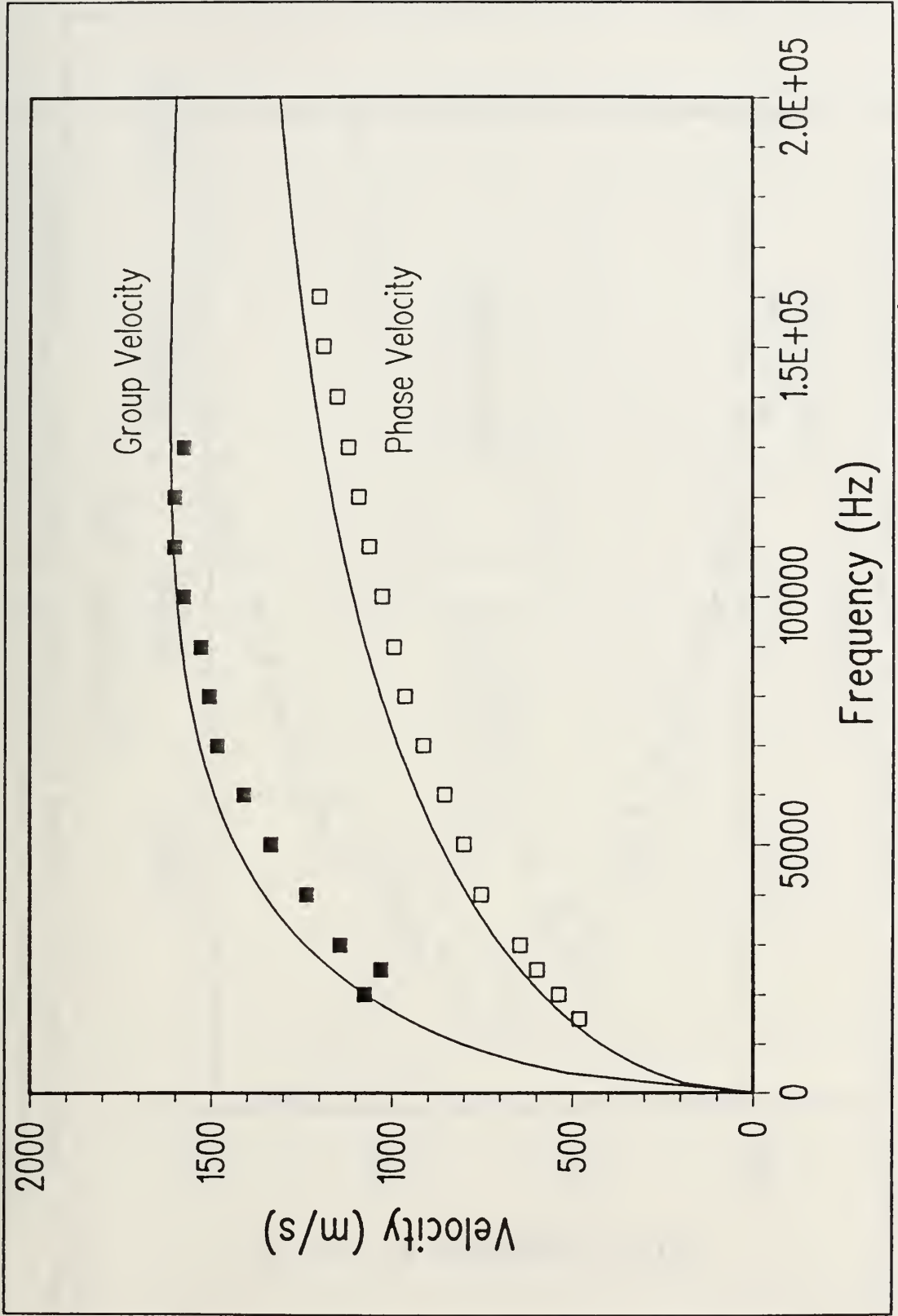
Figure 5.9. Theoretical dispersion curves and data for $[0_2/90_2]$, graphite/epoxy plate, 0^0 direction.

71
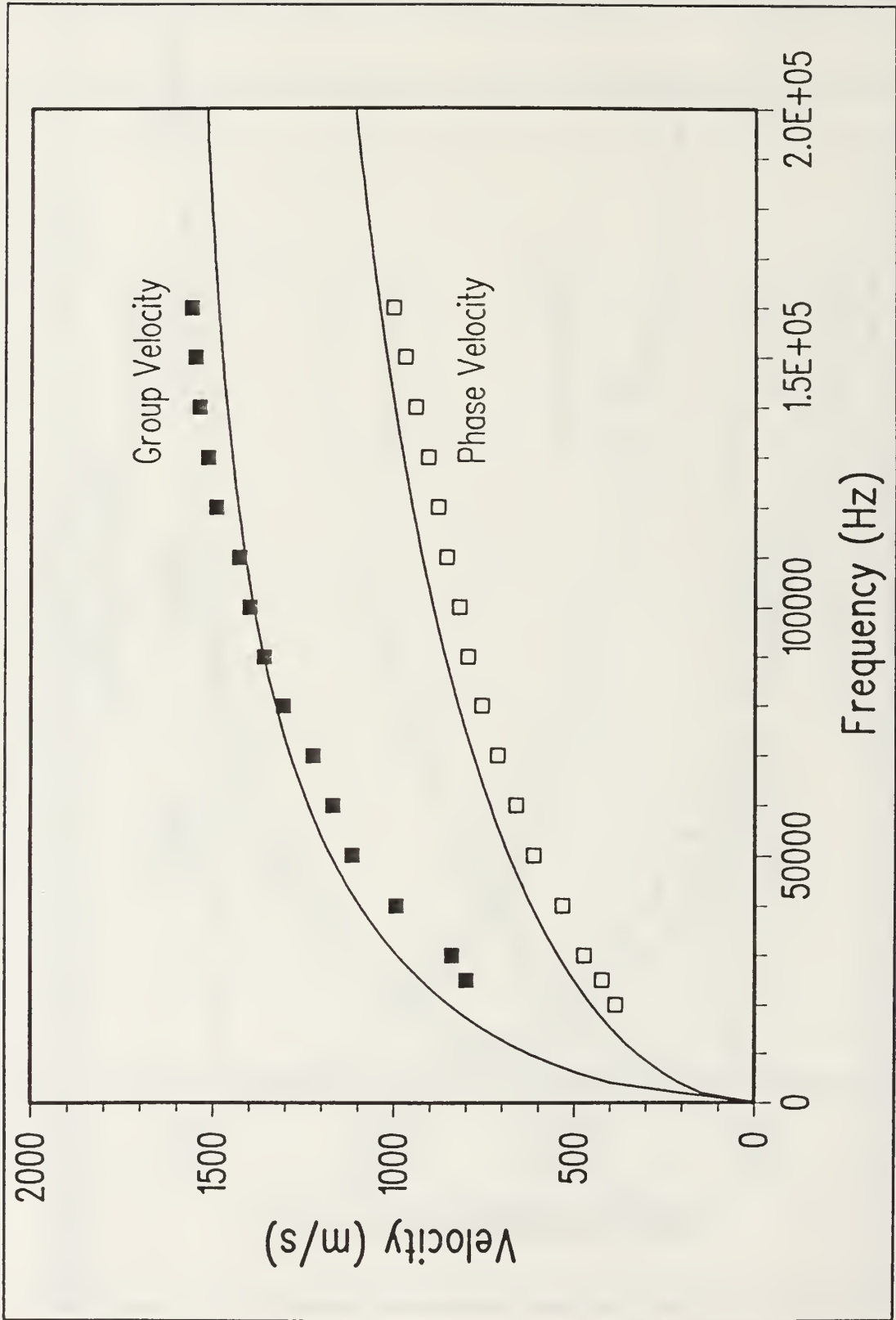
Figure 5.10. Theoretical dispersion curves and data for $[0_2/90_2]_s$ graphite/epoxy plate, 45^0 direction.
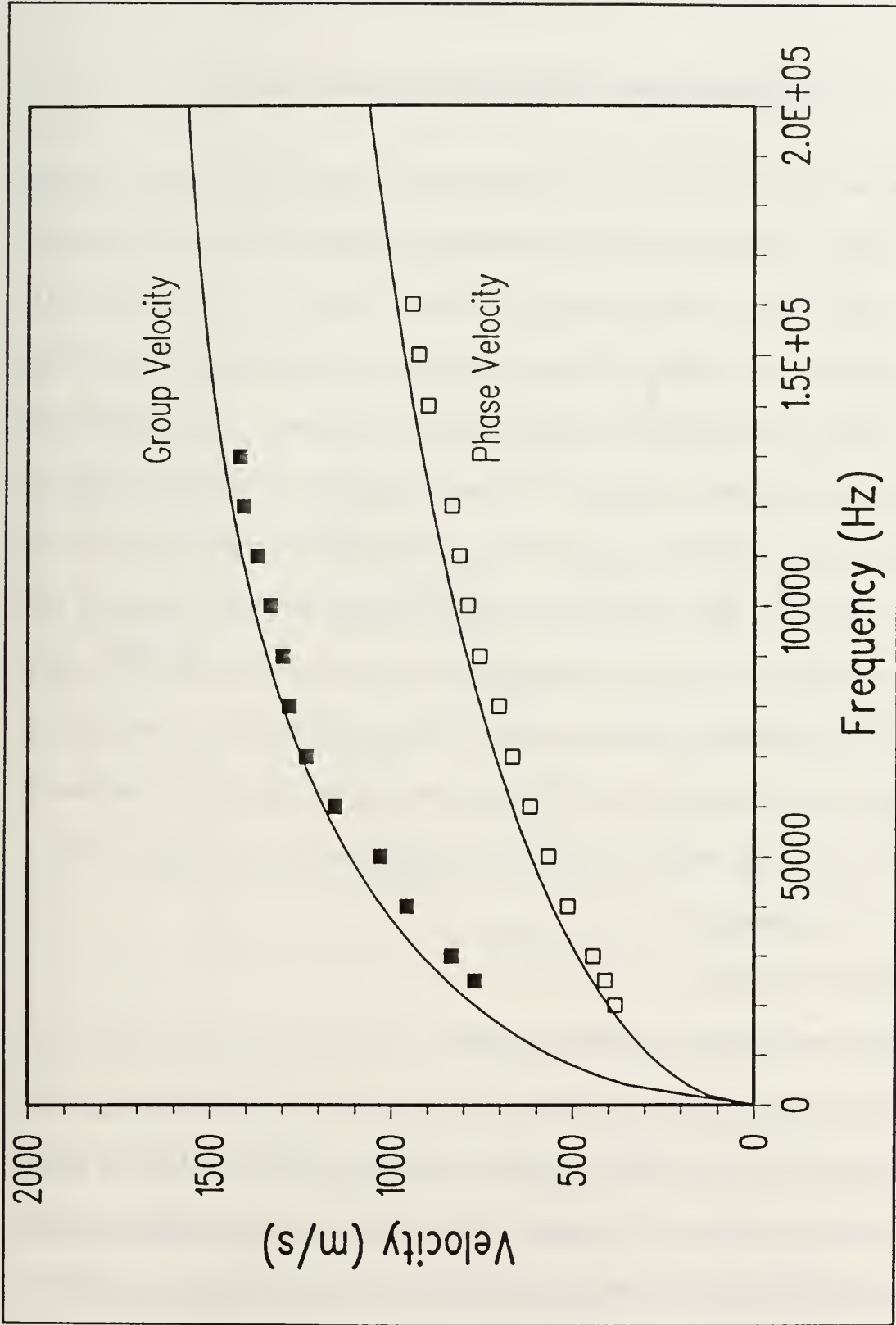
Figure 5.11. Theoretical dispersion curves and data for $[0_2/90_2]$, graphite/epoxy plate, 90^0 direction.

73

VI. EXPERIMENTAL SOURCE LOCATION RESULTS

Presented first in this section is the experimental set-up and the results from the source location experiments using an aluminum plate. The results for the aluminum plate include both crosscorrelation techniques along with conventional AE instrumentation and methods (resonant transducers and narrowband filtering) and the high gain/broadband filtering method discussed in Section I. The first threshold crossing techniques were included so that the crosscorrelation techniques could be compared with the methods currently in use. For the graphite/epoxy plate, only the crosscorrelation method using the narrowband filtering was used because it was discovered to be a more accurate method than the gaussian crosscorrelation method was used to determine the source location in the aluminum plate. Also, the first threshold crossing methods were not used for the graphite/epoxy plates because of the high attenuation which eliminated the extensional mode. Location data is presented in Appendix B.

A. ISOTROPIC PLATE

1. Experimental Set-up and Plate Material

For this case, an aluminum plate of 7178-T6 was used, with dimensions of 122 cm × 183 cm (4 ft × 6 ft), with a thickness of 0.142 cm (0.056 in). The AE source was a lead break, Pental 2H, 0.5 mm. Shown in Figure 6.1 is a schematic of the sensor arrangement and the locations of the lead breaks relative to the transducers.

74
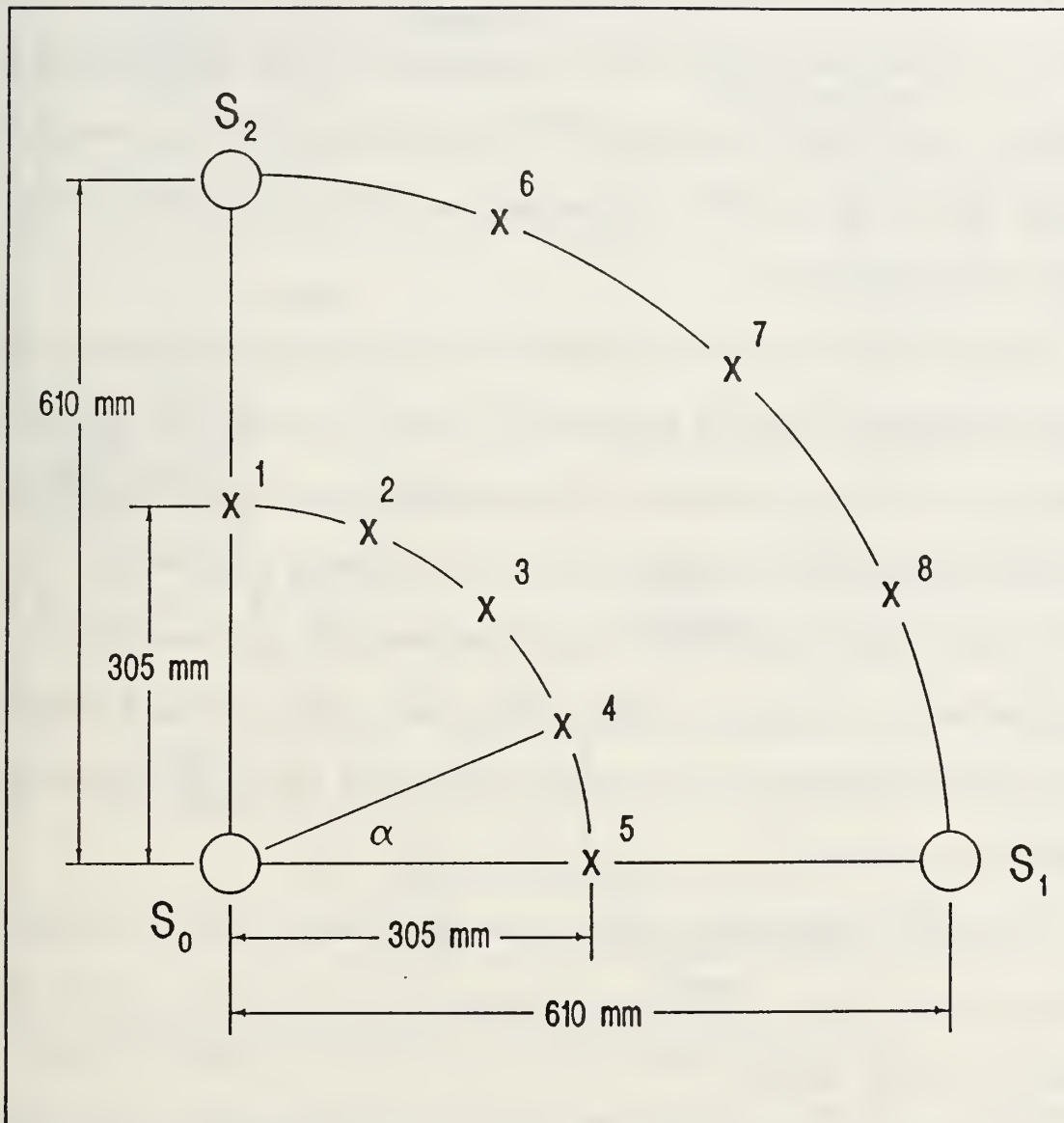
Figure 6.1. Lead break locations.

The values of α were 0^0, 22.5^0, 45^0, 67.5^0 and 90^0. Three lead breaks were performed at each of the locations to confirm the repeatability of the breaks. To acquire the waveforms for the crosscorrelation analysis a broadband system was used to capture the waveforms. Figure 6.2 shows a schematic of the instrumentation used for the

source location experiments. The transducers used to detect the wave in the plate were Harisonic G0504 ultrasonic transducers. These were coupled to the plate using Petro Wax (PCB Piezotronics, Inc.). The outputs from the transducers were amplified 60 dB using the broadband PAC preamplifiers. The signal was then digitized using the LeCroy DSO at a sampling rate of 20 nanoseconds/point, with 25,000 points being stored.

Because only two channels were available on the DSO, the signal from S_0 was input into channel 1, while the signals from S_1 and S_2 were input into the same preamplifier and then into channel 2. For measurements made at $\alpha = 45^0$, this could no longer be done, since the wave arrived at S_1 and S_2 nearly simultaneously. For these measurements separate lead breaks were used for the time difference determination for S_1 and S_2. Both the gaussian and narrowband filtering crosscorrelation techniques were used to determine the arrival time differences between S_0-S_1 and S_0-S_2.

The velocity used in the location analysis was determined by use of pulser-receiver method, which is detailed in Reference 42. For 100 kHz, the velocity measured was 2.001 mm/μs.

An Acoustic Emission Technology (AET) 4-channel 5500B AE analyzer was used for the conventional AE instrumentation location analysis. The preamplifiers used were AET model 160B, with 60 dB of amplification. For the high gain/broadband test the Harisonic G0504 piezoelectric transducers were used to detect the wave and the preamplifier filtering was 125 kHz - 1 MHz. For the

76
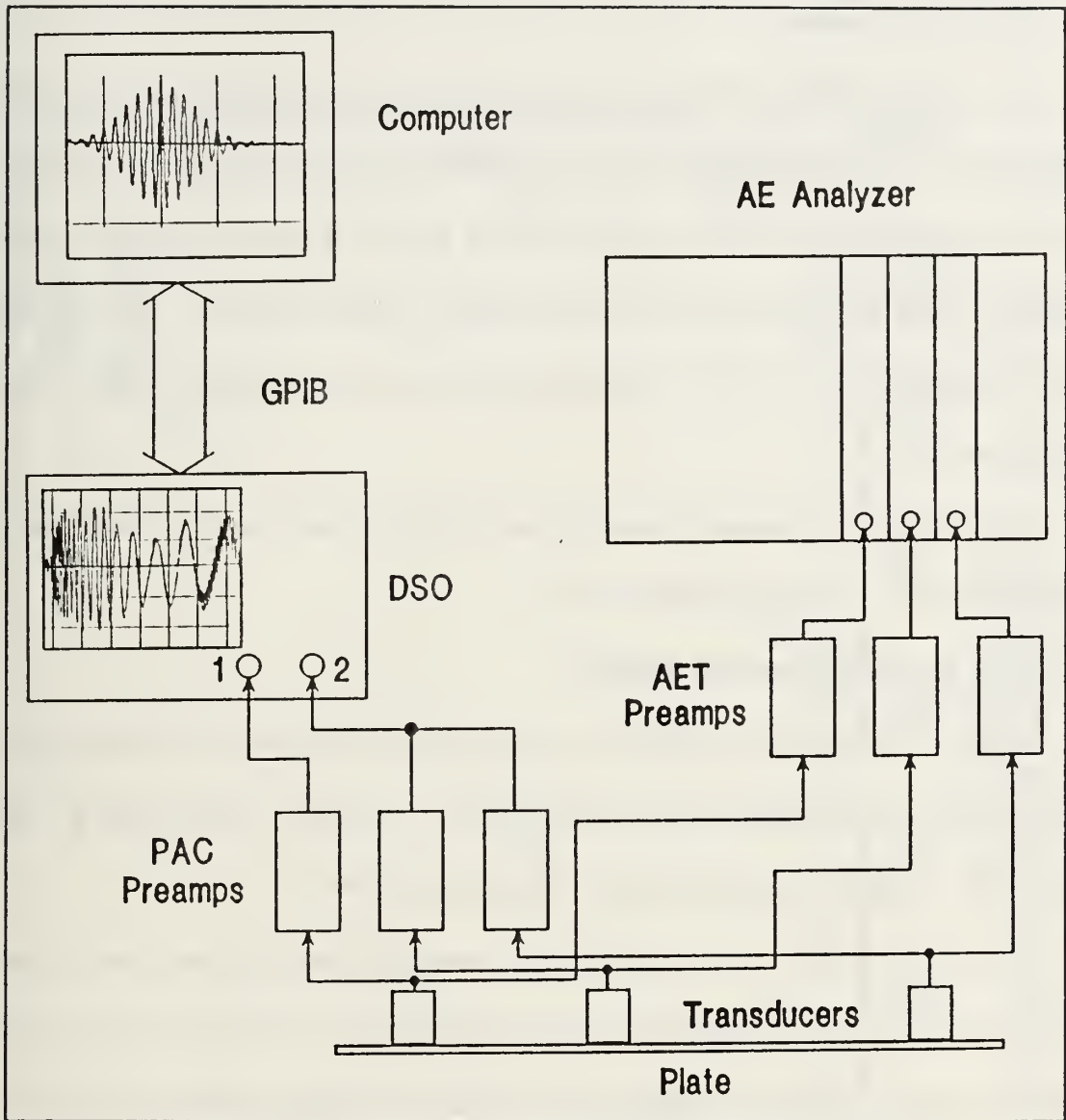
Figure 6.2. Schematic of instrumentation for location experiments.

conventional AE approach, PAC R-15 resonant transducers (150 kHz) and the AET

160B preamplifiers with narrowband filtering of 125 - 250 kHz were used. For the

broadband location tests, 80 dB of total system gain was used. At higher gains the

analyzer would continue to trigger on the reflections for some time, an undesirable

situation during an actual test. For the narrowband tests, both 80 and 60 dB of gain

were used for comparison with the high gain/broadband method and the

77

crosscorrelation methods.

The velocity measurements for the conventional AE instrumentation methods were made by placing the transducers a known distance apart, breaking the lead near one of the transducers, and then measuring the time of propagation using the AE analyzer. Three breaks were used and an average velocity calculated. For the high gain/narrowband test, $c = 5.339$ mm/μs, and for the low gain/narrowband test, $c = 5.041$ mm/μs.

The locations of the lead breaks for the aluminum plate were calculated using Tobias's location algorithm, Section IV-A.1.

2. First Threshold Crossing Methods

Shown in Figures 6.3, 6.4 and 6.5 are the data for the first threshold crossing techniques using conventional AE instrumentation. The three lead breaks at each position are plotted (+) along with the measured location (×).

Figures 6.3 and 6.4 show the high gain/broadband and high gain/narrowband data, respectively. These methods displayed the highest resolution with the least amount of scatter. This was expected since the high gain allowed the measurements to be based on the nondispersive extensional mode. The errors in the data can be attributed to an observed small amount of anisotropy in the plate, measurement errors in the placement of the transducers and location of the lead breaks. The limitations with this method would be the amount of gain available, the digitization rate of the system, the noise level and attenuation of the extensional mode.
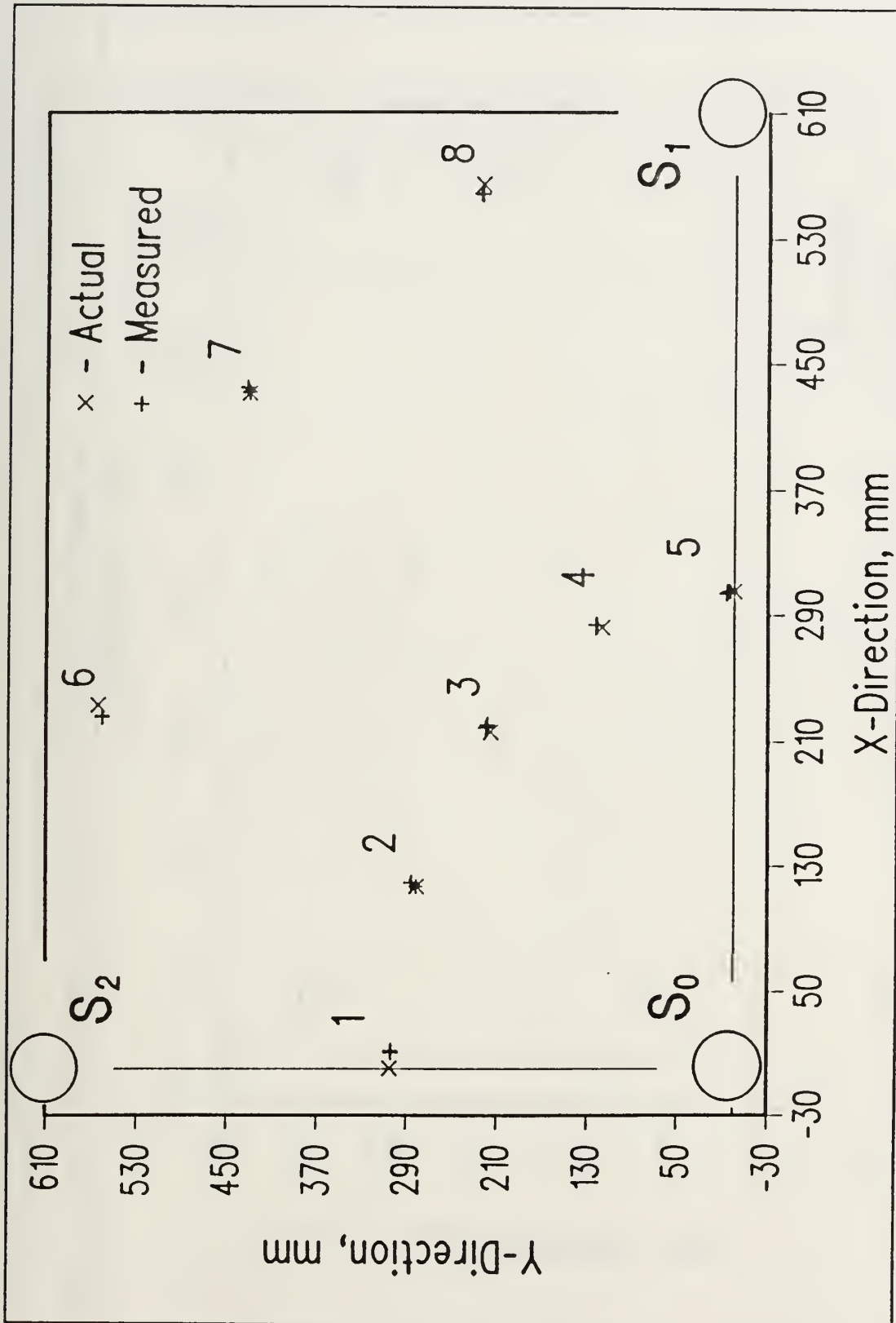
Figure 6.3. Source location data for high gain/broadband instrumentation.

79
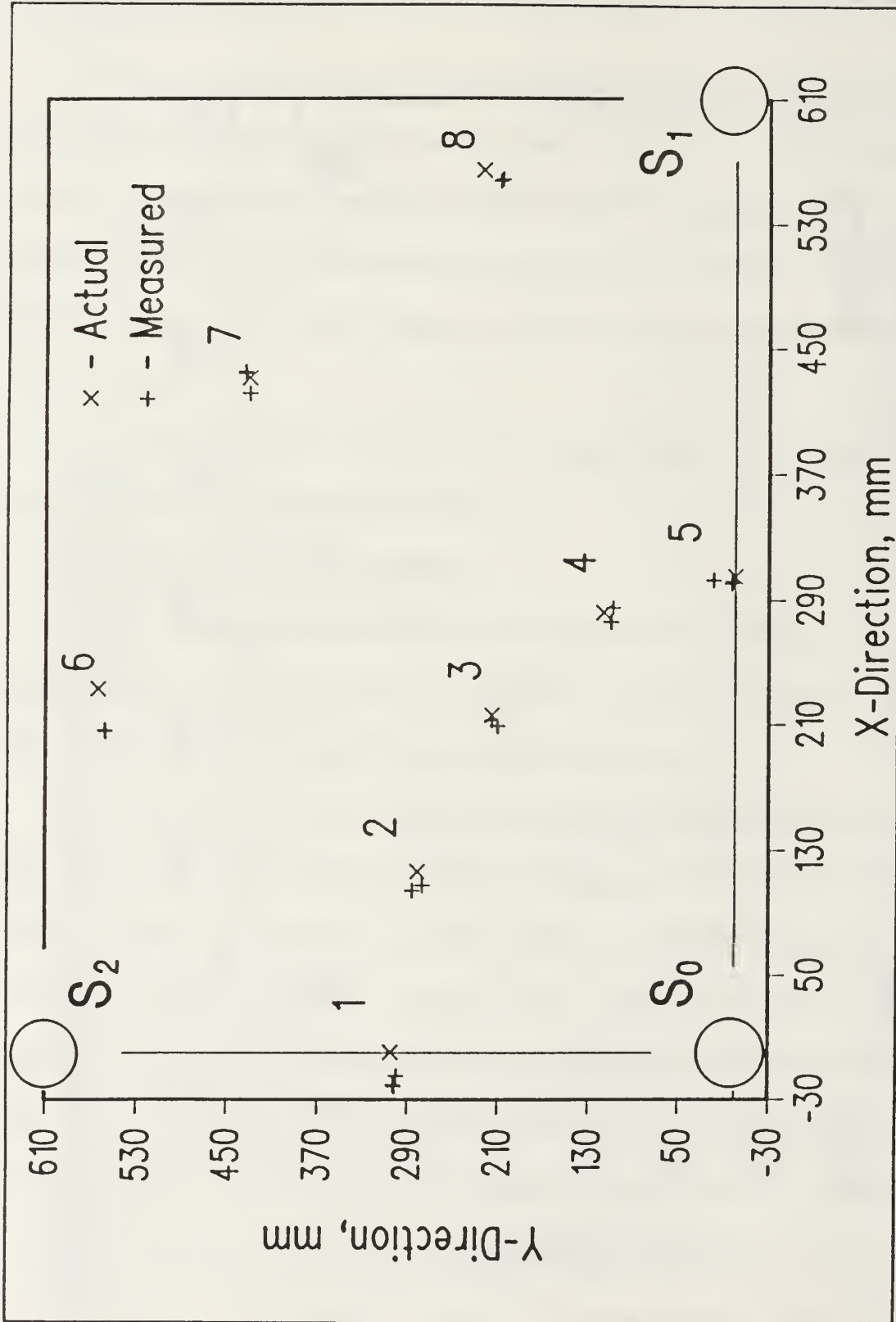
Figure 6.4. Source location data for high gain/narrowband instrumentation.

80
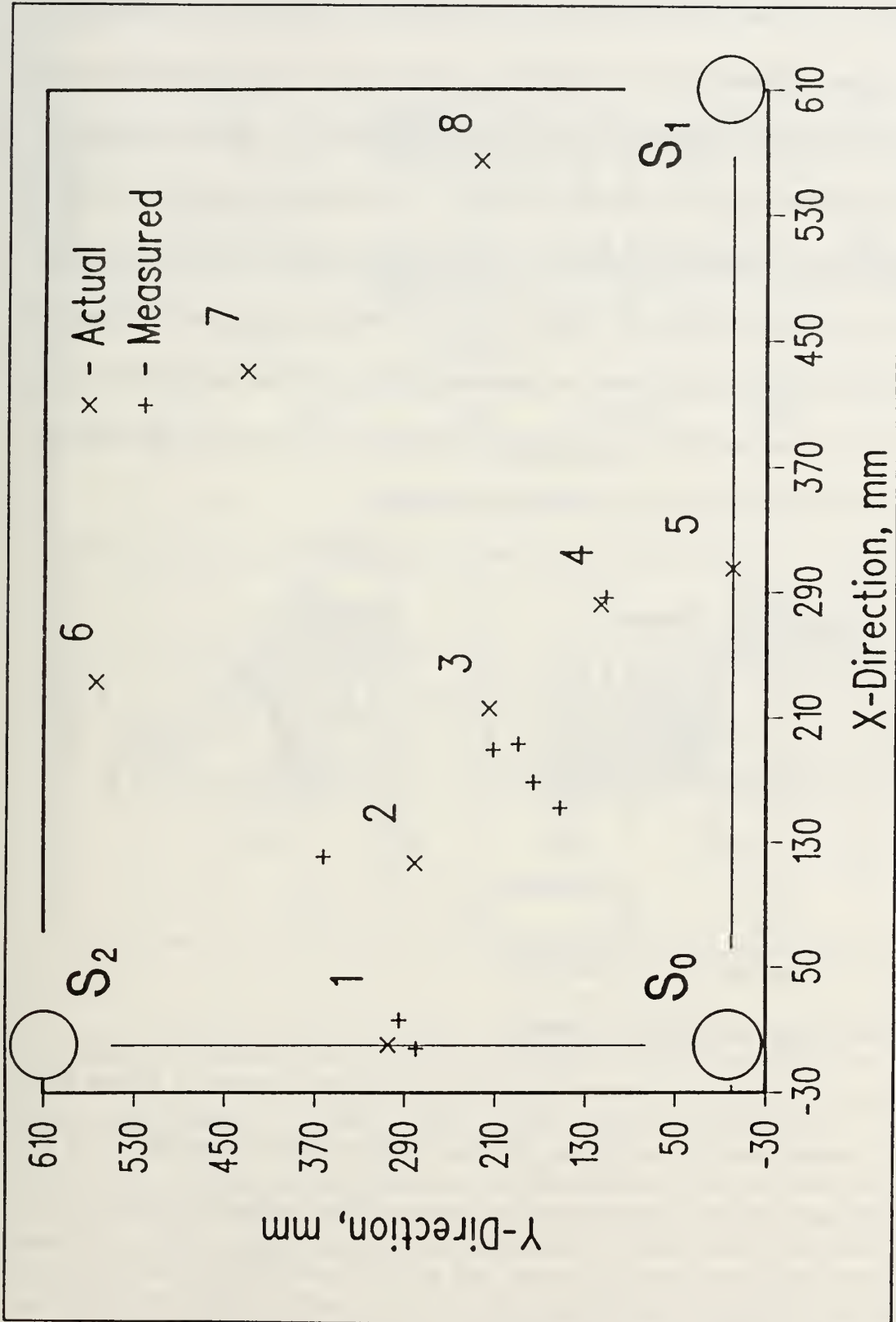
Figure 6.5. Source location data for low gain/narrowband instrumentation.

81

Figure 6.5 shows the 60 dB system gain data for the narrowband conventional AE instrumentation test. Location resolution in this case is reduced significantly, and at locations 6, 7 and 8 none of the lead breaks were located. Figure 6.6 shows a waveform captured using the broadband system. In this figure, both an extensional and flexural mode component are labeled, with the flexural mode being much larger, due to the out-of-plane nature of the source (lead break). For the gain setting used for this test the location clocks were no longer triggered by the extensional wave, but by the flexural wave, and from the previous discussions it is known that this leads to large source location errors, as evidenced by the data.
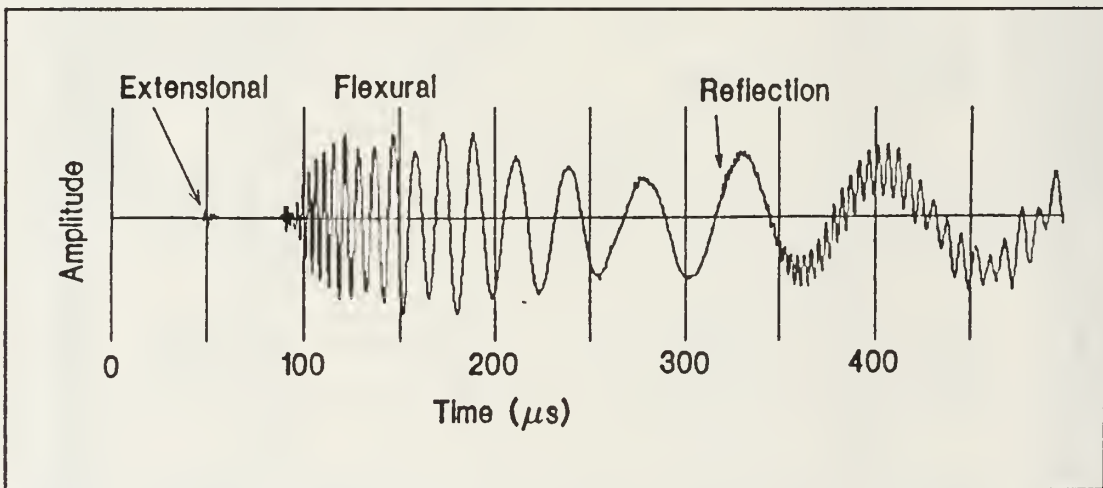
Figure 6.6. Waveform from a lead break.

3. Gaussian Crosscorrelation Method

Figure 6.7 shows typical waveforms from a lead break (location 1, Figure 6.1) and their crosscorrelations using the gaussian crosscorrelation method. Due to memory limitations of the computer and the amount of time needed to crosscorrelate 25,000 points, only every tenth point was used in the crosscorrelation (an effective sampling rate of 5 MHz). For the waveforms, the extensional and flexural portions

82
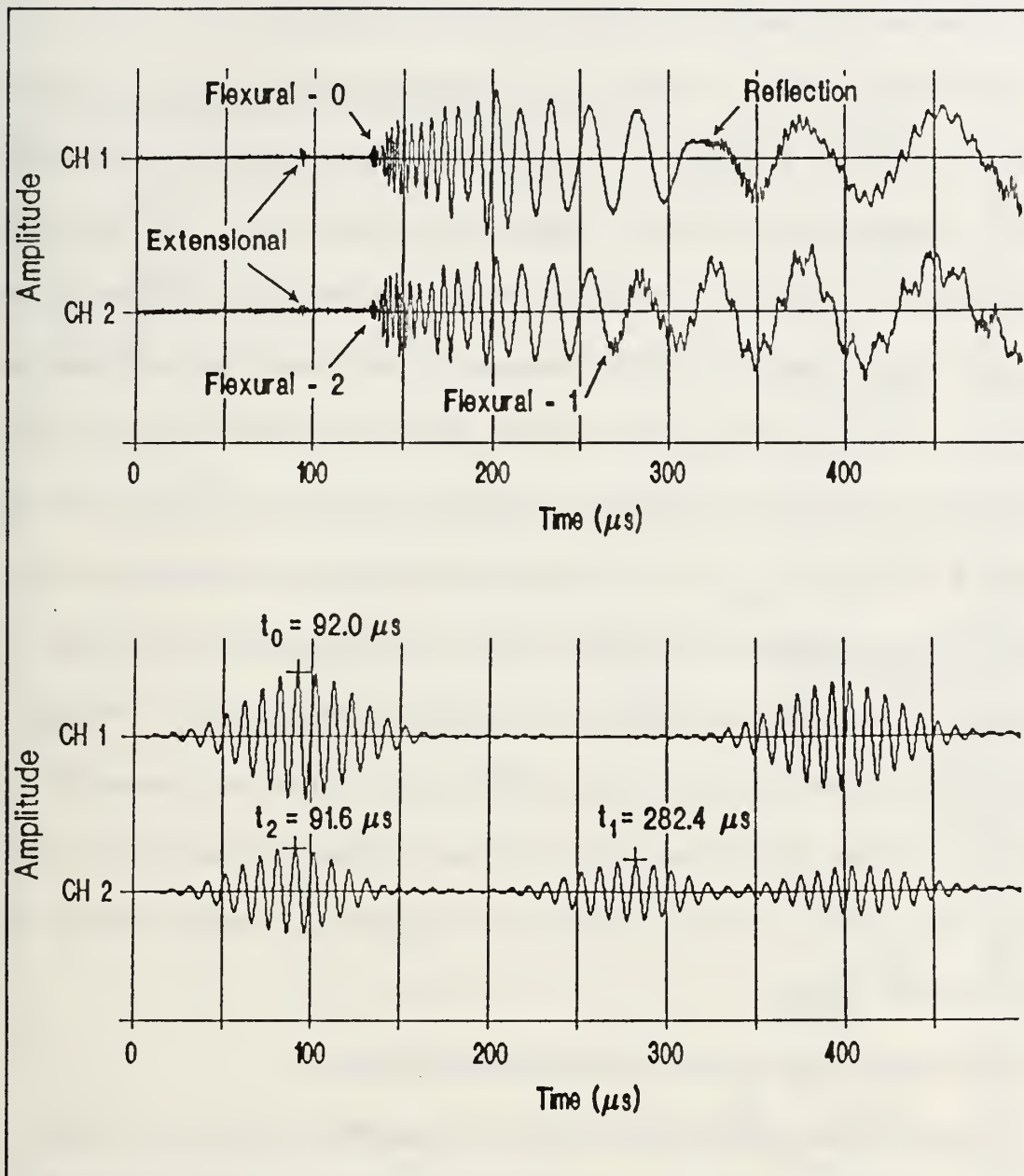
Figure 6.7. Gaussian crosscorrelation analysis for location 1, Figure 6.1.

have been labeled for each sensor, along with any reflections. For the
crosscorrelations the frequency used for the modulated cosine was 100 kHz, chosen
since a spectral analysis showed that this was a predominant frequency in the
waveforms from the lead break. Also given on the crosscorrelation plot are the times

83

at which the positive peaks of the crosscorrelations occurred.

Figure 6.8 shows the results of the location analysis using this method. Comparing Figures 6.5 and 6.8 the difference between using the first threshold crossing technique and locating known phase points using the gaussian crosscorrelation technique on the flexural wave becomes evident. In Figure 6.8 the data show good agreement with the measured values, except for two points at location 1, and all points at locations 6 and 7. The cause of this was found to be a phase shift of the frequency components, equation (4.25), as the AE pulse from the lead break propagated in the plate. This phase shift cannot be accounted for when using the gaussian crosscorrelation method since the initial phase and the length of the path that the wave has travelled are unknown. However, this error can be minimized by crosscorrelating at higher frequencies, if they are present in the waveform. Because of this phase shift, an arrival time determination method which is phase independent is needed, and leads use to the narrowband filtering and crosscorrelation method.

4. Narrowband Filtering and Crosscorrelation Method

By using this method, the phase shift of the frequency components in the pulse is no longer of concern. As long as the same point is chosen on the envelope of the crosscorrelation, the correct arrival times, based on the group velocity, can be determined. To verify that the resolution of the source location could be increased by the use of this method, the waveforms form the gaussian crosscorrelation experiment at locations 6, 7 and 8 were narrowband filtered at a center frequency of
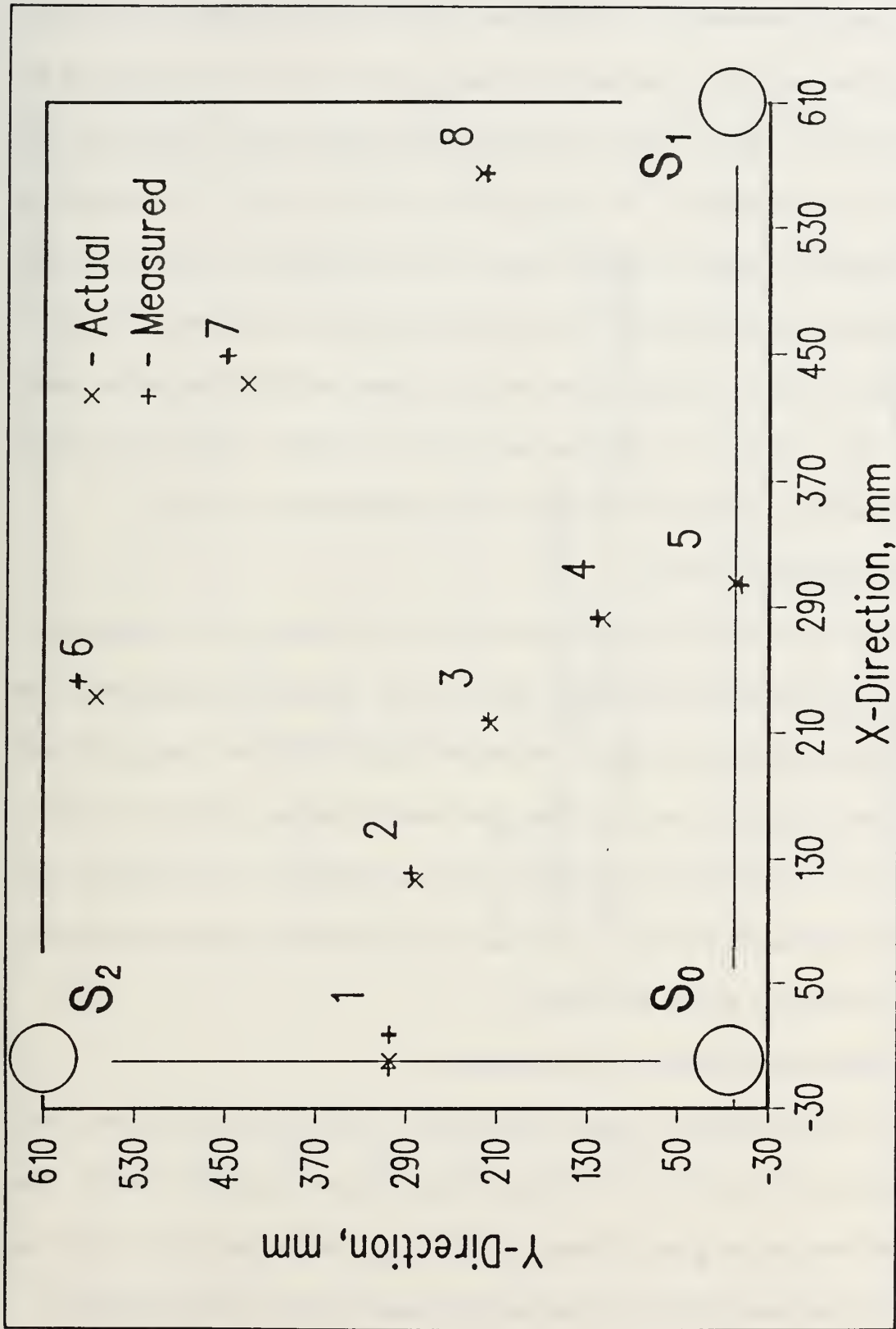
Figure 6.8. Source location data for Gaussian crosscorrelation method.

100 kHz and a bandwidth of 1/2 octave (80-120 kHz), and then crosscorrelated. The arrival times were then determined by choosing the peak of the envelope of the crosscorrelation. The 1/2 octave bandwidth was chosen since it provided a well defined crosscorrelation. As the bandwidth of the filter is narrowed, the crosscorrelation begins to "spread" and the peak becomes less defined, thereby making peak detection difficult. The source location results are shown in Figure 6.9. It can be seen that by using this method the location resolution can be increased. While this method is computationally more intensive that the gaussian crosscorrelation technique, it resulted in the highest resolution overall.

B. ORTHOTROPIC PLATE

For the orthotropic plate, only the narrowband filtering and crosscorrelation method was used for the arrival time determination. Because of the response of the broadband conical point transducer, the extensional portion of the wave was virtually nonexistent, Figures 5.6 and 5.7, so the first threshold crossing techniques could not be employed. Furthermore, the higher frequency components in the flexural wave were also attenuated, and thus the gaussian crosscorrelation technique could not be employed with any degree of accuracy.

1. Experimental Set-up and Plate Material

For the orthotropic location experiment, a $[0_2/90_2]_s$ plate was used, with dimensions of 51 cm × 76 cm (20 in × 30 in) by 0.1143 cm (0.045 in) thick. The material constants are given in Section V-B. The same sensor configuration and lead break locations were used as for the isotropic case, Figure 6.1, but the distance

86
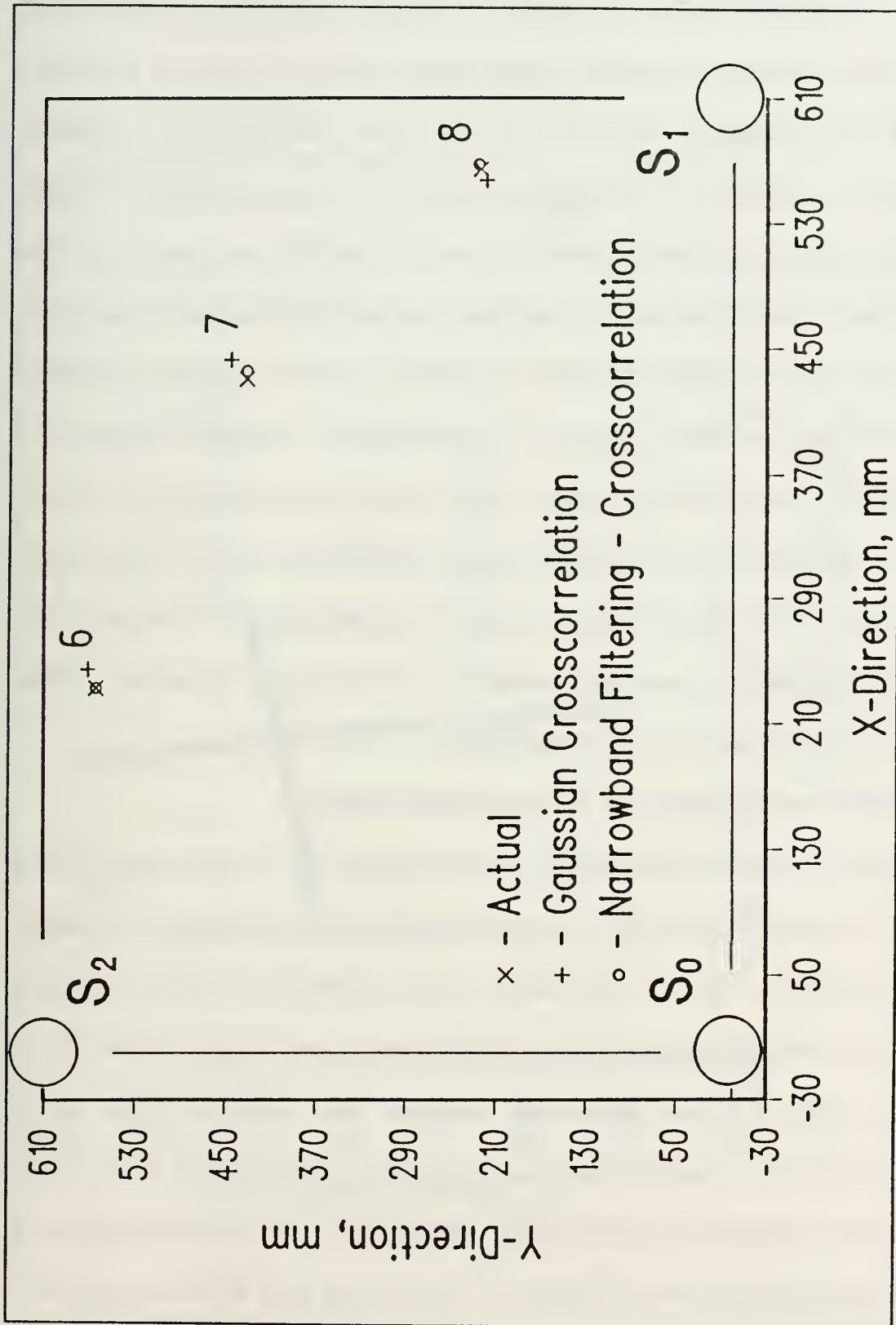
Figure 6.9. Source location data for narrowband filtering and crosscorrelation method.

87

between the sensors was 200 mm, and the lead breaks were performed on arcs of 100 and 200 mm. Because of the high degree of attenuation in the plate, a broadband conical point transducer was used in place of the Harisonic G0504 ultrasonic transducers employed for the aluminum plate. This was done since the point transducer had a better low frequency response that the Harisonic transducer. The signal from the transducer was then amplified using the PAC broadband preamplifier with 60 dB of gain, and then captured using the LeCroy DSO. Since only one point transducer was available, in order to obtain the three waveforms necessary to perform the crosscorrelation analysis, a trigger sensor was placed near the position of the lead break, and the point transducer at transducer location 0. The lead was then broken, and the signal from the point transducer was captured. This procedure was then repeated for transducer locations 1 and 2. Thus, to obtain one location point, three lead breaks had to be performed.

2. Narrowband Filtering and Crosscorrelation Method

For each location, the signal from the point transducer was narrowband filtered at center frequencies of 40, 50, 60, 80 and 100 kHz, with a bandwidth of 1/2 octave at each frequency. The Δt's determined by the crosscorrelation method were then input into a computer program which calculated the source location. Values for θ_0, θ_1 and θ_2, Figure 4.4, were incremented in steps of 0.25^0. Shown in Figure 6.10 is a plot of the loci of points which are determined using equation (4.14). The intersection of the these loci is the location of the source. The locations determined at each frequency are shown in Figure 6.11. While some large errors are apparent,

88
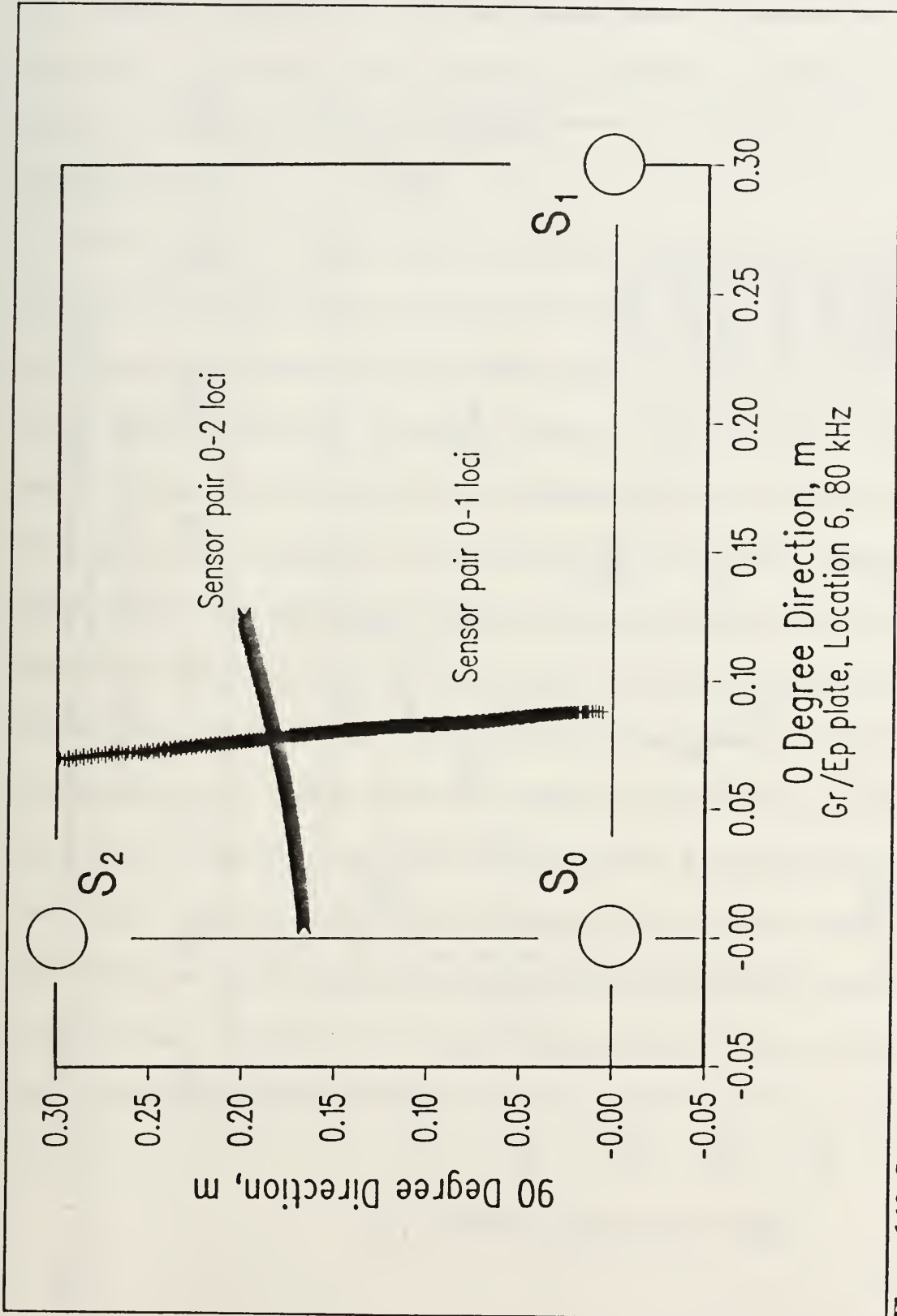
Figure 6.10. Source location loci.
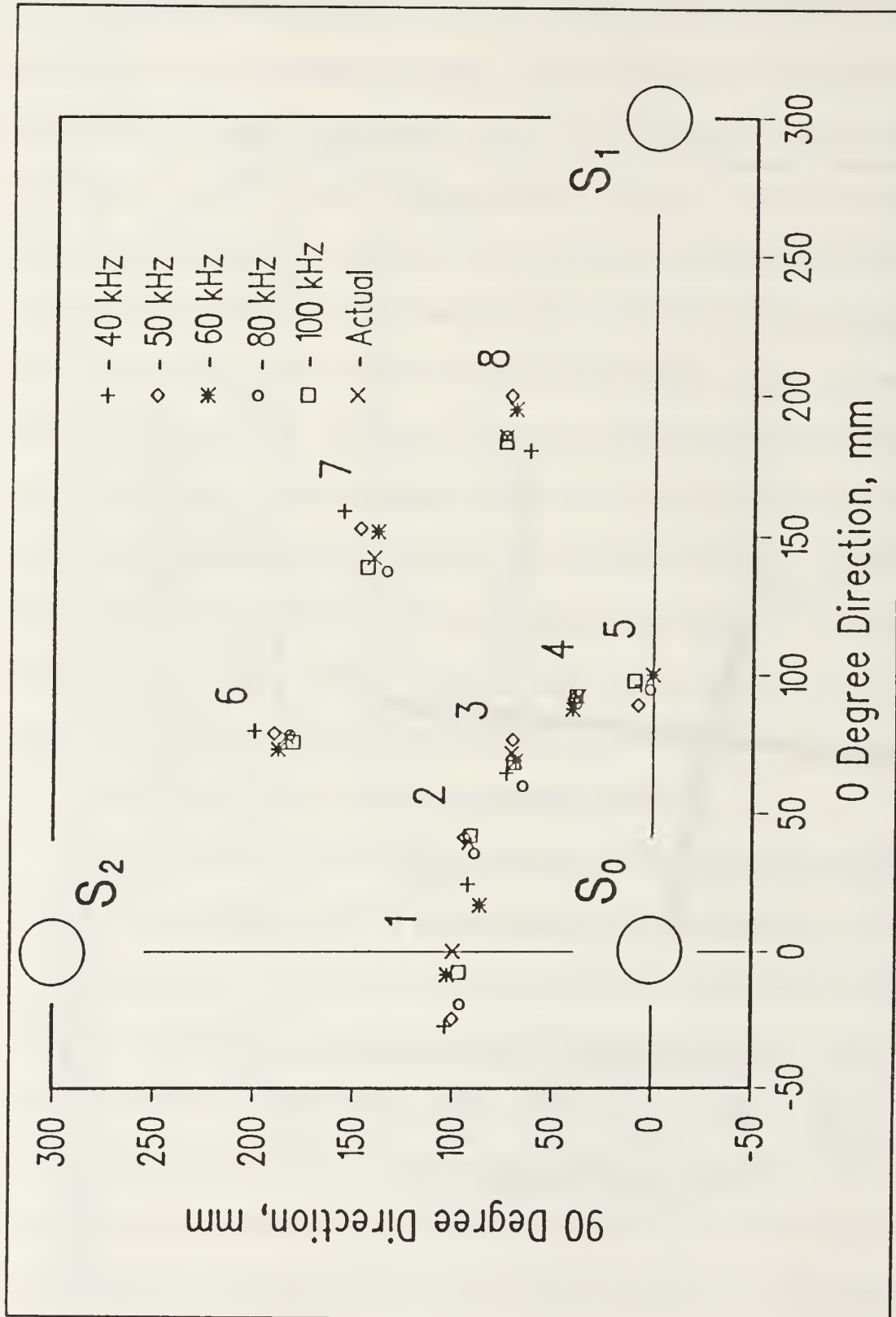
Figure 6.11. Source location data for narrowband filtering and crosscorrelation method.

90

these again are likely due to errors in the enveloping of the crosscorrelation, transducer and source positioning since only one transducer was available and the step size of 0.25^0 used in the location program.

C. DISCUSSION

Several methods for determination of arrival times have been presented. For the first threshold crossing techniques, as long as the location clocks were triggered by the nondispersive extensional portion of the plate wave, the location of the lead breaks was determined quite accurately. However, if the gain cannot be set high enough (for example, high noise levels) the location clocks for transducers remote from the source are triggered by the flexural portion of the wave. Triggering on different wave modes leads to large errors in the determination of the location of the lead break, even in the case of an aluminum plate. This was corrected by the use of crosscorrelation techniques. While the gaussian crosscorrelation method can be in error by up to one cycle of the crosscorrelation frequency due to phase shifts as the AE pulse propagates, if the crosscorrelation frequency is high enough, this error can be made negligible. This however is dependent on the frequency content of the signal. The narrowband filter crosscorrelation, while computationally more intense, provides a way to determine arrival times accurately without having to account for the problem of the unknown phase.

VII. CONCLUSIONS

The ability to detect the growth of defects is important if catastrophic failures of engineering structures are to be prevented. One method for detection of these defects is acoustic emission (AE). AE has the benefits of being able to be applied to the structure while it is in service, and the energy used for defect detection is supplied by the defect in the form of a stress wave propagating through the structure. However, if maximum use of the stress wave is to be made, the propagation of the wave through the medium must be understood.

In this thesis, a study of the propagation of stress waves in thin plates was presented, along with methods for determining the defect source location. In thin plates, it was shown that dispersion can cause large errors if threshold crossing techniques are used for source location, since the stress wave changes shape as it propagates. By using broadband transducers and filtering and applying crosscorrelation techniques, stress wave arrival times from the dispersive flexural mode that were independent of voltage threshold or gain settings were determined. This could be important in large structures where, due to attenuation, only the low frequency components of the flexural plate wave can propagate any distance, and in impact studies, where due to the source motion a large flexural wave is produced with little or no extensional component.

The presence of reflections, and their effect on the ability of the crosscorrelation

methods to correctly determine arrival times has not been examined. This problem was avoided in this work by the use of large plates. To make these location methods applicable in real engineering structures, accounting for the effect of reflections would be a logical next step.

APPENDIX A - HILBERT TRANSFORM

The Hilbert transform of a real-valued time domain signal $x(t)$ is another real-valued time domain signal, denoted by $\tilde{x}(t)$, such that $z(t)=x(t)+j\tilde{x}(t)$ is an analytical signal. From $z(t)$, one can define a magnitude function $A(t)$ and a phase function $\theta(t)$, where $A(t)$ describes the envelope of the original function $x(t)$ versus time, and $\theta(t)$ describes the instantaneous phase of $x(t)$ versus time [Ref. 36]. In this appendix, the mathematical definition of the Hilbert transform will be given, along with the computation of the transform.

We begin with an analytic signal $z(t)$, defined by

$$z(t) - x(t) + j\tilde{x}(t). \qquad \text{(B.1)}$$

This can also be written as

$$z(t) - A(t)e^{j\theta(t)} \qquad \text{(B.2)}$$

where $A(t)$ is called the envelope signal of $x(t)$ and $\theta(t)$ is called the instantaneous phase signal of $x(t)$. In terms of x(t) and $\tilde{x}(t)$, it is clear that

$$A(t) - \left[x^2(t) + \tilde{x}^2(t)\right]^{1/2} \qquad \text{(B.3)}$$

$$\theta(t) - \tan^{-1}\left[\frac{\tilde{x}(t)}{x(t)}\right] - 2\pi f_0 t. \qquad \text{(B.4)}$$

94

The instantaneous frequency, f_0, is given by

$$f_0 = \left(\frac{1}{2\pi}\right)\frac{d\theta(t)}{dt}. \tag{B.5}$$

Now let $Z(f)$ be the Fourier transform of $z(t)$,

$$\begin{aligned}Z(f) &= \mathcal{F}[z(t)] = \mathcal{F}[x(t)+j\tilde{x}(t)]\\ &= \mathcal{F}[x(t)]+j\mathcal{F}[\tilde{x}(t)] = X(f)+j\tilde{X}(f).\end{aligned} \tag{B.6}$$

The inverse Fourier transform of $Z(f)$ yields

$$z(t) = \mathcal{F}^{-1}[Z(f)] = x(t)+j\tilde{x}(t) \tag{B.7}$$

where

$$\tilde{x}(t) = \mathrm{Im}[z(t)] \tag{B.8}$$

which is the definition of the Hilbert transform.

It can be shown that [Ref. 36]

$$\tilde{X}(f) = (-j\,\mathrm{sgn}\,f)X(f) \tag{B.9}$$

This result can be substituted into equation (B.6) to get

$$Z(f) = [1+\mathrm{sgn}\,f]X(f) = B(f)X(f) \tag{B.10}$$

where, as shown in Figure B.1, $B(0)=1$ and

$$B(f) = \begin{cases} 2 & \text{for } f>0 \\ 0 & \text{for } f<0 \end{cases} \tag{B.11}$$

95

To obtain $Z(f)$ from $X(f)$ compute $X(f)$ for all f and then define $Z(f)$ by $Z(0)=X(0)$ and

$$Z(f) = \begin{cases} 2X(f) & \text{for } f>0 \\ 0 & \text{for } f<0 \end{cases} \tag{B.12}$$

The inverse Fourier transform of $Z(f)$ then gives $z(t)$ with $\tilde{x}(t) = \text{Im}[z(t)]$.
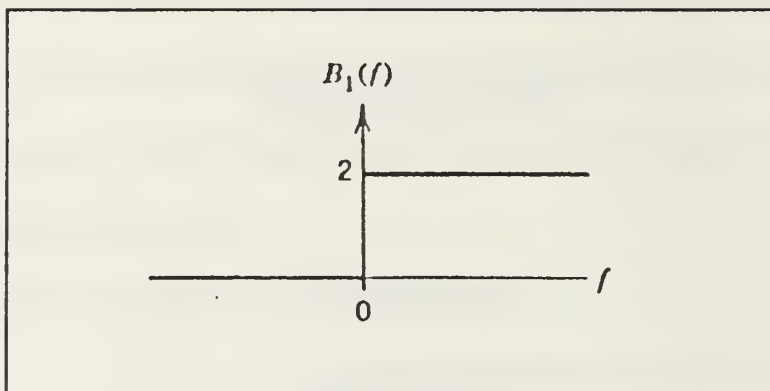
Figure 1. Sketch of $B(f)$.

APPENDIX B - LOCATION DATA

A. SOURCE LOCATION DATA FOR ALUMINUM PLATE

Given in Table I are the actual locations of the lead breaks on the aluminum plate. Shown in Tables II-IV are the location data points for each of the location methods discussed in Section VI-A.2. In the tables, *'s refer to to arrival times which resulted in mathematically intractable solutions in the isotropic location algorithm. Table V shows the data for the Gaussian crosscorrelation method, Section VI-A.3. Averages and standard deviations for the three lead breaks at each location have been calculated, except for the low gain/narrowband data. In Table VI the data points for the narrowband filtering and crosscorrelation method, Section VI-A.4, at locations 6, 7 and 8 are presented. All measurements are in millimeters (mm).

Table I. ACTUAL LEAD BREAK LOCATION, ALUMINUM PLATE

Location	x	y
1	0	305
2	117	282
1	216	216
4	282	117
5	305	0
6	233	564
7	431	431
8	564	224

97

Table II. LOCATION DATA FOR HIGH GAIN/BROADBAND INSTRUMENTATION, ALUMINUM PLATE.

Location	x	y	AVE - x	STD - x	AVE - y	STD - y
1	10.68	304.02	10.67	0.70	304.2	0.0
	9.97	304.02				
	11.38	304.02				
2	118.96	286.13	117.5	1.29	283.4	2.39
	116.72	281.99				
	116.72	281.99				
3	220.56	218.64	219.5	0.96	219.5	0.77
	219.18	219.66				
	218.70	220.14				
1	283.60	122.40	283.6	0.01	122.0	0.60
	283.62	121.36				
	283.60	122.40				
5	303.70	6.63	304.5	0.67	4.74	1.75
	304.67	3.18				
	305.00	4.42				
6	226.27	560.10	226.0	0.41	560.2	0.11
	225.55	560.29				
	226.27	560.10				
1	431.32	430.82	432.6	1.79	431.5	1.75
	434.69	432.69				
	431.94	430.94				
8	557.47	224.48	557.9	0.36	224.5	0.77
	558.15	225.79				
	558.00	224.42				

Table III. LOCATION DATA FOR HIGH GAIN/NARROWBAND INSTRUMENTATION, ALUMINUM PLATE.

Location	x	x	AVE - x	STD - x	AVE - y	STD - y
2	-21.89	301.66	-19.21	3.70	301.2	1.39
	-20.74	302.32				
	-14.99	299.65				
2	107.79	277.03	106.7	1.88	280.0	5.15
	104.53	285.95				
	107.79	277.03				
3	208.69	210.17	210.2	1.99	212.3	3.12
	209.42	210.90				
	212.45	215.90				
7	276.23	110.76	279.0	0.89	109.6	1.28
	275.90	109.80				
	284.81	108.22				
5	302.00	2.52	301.8	1.02	8.41	9.50
	302.66	19.37				
	300.66	3.34				
6	206.05	557.51	206.3	0.39	557.6	0.20
	206.05	557.51				
	206.72	557.86				
7	421.21	430.86	430.0	7.65	433.2	2.10
	434.83	434.83				
	434.06	434.06				
8	557.33	208.93	557.8	0.62	208.2	1.09
	•	•				
	558.21	207.39				

Table IV. LOCATION DATA FOR LOW GAIN/NARROWBAND INSTRUMENTATION, ALUMINUM PLATE.

Location	x	y	AVE - x	STD - x	AVE - y	STD - y
6	.	.				
	-2.08	279.8				
	15.8	294.9				
2	.	.				
	.	.				
	.	.				
3	193.6	181.9				
	152.2	152.2				
	189.5	212.1				
4	286.2	111.9				
	.	.				
	.	.				
5	.	.				
	.	.				
	.	.				
6	.	.				
	.	.				
	.	.				
7	120.9	362.1				
	168.3	176.1				
	168.3	176.1				
8	.	.				
	.	.				
	.	.				

100

Table V. LOCATION DATA FOR GAUSSIAN CROSSCORRELATION, ALUMINUM PLATE.

Location	x	y	AVE - x	STD - x	AVE - y	STD - y
1	-4.67	305.40	9.71	12.47	305.1	0.31
	17.59	304.80				
	16.21	305.00				
2	121.24	284.97	121.32	0.29	285.3	0.33
	121.46	286.61				
	121.17	285.19				
3	217.44	217.44	217.7	0.24	217.6	0.12
	217.66	217.66				
	217.92	217.63				
4	282.38	121.46	282.4	0.96	121.6	0.36
	283.44	122.06				
	281.52	121.43				
5	303.40	-5.68	303.5	0.61	-5.3	0.44
	303.00	-5.42				
	304.20	-4.82				
4	242.53	579.08	243.0	0.59	579.8	1.63
	243.62	581.63				
	243.00	578.59				
7	449.21	447.96	448.6	0.59	449.2	1.12
	448.54	450.10				
	448.04	449.61				
8	563.08	220.42	563.8	0.72	220.0	0.32
	564.51	219.83				
	563.85	219.90				

Table VI. LOCATION DATA FOR NARROWBAND FILTERING AND CROSSCORRELATION, ALUMINUM PLATE.

Location	Actual		Gaussian X-Corr		NBF X-Corr	
	x	y	x	y	x	y
6	233	564	243	579	233	564
7	431	431	448	450	436	431
8	564	224	564	220	567	226

B. SOURCE LOCATION DATA FOR GRAPHITE/EPOXY PLATE

Table VII shows the actual leadbreak positions, while Table VIII gives the calculated positions using the method outlined in Section VI-B.2. Again, all measurements are in millimeters (mm).

Table VII. ACTUAL LOCATIONS OF LEAD BREAKS, GR/EP PLATE.

Location	x	●
1	0	100
2	39.2	92.0
3	71.6	71.0
2	92.2	37.5
5	100	0
6	77.6	184
7	142	140.5
8	185	75.0

Table VIII. LOCATION DATA FOR GRAPHITE/EPOXY PLATE.

Location 1	x	y	Location 2	x	y
Actual	0.0	100.0	Actual	39.2	92.0
40 kHz	-27.3	103.6	40 kHz	88.0	92.0
60 kHz	-24.5	99.9	50 kHz	41.1	94.5
60 kHz	-8.5	102.8	60 kHz	16.4	86.6
80 kHz	-19.2	96.4	80 kHz	39.2	89.5
100 kHz	-7.6	96.8	100 kHz	71.0	91.2
Location 3	x	y	Location 4	x	y
Actual	41.1	71.0	Actual	92.2	37.5
40 kHz	64.5	73.6	40 kHz	91.7	39.4
50 kHz	76.4	70.6	50 kHz	91.2	40.1
60 kHz	68.9	98.6	60 kHz	87.6	40.4
80 kHz	59.9	65.3	80 kHz	97.7	38.5
100 kHz	68.2	70.1	100 kHz	78.3	38.7
Location 5	x	y	Location 6	x	y
Actual	100.0	0.0	Actual	77.6	184.0
40 kHz	96.5	6.3	40 kHz	79.8	200.0
50 kHz	88.8	0.0	50 kHz	78.8	190.2
60 kHz	100.0	0.0	60 kHz	73.1	188.1
80 kHz	94.6	1.7	80 kHz	78.3	182.2
100 kHz	97.7	0.0	100 kHz	75.8	180.7
Location 7	x	y	Location 8	x	y
Actual	142.2	140.5	Actual	185.0	75.0
40 kHz	159.0	156.1	40 kHz	130.8	62.9
50 kHz	152.8	147.5	50 kHz	199.7	72.2
60 kHz	151.5	138.8	60 kHz	194.8	69.9
80 kHz	137.5	134.0	80 kHz	185.4	74.9
100 kHz	138.9	143.9	100 kHz	183.4	75.0

103

LIST OF REFERENCES

1. Baker, D., "Why Challenger Failed," *New Scientist*, v. 11, pp. 52-56, September 1986.

2. "Safety of Aging Aircraft Undergoes Reassessment," *Aviation Week and Space Technology*, pp. 16-18, 16 May 1988.

3. Smith Jr., W. D., *Acoustic Emission from Spectrum Fatigue Cracks in 7075 Aluminum*, Master's Thesis, Naval Postgraduate School, Monterey, California, December 1990.

4. Votava, E., and Jax, P., "Inspection of Nuclear Reactors by Means of Acoustic Emission During Hydrostatic Test," *Acoustic Emission Monitoring of Pressurized Systems*, ASTM STP 697, pp.149-164, 1979.

5. Le Floc'h, C., "Acoustic Emission Monitoring of Composite High-Pressure Fluid Storage Tanks," *NDT International*, v. 19, n. 4, pp. 259-262, August 1986.

6. Gorman, M. R., Ziola, S. M., and Koury, J. L., *Proc. Third Int. Symp. Acoustic Emission from Composite Materials (AECM-3)*, American Society for Nondestructive Testing, Columbus, Ohio, USA, p. 286, 1989.

7. Gorman, M. R., "Plate Wave Acoustic Emission," *Journal of the Acoustical Society of America*, v. 90, n. 1, pp. 358-364, July 1991.

8. Gorman, M. R., and Ziola, S. M., "Plate Waves Produced by Transverse Matrix Cracking," *Ultrasonics*, v. 29, n. 3, pp. 245-251, May 1991.

9. Beattie, A. G., "Acoustic Emission, Principles and Instrumentation," *Journal of Acoustic Emission*, v. 2, n. 1/2, pp. 95-128, 1983.

10. Bendat, J. S., and Piersol, A. G., *Engineering Applications of Correlation and Spectral Analysis*, 2d ed., John Wiley & Sons, Inc., 1986.

11. Special Issue on Time Delay Estimation, *IEEE Trans. Acoust., Speech, Signal Processing*, v. 29, n. 3, June 1981.

12. Smith, M. W., and Lambert, R. F., "Propagation of Band Limited Noise," *Journal of the Acoustical Society of America*, v. 32, n. 4, pp. 512-514, April 1960.

13. Winter, E. F., and Bies, D. A., "Correlation Properties of Flexural Waves in Long Thin Bars," *Journal of the Acoustical Society of America*, v. 34, n. 4, pp. 472-475, April 1962.

14. White, P. H., "Cross Correlation in Structural Systems: Dispersion and Nondispersion Waves," *Journal of the Acoustical Society of America*, v. 45, n. 5, pp. 1118-1128, 1969.

15. Novikov, A. K., "Spatial Correlation of Plane Bending Waves," *Soviet Physics - Acoustics*, v. 7, n. 4, pp. 374-379, April-June 1962.

16. Castagnede, B., Roux, J., and Hosten, B., "Correlation Method for Normal Mode Tracking in Anisotropic Media Using an Ultrasonic Immersion System," *Ultrasonics*, v. 27, n. 5, pp. 280-287, September 1989.

17. Aussel, J. D., and Monchalin, J. P., "Precision Laser-Ultrasonic Velocity Measurement and Elastic Constant Determination," *Ultrasonics*, v. 27, n. 3, pp. 165-177, May 1989.

18. Nagano, K., Niitsuma, H., and Chubachi, N., "Automatic Algorithm for Triaxial Hodogram Source Location in Downhole Acoustic Emission Measurement," *Geophysics*, v. 54, n. 4, pp. 508-513, April 1989.

19. Hsu, N. N., and Hardy, S. C., "Experiments in Acoustic Emission Waveform Analysis for Characterization of AE Sources, Sensors and Structures," *Elastic Waves and Non-Destructive Testing of Materials*, Applied Mechanics Division, v. 29, pp. 85-106, December 1978.

20. Harris, R. W., and Wood, B. R. A., "The Detection, Transmission and Interpretation of Acoustic Emission Signals," *Metals Forum*, v. 5, n. 4, pp. 210-216, 1982.

21. Pollock, A. A., "Acoustic Emission - 2, Acoustic Emission Amplitudes," *Non-Destructive Testing*, v. 6, n. 5, pp. 63-70, October 1973.

22. Brindley, B. J., Holt, J. and Palmer, I. G., "Acoustic Emission - 3, The Use of Ring-Down Counting," *Non-Destructive Testing*, v. 6, n. 6, pp. 299-306, December 1973.

23. Baram J., and Rosen, M., "Fatigue Life Prediction by Distribution Analysis of Acoustic Emission Signals," *Materials Science and Engineering*, v. 41, n. 1, pp. 25-30, November 1979.

24. Graff, K. F., *Wave Motion in Elastic Solids*, Ohio State University Press, 1975.

25. Mindlin, R. D., and Medick, M. A., "Extensional Vibrations of Elastic Plates," *Journal of Applied Mechanics*, v. 32, n. 5, pp. 561-569, December 1959.

26. Mindlin, R. D., "Influence of Rotary Inertia and Shear on Flexural Motions of Isotropic, Elastic Plates," *Journal of Applied Mechanics*, v. 18, pp. 31-38, March 1951.

27. Tang, B., Henneke II, E. G., and Stiffler, R. C., "Low Frequency Flexural Wave Propagation in Laminated Composite Plates," *Acousto-Ultrasonics Theory and Application*, pp. 45-65, Plenum Press, 1988.

28. Noiret, D., and Roget, J., "Calculation of Wave Propagation in Composite Materials Using the Lamb Wave Concept," *Journal of Composite Materials*, v. 23, n. 2, pp. 195-206, February 1989.

29. Datta, S. K., Shah, A. H., Bratton, R. L., and Chakraborty T., "Wave Propagation in Laminated Composite Plates," *Journal of the Acoustical Society of America*, v. 86, n. 6, pp. 2020-2026, June 1988.

30. Stokes, G. G., *Mathematics and Physics Papers*, v. 5, p. 362, Cambridge University Press, 1905.

31. Tobias, A., "Acoustic-Emission Source Location in Two Dimensions by an Array of Three Sensors," *Non-Destructive Testing*, v. 9, n. 1, pp. 9-12, February 1976.

32. Castagnede, B., Sachse, W., and Kim, K. Y., "Location of Pointlike Acoustic Emission Sources in Anisotropic Plates," *Journal of the Acoustical Society of America*, v. 86, n. 3, pp. 1161-1171, September 1989.

33. Buttle D. J., and Scruby, C. B., "Acoustic Emission Source Location in Fiber Reinforced Plastic Composites," *Journal of Acoustic Emission*, v. 7, n. 4, pp. 211-223, 1988.

34. Medick, M. A., "On Classical Plate Theory and Wave Propagation," *Journal of Applied Mechanics*, v. 28, n. 2, pp. 223-228, June 1961.

35. Jahnke, Emde, and Loshch, *Tables of Higher Functions*, 6th ed., pp. 18-22, McGraw-Hill, Inc., 1960.

36. Bendat, J. S. and Piersol, A. G., *Random Data: Analysis and Measurement Procedures*, 2d ed., John Wiley and Sons, Inc., 1986.

37. Bassim, M. N., Houssny-Emam, M., "Time and Frequency Analysis of Acoustic Emission Signals," *Acoustic Emission*, v. 2, pp. 139-163, Gordon and Breach Science Publishers, 1983.

38. Habeger, C. C., Mann, R. W., and Baum, G. A., "Ultrasonic Plate Waves in Paper," *Ultrasonics*, v. 17, n. 2, pp. 57-62, March 1979.

39. Dayal, V., and Kinra, V. K., "Leaky Lamb Waves in an Anisotropic Plate. I: An Exact Solution and Experiments," *Journal of the Acoustical Society of America*, v. 85, n. 6, pp. 2268-2276, June 1989.

40. Chimenti, D. E., and Nayfeh, A. H., "Experimental Ultrasonic Reflection and Guided Wave Propagation in Fibrous Composite Laminates," *Wave Propagation in Structural Composites*, Applied Mechanics Division, v. 90, pp. 29-37, 1988.

41. NASA Contractor Report, *Low Frequency Plate Wave Modes*, by R. C. Stiffler and E. G. Henneke II, May 1986.

42. Ziola, S. M., and Gorman, M. R., "Experimental Plate Wave Dispersion Analysis," *Review of Progress in Quantitative Nondestructive Evaluation*, v. 10B, pp. 1921-1928, Plenum Press, 1990.

INITIAL DISTRIBUTION LIST

1. Defense Technical Information Center   2
   Cameron Station
   Alexandria, Virginia 22304-6145

2. Library, Code 0142   2
   Naval Postgraduate School
   Monterey, California 93943-5000

3. Prof. Michael R. Gorman   6
   Code AA/Go
   Naval Postgraduate School
   Monterey, California 93943-5000

4. Prof. Edward M. Wu   1
   Code AA/Wu
   Naval Postgraduate School
   Monterey, California 93943-5000

5. Mr. James L. Koury   1
   Phillips Laboratory
   VSSC
   Edwards Air Force Base, California 93523-5000

6. Dr. William H. Prosser   1
   NASA Langley Research Center
   Mail Stop 231
   Hampton, Virginia 23665

7. Dr. John W. Gillespie, Jr.   1
   Center for Composite Materials
   Composite Manufacturing Science Laboratory
   University of Delaware
   Newark, Delaware 19716

8. Steven M. Ziola   1
   Code AA/Zi
   Naval Postgraduate School
   Monterey, California 93943-5000

Thesis
Z5
c.1   Ziola
              Source location in
           thin plates using cross-
           correlation.

Thesis
Z5
c.1   Ziola
              Source location in
           thin plates using cross-
           correlation.